OAK RIDGE
NATIONAL LABORATORY

MANAGED BY UT-BATTELLE
FOR THE DEPARTMENT OF ENERGY

Preliminary Multiphysics Analyses of HFIR LEU Fuel Conversion using COMSOL

June 2011

Prepared by

J. D. Freels
I. T. Bodey
R. V. Arimilli
F. G. Curtis
K. Ekici
P. K. Jain
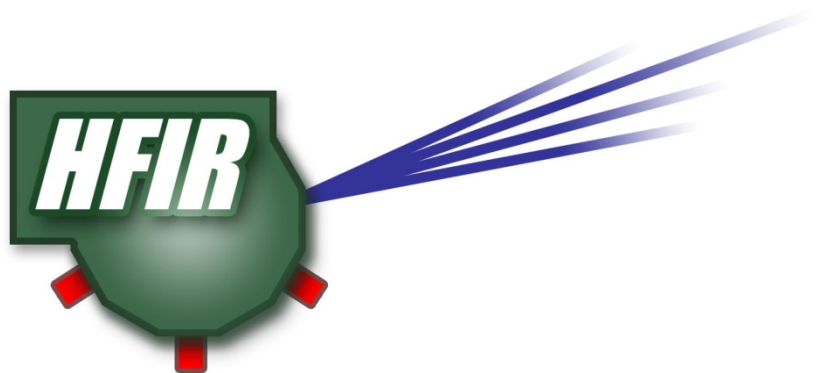
UT-BATTELLE

ORNL-27 (4-00)

DOCUMENT AVAILABILITY

Reports produced after January 1, 1996, are generally available free via the U.S. Department of Energy (DOE) Information Bridge.

Web site http://www.osti.gov/bridge

Reports produced before January 1, 1996, may be purchased by members of the public from the following source.

National Technical Information Service
5285 Port Royal Road
Springfield, VA 22161
Telephone 703-605-6000 (1-800-553-6847)
TDD 703-487-4639
Fax 703-605-6900
E-mail info@ntis.gov
Web site http://www.ntis.gov/support/ordernowabout.htm

Reports are available to DOE employees, DOE contractors, Energy Technology Data Exchange (ETDE) representatives, and International Nuclear Information System (INIS) representatives from the following source.

Office of Scientific and Technical Information
P.O. Box 62
Oak Ridge, TN 37831
Telephone 865-576-8401
Fax 865-576-5728
E-mail reports@osti.gov
Web site http://www.osti.gov/contact.html

PRELIMINARY MULTIPHYSICS ANALYSES OF
HFIR LEU FUEL CONVERSION USING COMSOL

J. D. Freels
I. T. Bodey*
R. V. Arimilli*
F. G. Curtis*
K. Ekici*
P. K. Jain

*University of Tennessee, Knoxville, TN

June 2011

CONTENTS

LIST OF TABLES

LIST OF FIGURES

ACKNOWLEDGEMENTS

ABSTRACT

The research documented herein was performed by several individuals across multiple organizations. We have previously acknowledged our funding for the project, but another common thread among the authors of this document, and hence the research performed, is the analysis tool COMSOL. The research has been divided into categories to allow the COMSOL analysis to be performed independently to the extent possible. As will be seen herein, the research has progressed to the point where it is expected that next year (2011) a large fraction of the research will require collaboration of our efforts as we progress almost exclusively into three-dimensional (3D) analysis. To the extent possible, we have tried to segregate the development effort into two-dimensional (2D) analysis in order to arrive at techniques and methodology that can be extended to 3D models in a timely manner. The Research Reactors Division (RRD) of ORNL has contracted with the University of Tennessee, Knoxville (UTK) Mechanical, Aerospace and Biomedical Engineering Department (MABE) to perform a significant fraction of this research. This group has been chosen due to their expertise and long-term commitment in using COMSOL and also because the participating students are able to work onsite on a part-time basis due to the close proximity of UTK with the ORNL campus. The UTK research has been governed by a statement of work (SOW) which clearly defines the specific tasks reported herein on the perspective areas of research. Ph.D. student Isaac T. Bodey has focused on heat transfer, fluid flow, modeling, and meshing issues and has been aided by his major professor Dr. Rao V. Arimilli and is the primary contributor to Section 2 of this report. Ph.D student Franklin G. Curtis has been focusing exclusively on fluid-structure interaction (FSI) due to the mechanical forces acting on the plate caused by the flow and has also been aided by his major professor Dr. Kivanc Ekici and is the primary contributor to Section 4 of this report. The HFIR LEU conversion project has also obtained the services of Dr. Prashant K. Jain of the Reactor & Nuclear Systems Division (RNSD) of ORNL. Prashant has quickly adapted to the COMSOL tools and has been focusing on thermal-structure interaction (TSI) issues and development of alternative 3D model approaches that could yield faster-running solutions. Prashant is the primary contributor to Section 5 of the report. And finally, while incorporating findings from all members of the "COMSOL team" (i.e., the team) and contributing as the senior COMSOL leader and advocate, Dr. James D. Freels has focused on the 3D model development, cluster deployment, and has contributed primarily to Section 3 and overall integration of this report. The team has migrated to the current release of COMSOL at version 4.1 for all the work described in this report, except where stated otherwise. Just as in the performance of the research, each of the respective sections has been originally authored by the respective authors. Therefore, the reader will observe a contrast in writing style throughout this document.

1.0   INTRODUCTION

During the original design of HFIR, the design engineers and analysts at the time wrote an original computer code that has come to be known at HFIR as the "Steady-State Heat Transfer Code" (SSHTC). The SSHTC includes most of the physics required to analyze the thermal hydraulics, structural mechanics, and other phenomena related to the normal and abnormal operation of the HFIR HEU fuel plates and fuel elements. The analysis is carried out in a conservative manner such that safe operation of the HFIR is assured with large margins of safety. The code source is available, but it is not well documented or source-commented, and is very difficult to change without creating unpredictable results. Furthermore, many of the correlations and empirical relationships embedded in the SSHTC are based on tests, experiments, and fabrication tolerances that are not applicable to LEU fuel.

The input for the SSHTC is structured specifically for the HFIR HEU fuel. Some of the inputs to the code can be changed from HEU fuel to LEU fuel such as material properties. However, several of the most important parameters are the uncertainty factors (U factors as they are called in the SSHTC input) applied to the local heat generation used to generate a conservatively high wall temperature adjacent to the coolant. At the present time, these factors cannot be determined for the LEU counterpart.   In the absence of LEU-specific equivalent data, we have chosen to use the SSHTC with HEU surrogate inputs as a scoping analysis and use our best engineering judgment in interpreting the results of the analysis in order to meet program goals.[1] The result of this LEU-based SSHTC feasibility analysis has indicated that an axially-contoured fuel along with radially-contoured fuel (also in the present HEU fuel, but a different radial contour design) will produce a sufficient margin in the clad surface temperature to allow for 100-MW operation of the HFIR. Recall that a change in power level from HEU/85-MW to LEU/100-MW operation is required to maintain HFIR research performance capabilities.

More accurate analyses are therefore necessary and can be done by either: (1) repeating most of the past HEU tests and experiments that were required to develop the original SSHTC, and modifying the SSHTC to change the HEU characteristics of the code to the LEU counterpart, or (2) utilizing a modern multi-physics engineering analysis code such as COMSOL to validate with HEU fuel and build a new design basis for the HFIR LEU fuel. RRD has selected COMSOL for several reasons, including that the COMSOL code is a modern, state-of-the-art, 3D integrated multi-physics engineering simulation toolbox. The investment in a COMSOL-based analysis tool is justifiable because we anticipate at least 20 years of operation with LEU fuel after the conversion, which will involve over 75,000 individual fuel plates to be manufactured. We must produce a high quality and superior fuel at a reasonable cost. This will ultimately mean a transition from the ultra-conservatism of the SSHTC to the increased accuracy of the COMSOL results, with selective conservatism, while taking advantage of the modern analysis methods included in the code.

This report primarily documents progress that has been made in the thermal-hydraulic (T-H) technical area during the calendar year 2010 (CY 2010). A significant amount of the research reported here was performed by a group out of the University of Tennessee, Knoxville Department of Mechanical, Aerospace, Biomedical Engineering (UTK-MABE) on a contract that also started at the beginning of the CY 2010. Some of the material may span periods of time across the contracting period and/or calendar years.

The purpose of this research is to develop an accurate and robust simulation capability that will encompass essentially all of the physics associated with thermal effects of a HFIR LEU fuel element. The primary tool to be used is "COMSOL-Multiphysics," or COMSOL, which is commercially available from COMSOL, Inc. The developed COMSOL models are anticipated to be used to simulate both normal operation and accident (or abnormal) conditions to the extent possible given the capabilities of the COMSOL code.

The need for a thermal simulation capability is driven by the difficulty in performing tests to the extent that the HEU fuel was tested during the original design and construction of the HFIR facility. Therefore, many of the phenomena that were measured or witnessed directly by testing the original HEU fuel elements will now be simulated by a computer for the development of the HFIR LEU fuel. There are several reasons for this modified approach to fuel design: (1) the simulation capabilities brought about by improved computer hardware and software allow for precise estimates of the fuel thermal performance that were not possible at the time of the HEU fuel design, (2) the costs associated with nuclear-related testing have become prohibitively high relative to the costs of computer simulation, and (3) the regulatory requirements that exist today for operating a nuclear facility demand thorough and rigorous quality assurance for both testing and analytical approaches such that testing alone will not be sufficient to develop a new fuel. In other words, because we will need to perform the computer simulations anyway, and if it is sufficient to achieve the desired goals without testing, then it is more cost effective to only perform simulations of the thermal effects in some cases. However, it is emphasized that there are some phenomena that must also be tested since validation data supporting the simulations may not be available. Hence, the quality assurance issues will dictate whether testing is required in addition to the simulations.

The thermal-related physics we are addressing in this research and development documented to some extent in this report are: (1) thermal heat conduction in both fuel and coolant materials and associated structures, (2) thermal convection between the fuel and coolant and advection to and from the fuel regions by the coolant, (3) the thermal expansion and contraction of all the materials modeled within the fuel element domain (i.e., thermal-structure interaction or TSI), and (4) the movement of the structures relative to the coolant caused by the forces of the coolant acting on the structures (i.e., fluid-structure interaction or FSI). There are additional physics that are being considered for investigation under this project and/or coupled with this work at a later time. These include reactor kinetics (space-time), radiation-induced material damage, and corrosion buildup during a cycle. Indeed, the physical effects associated with the change in material properties during the fuel cycle will need to be examined and included in this multiple-physics approach to fuel design.

As stated earlier, this report summarizes the thermal-hydraulic research performed primarily during CY 2010, but some of the work was done during the early part of FY 2011. The research and analysis is divided into two-dimensional (2D) and three-dimensional (3D) parts in the discussion. Our goal is to consider only the 3D geometry, but much can be learned about methods and techniques in the 2D framework such that significant resource savings can occur. Therefore, we always study in 2D to the extent possible before exploring the 3D details.

Other reports related to this work have been completed recently. The research from CY 2009 was completed during FY 2010 and documented by the following publication:

ORNL/TM-2010/018 , 2D Thermal Hydraulic Analysis and Benchmark in Support of HFIR LEU Conversion using COMSOL, 09/18/2010, http://info.ornl.gov/sites/publications/Files/Pub23015.pdf.

Two papers related to this work were submitted and presented at the COMSOL Conference 2010 Boston, October 7-9, 2010. Copies of the full conference proceedings are available from COMSOL which includes these two papers. The papers are also publically available from ORNL here:

http://info.ornl.gov/sites/publications/Files/Pub26121.pdf
Upgrading the HFIR Thermal-Hydraulic Legacy Code Using COMSOL

http://info.ornl.gov/sites/publications/Files/Pub26110.pdf -- paper
http://info.ornl.gov/sites/publications/Files/Pub26490.pdf -- presentation
Exploiting New Features of COMSOL version 4 on Conjugate Heat Transfer Problems

A presentation was made to the Joint Meeting of TRTR and IGORR in Knoxville, TN on September 20, 2010. The presentation was entitled Multiphysics Modeling to Support HFIR LEU Fuel Conversion, and is available here http://info.ornl.gov/sites/publications/Files/Pub24478.pdf .

A presentation was made to the U.S. High-Performance Reactors Working Group Thermal-Hydraulics Experts Meeting on June 10, 2010 at the campus of Oregon State University, Corvallis, Oregon. The presentation was entitled Status of Multiphysics Modeling for the Conversion of HFIR Fuel Elements to LEU, and is available here http://info.ornl.gov/sites/publications/Files/Pub24483.pdf .

An invited presentation was made at a CFD Colloquium in honor of the retirement of Professor A. J. Baker of UT-Knoxville on May 27, 2010 at the UTK campus. The presentation was entitled Recent CFD-Related Activities at the High Flux Isotope Reactor of ORNL, and includes a considerable amount of discussion related to this LEU conversion project. The presentation is available here http://info.ornl.gov/sites/publications/Files/Pub24235.pdf and http://cfdlab.utk.edu/html/colloquium/colloq.htm.

2.0   2D THERMAL-HYDRAULIC METHODS DEVELOPMENT

2.1   INVESTIGATION OF TURBULENT PRANDTL NUMBER

The formulations of the turbulent Prandtl number used in COMSOL are the Kays-Crawford, Extended Kays-Crawford, and User Defined. COMSOL versions 3.4 and earlier only provided for the "User Defined" option, which usually was represented as a constant such as 1.0 or 0.85. The Kays-Crawford turbulent Prandtl number is chosen by default. The COMSOL documentation states that this formulation of the turbulent Prandtl number is found to be sufficient for "most turbulent wall bounded flows except for liquid metals."[2] Formally it is expressed as

$$\text{Pr}_T = \left[\frac{1}{2\text{Pr}_{T\infty}} + \frac{0.3}{\sqrt{\text{Pr}_{T\infty}}} \frac{C_p \eta_T}{k} - \left(0.3 \frac{C_p \eta_T}{k} \right)^2 \left(1 - e^{\frac{-k}{0.3 C_p \eta_T \text{Pr}_{T\infty}}} \right) \right]^{-1},$$ (2.1)

where $\text{Pr}_{T\infty} = 0.85$, k is the thermal conductivity of the fluid, C_p is the specific heat of the fluid, and η_T is the eddy viscosity. This equation is based on the idea that the mechanism for heat transfer in an eddy is by molecular diffusion only and "when compared with experiment it fits the available data reasonably well".[3]

The extended Kays-Crawford turbulent Prandtl number includes liquid metals by modifying the free stream turbulent Prandtl number

$$\text{Pr}_{T\infty} = 0.85 + \frac{100 \, k}{C_p \eta \text{Re}_\infty^{0.888}}$$ (2.2)

Where Re_∞ is the free stream Reynolds number and η is the dynamic viscosity of the fluid.
The "User defined" option also gives the COMSOL user the freedom to define a value or expression for the turbulent Prandtl number.

It is clear from the descriptions that the default input of v4+ of COMSOL specifying the Kays-Crawford turbulent Prandtl number is the correct input for the HFIR fuel element application.

2.2   LOW REYNOLDS NUMBER TURBULENT MODEL IN COMSOL 4

Earlier versions of COMSOL, i.e. version 3.5a and before, used empirical relationships between the time-averaged velocity and the wall shear stress known as 'wall functions' to model turbulence close to a fluid-solid interface. These wall functions are of a form

$$u^+ = \frac{\bar{u}}{u_\tau} = \frac{1}{\kappa} \ln(y^+) + C^+$$ (2.3)

where $\bar{u}$ is the average velocity of the flow, κ is a von Karman's constant and is set equal to 0.42 according to the COMSOL documentation [ref. 3], C^+ is a "universal constant for smooth walls"[4] and is set to a default value of 5.5 in COMSOL. Note that the default values of both κ and C^+ are allowed to be changed in COMSOL if needed. The term u_τ, in equation 2.3, is the friction velocity and is represented by

4

$$u_\tau = \sqrt{\frac{\tau_s}{\rho}} \tag{2.4}$$

with τ_s being the wall shear stress and ρ being the fluid density. The y^+ term in equation 2.3 is a way of expressing the effective thickness of the viscous sublayer which is the region of the turbulent boundary layer that is laminar, i.e. adjacent to the wall subject to a no slip boundary condition. Formally y^+ is represented by the following equation

$$y^+ = \frac{y u_\tau}{\upsilon} \tag{2.5}$$

with υ being the kinematic viscosity of the fluid and y being the distance from the physical wall. These wall functions show good agreement with experiments in the range $30 \leq y^+ \leq 100$. A divergence of the wall function model with experiment for values of $y^+ < 30$ is shown in Fig. 2.1. In fact, one could potentially over-predict the average velocity by a factor of 5 near the wall which would result in significantly lower wall temperatures than those physically observed.

Not shown in Fig. 2.1 is the deviation of the data relative to the wall function for $y^+ > 100$. While the data do indeed diverge relative to the model in this region, it is not as pronounced as the deviation close to the physical wall. Indeed, higher Reynolds number flows tend to diverge less in this region. While this region is important for turbulence dissipation,[5] the primary objective of this research is to accurately determine the amount of thermal energy removed from and the forces acting upon the HFIR fuel plate, which are effects of the fluid-solid interaction.

COMSOL 3.5a requires the user to provide the wall offset or in the present context, y^+. The COMSOL specific variable for y^+ is δ_w^+. Choosing a useful value of y^+ is not a trivial task. In COMSOL 3.5a, this value is strongly dependent on the mesh density of the finite element discretization, and the wall temperature is affected by the value chosen for y^+ (i.e., the clad surface temperature is subject to user input). The dependence of the clad surface temperature on y^+ is shown in Fig. 2.2. Figure 2.2 was completed as part of CY 2009 work.[6]
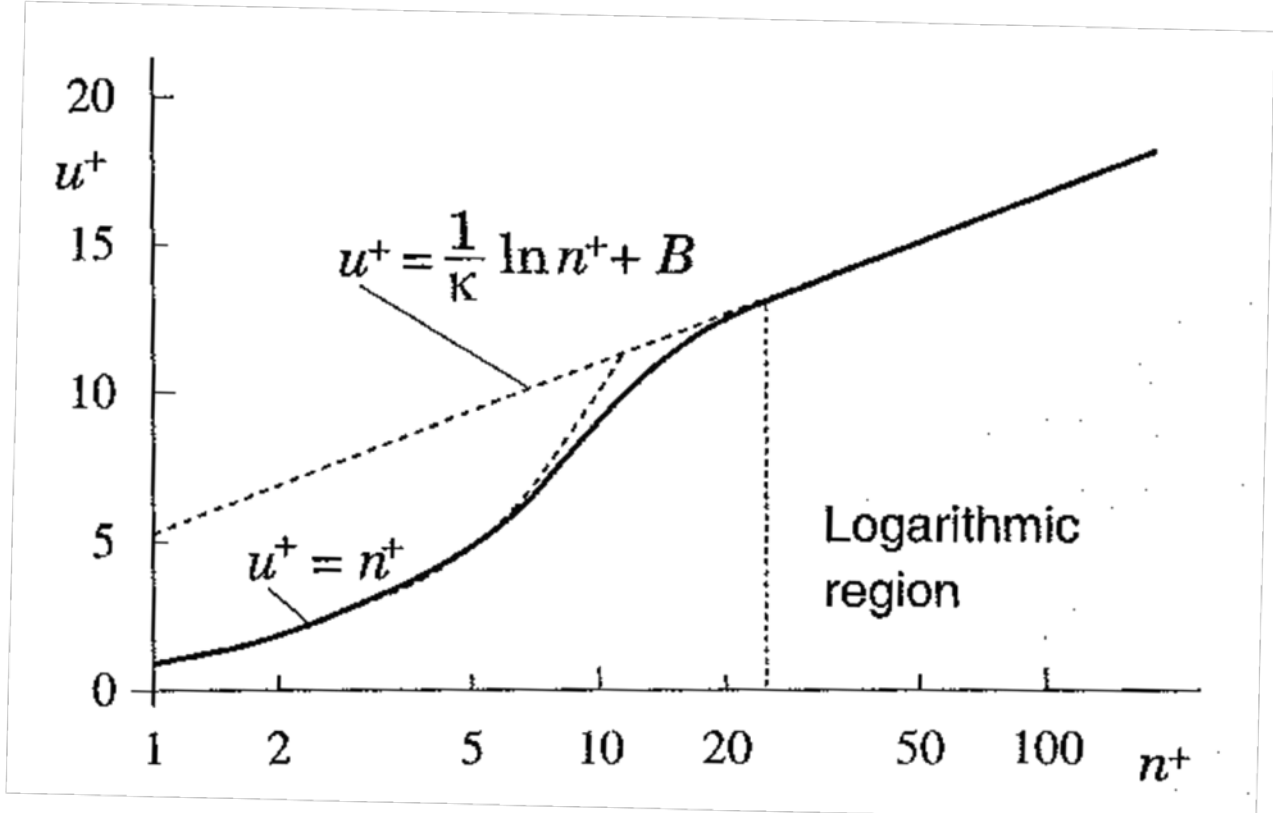
Fig. 2.1. Turbulent boundary layer regions.
Here $n^+ = y^+$ in the context of Equation 2.3. Experimental data fall along the solid line.
Figure obtained from ref 4.
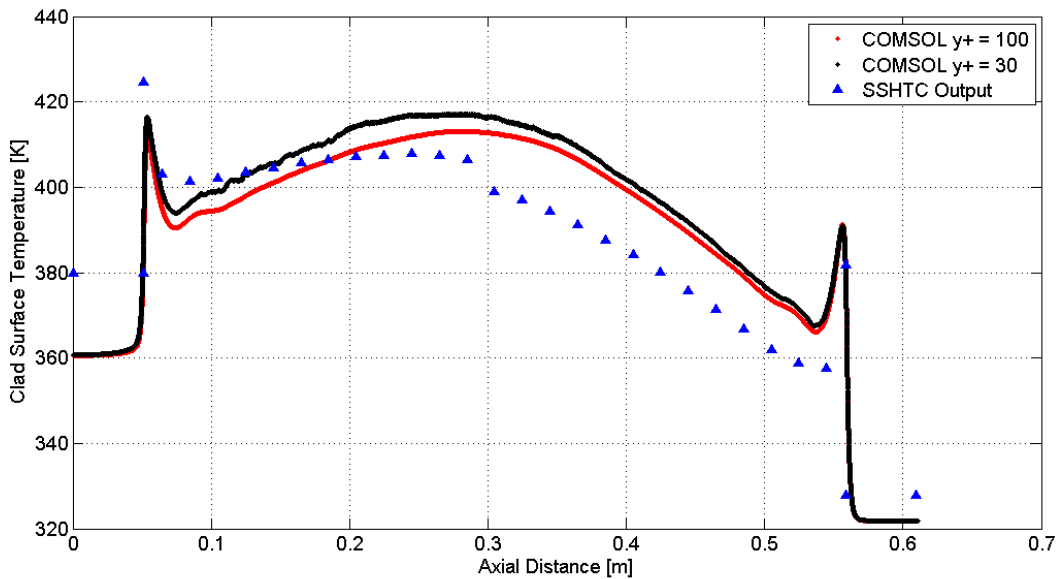
**Fig. 2.2. Clad surface temperature profile for involute arc length position 6 of
an inner fuel plate based on the SSHTC discretization procedure.**
Flow is from right to left.

Due to the necessity of using a wall offset in these turbulence models, important flow dependent parameters such as the convection heat transfer coefficient and the wall shear stress are not calculable from the field variables. These parameters are calculated using gradients in the viscous sublayer at the wall, which is not represented in the simulation. Thus the best the analyst can do is assume linear velocity and temperature profiles in the viscous sublayer based on the physics at the wall and local values in the simulation at the wall offset to aid in the calculation of these quantities.

In version 4 of COMSOL, the user has another option for turbulence modeling known as the Low Reynolds Number k-ε model (LRN). The LRN refers to the decrease in the Reynolds number as the physical wall is approached due to the no slip wall boundary condition. With this formulation, a user-input for the wall offset is not required for the turbulent thermal-fluid interaction; but rather, is computed automatically by COMSOL as an integral part of the solution process. The LRN essentially includes the viscous sublayer, i.e., $u^+ = y^+$, in the model as well as the logarithmic layer shown in Fig. 2.1. Thus the LRN model potentially represents a more physically accurate simulation of the turbulent thermal-hydraulic phenomena. In particular, the COMSOL documentation states that where accurate representation of the wall temperature is important, the LRN model should be used. The tradeoff in using the LRN model is that the mesh density requirements are increased adjacent to the wall; hence, the computer resource requirements and run-time requirements are likewise increased.

The clad surface temperature profile, at involute arc-length position 6,[7] found using the LRN is overlaid with the COMSOL 3.5a results and the SSHTC results, at the same location, in Fig. 2.3. The COMSOL models use isotropic plate material thermal conductivities.
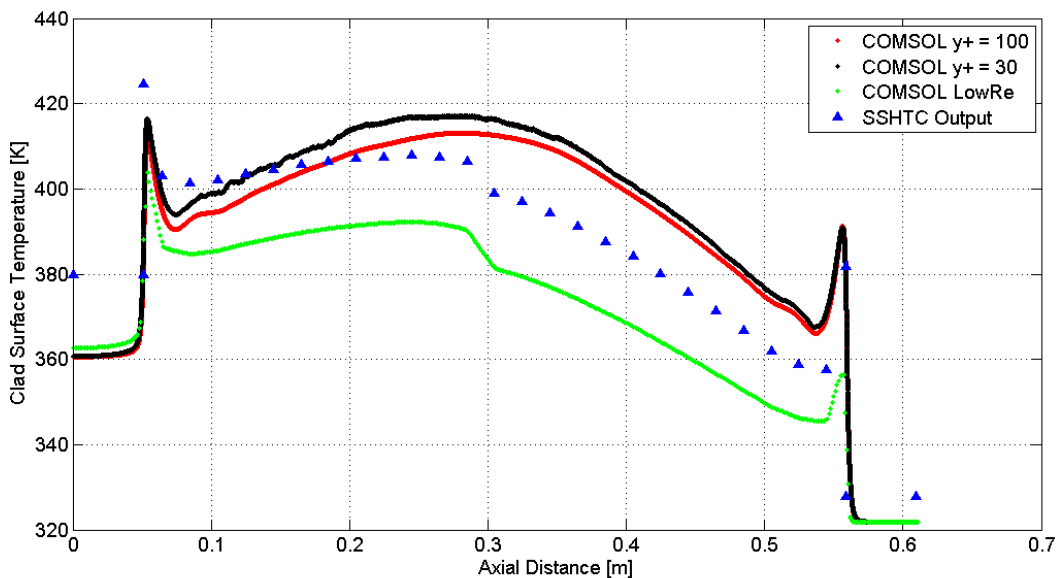
Fig. 2.3. Comparison of clad surface temperatures.
Flow is from right to left.

This LRN model consists of 107,152 finite elements and the solution presented in Fig. 2.3 is mesh convergent. The error in global energy conservation for the LRN model is 0.01748 % and the error in global mass conservation is essentially machine accurate (zero). The details of the model itself are discussed later.

From Fig. 2.3, it is observed that the LRN temperature distribution has the same basic shape as the SSHTC profile with a decrease in magnitude. This is expected as the SSHTC produces conservatively high clad surface temperatures due to uncertainties in the power density and unidirectional thermal conductivities in the plate, i.e., thermal energy is only conducted in a direction normal to the 24 inch portion of the clad.

A quantity that gives a measure of the quality of the LRN is L_c^*. This quantity is a measure of the distance from the wall, in viscous units, to the center of the wall-adjacent cell.[4] Thus, this quantity is grid-dependent and must be less than one to ensure a valid LRN solution[3] (i.e., if $L_c^* > 1$ then the mesh along the wall needs to be refined and the solution is suspect, but not necessarily inaccurate). Figure 2.4 shows the clad surface value of L_c^* for the LRN model used to produce the temperature profile in Fig. 2.3.
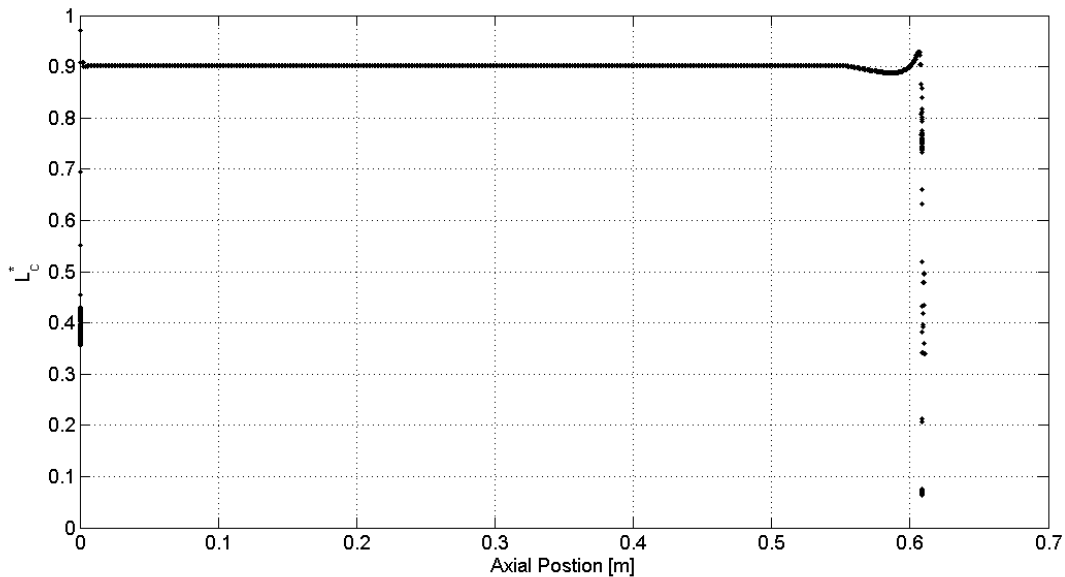
Fig. 2.4. L_c^* as a function of axial position of the fuel plate for the LRN model.

2.3   FUEL-CLAD NON-BOND MODELING

In order to characterize and model the non-bond physics associated with the fuel-clad interface, we first review and validate our methods based on the existing HEU fuel analysis. It is expected that similar, or slightly altered, methods might be developed for the LEU fuel as it matures in fabrication capability. Therefore, the entire discussion here is associated with the present HEU fuel for HFIR. The non-bond is an important phenomenon to investigate as its presence creates local increases in fuel plate temperatures and heat fluxes, due to a locally significant increase in thermal resistance caused by "blistering". The term non-bond or blister is used to describe a region in the fuel, usually at an interface, where a void exists. Non-bonds can exist at the fuel-clad interface, the filler-clad interface, and/or at the fuel-filler interface.[8] The CY 2010 model does not incorporate the filler material between the fuel and clad, thus the non-bond models presented here are those of fuel-clad blisters. It was, however, stated in ref. 8 that the study conducted by Hilvety and Chapman had a non-bond at the fuel-filler interface. It was conjectured by Kirkpatrick that this location was chosen to produce the "largest peaking factors."[8]

Calendar year 2011 non-bond modeling with COMSOL will indeed incorporate the blister at the fuel-filler and filler-clad interfaces.

The reduced mesh model, a.k.a. CY 2010 best estimate, employs a mapped meshing (MM) scheme in the fueled portion of the HFIR fuel plate. As explained in the reduced mesh discussion of this report, the MM scheme could depend on matching edge discretizations in each domain. Thus to create a non-bond region of the fuel, the subdomain and the mesh structure of the fueled region of the plate had to be modified since imprinting was not used in this study. The modification of the subdomain is shown in Fig. 2.5.
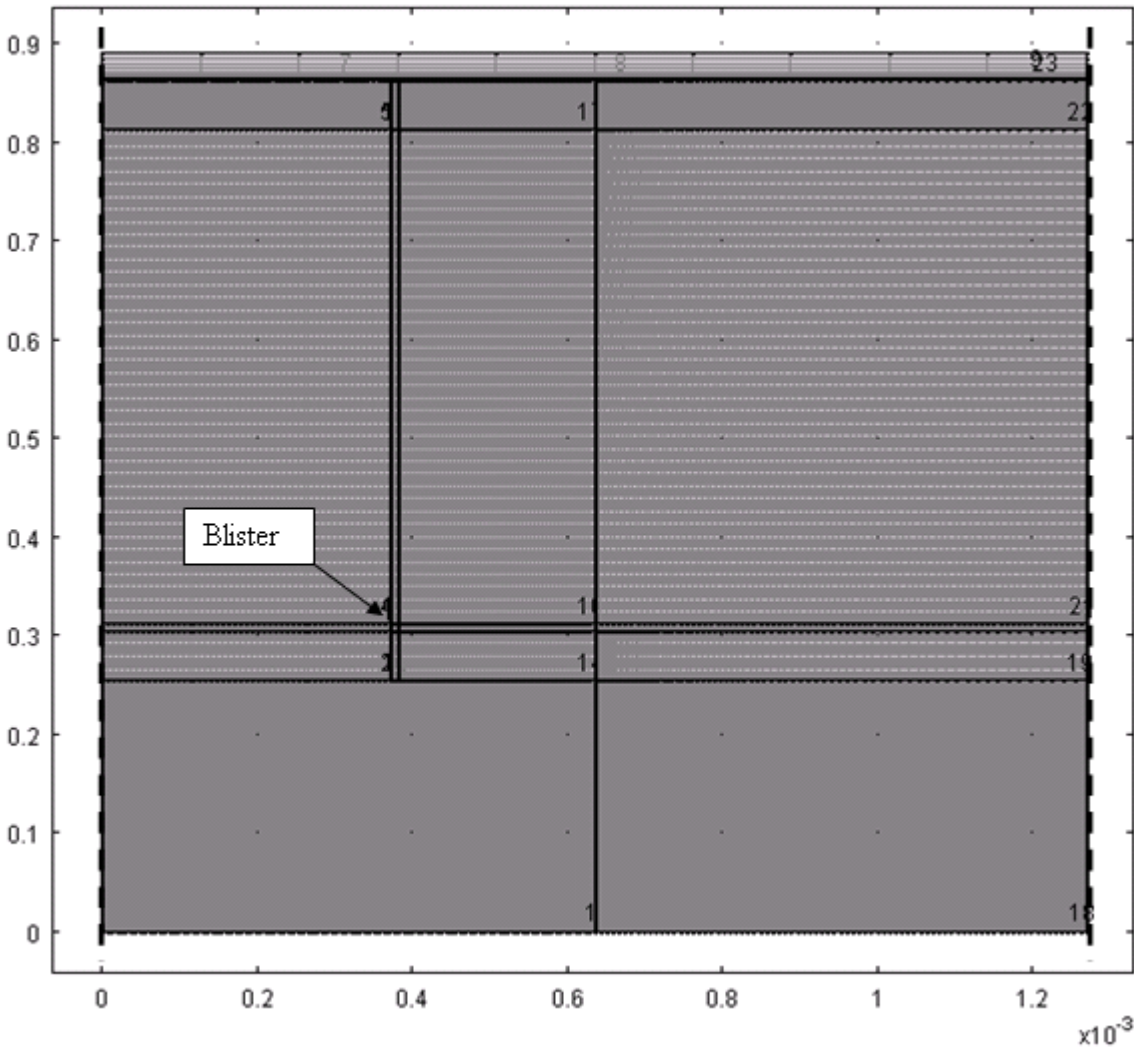
Fig. 2.5. Subdomain modification for the accommodation of a non-bond labeled as blister.
Symmetry boundaries are indicated with heavy dashed lines.

The narrow strip that spans the horizontal direction of the geometry is necessary to match edge discretizations. The vertical strip that intersects the horizontal strip serves the same purpose and the intersection of the two is the location of the blister. These locations represent the regions of the plate where the highest temperatures occur. The blister created in this model is 0.0625 square inches (40.3225 square millimeters).

A thermal conductivity value of zero was initially intended for the blister subdomain to maximize thermal resistivity, however this created a singular matrix in the simulation and thus could not produce a result. The blister was modeled with a relatively low thermal conductivity, 1×10^{-6} W/m/K. No thermal energy generation was modeled in the blister region. A more realistic case would be to model the blister with a thermal conductivity of some typical gas found in blister regions and thermal energy generation in those regions as well. Also, since the model employs the symmetry condition at the left global boundary, another blister is implied for the half of the plate that is not modeled. Therefore, the bulk of the thermal energy in the vicinity of the blister must be conducted axially.

Questions that arise in setting up such a model (i.e., nonzero thermal conductivity and nonzero internal heat generation) are as follows: what material would reside in the blister, are surface to surface thermal radiation effects to be incorporated into the model, is the blister material a participating medium in the thermal radiation environment, will natural convection occur in the blister material, etc. In this quasi-vacuum void model, no surface to surface thermal radiation effects are simulated. Natural convection is also neglected in the quasi-vacuum model.

The results of the simulation are shown in Fig. 2.6.
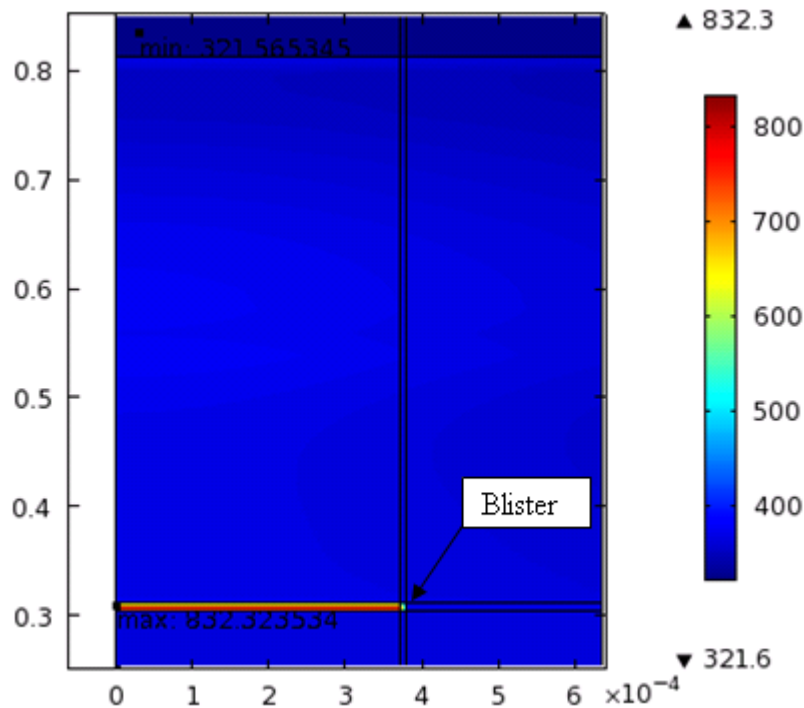
Fig. 2.6. Temperature result, in Kelvin, of quasi-vacuum nonbond model.
Only the plate is shown.

The global symmetry condition at the left boundary of the model (refer to Fig. 2.5) implies that a blister exists on the other side of the plate as well. This further exaggerates the temperature distribution in the blister region. No observed changes in the flow field occurred as a result of the blister, therefore the fluid domain is not shown in Fig. 2.6. Figure 2.6 shows that the highest temperatures do indeed occur at the site of the blister, with a maximum value of 832.3 K. However, the axial diffusion of thermal energy is very slight from this high temperature region.

A close up of the temperature distribution in the blister is shown in Fig. 2.7.
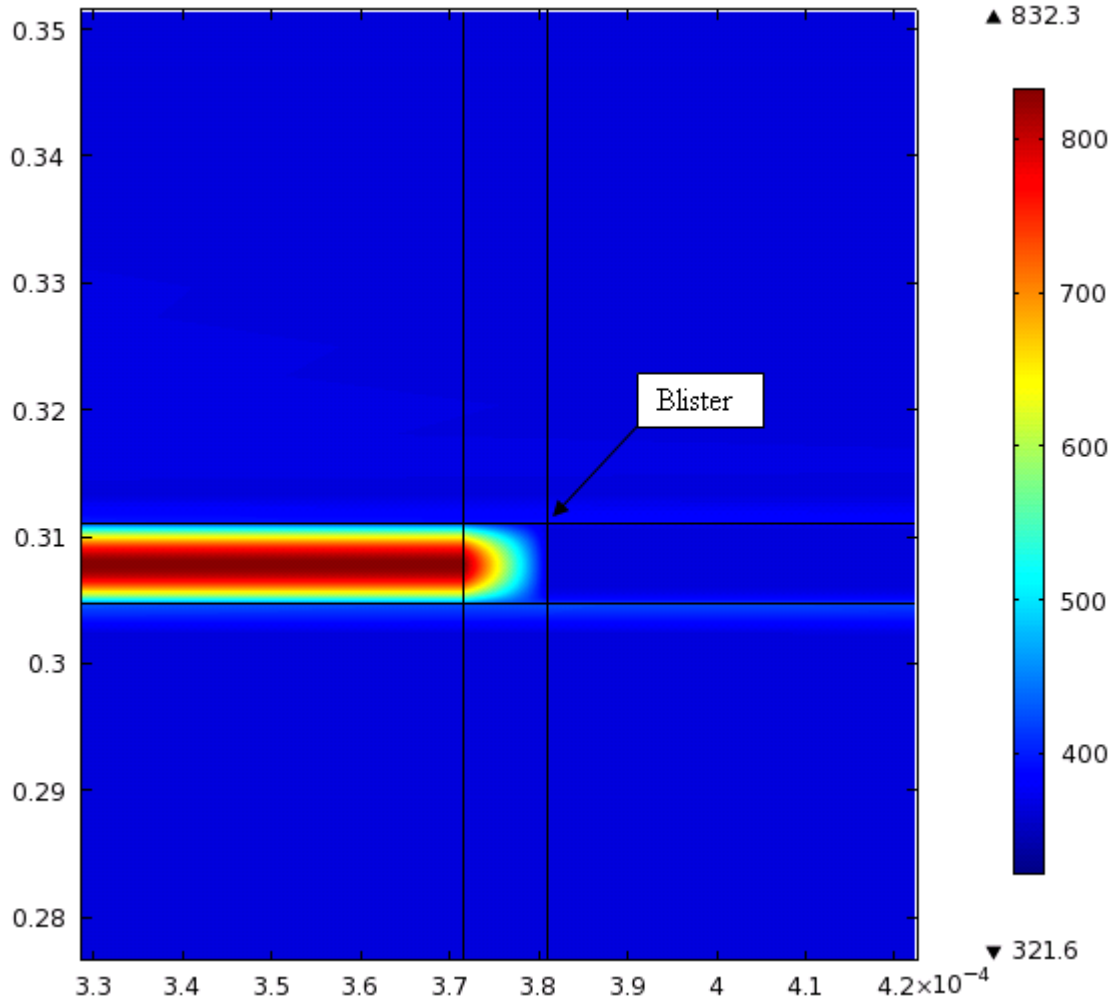
Fig. 2.7. Close-up of blister region.

Figure 2.7 shows the thermal energy passing around the bottom of the blister region through the clad.

From this study it has been determined that a different geometry must be used to accurately model an anomaly in the fuel such as a blister or a segregation region. The above simulation incorporates too much symmetry. Based on the lessons learned from this simulation, a good candidate geometry for 2-D hotspot modeling consists of two flow channels with a full fuel plate between them. This would allow the thermal energy to pass through the opposing side of the blister into the fluid as Kirkpatrick has stated. Further investigations into nonbond modeling are currently underway in CY 2011.

2.4   MINIMIZING THE AXIAL SPACING OF THE FINITE ELEMENTS

The CY 2009 best estimate 2-D turbulent thermal-hydraulic model consisted of 309,006 free mesh (FM) elements which yielded 2,824,416 degrees of freedom (DOF).[6] This mesh is quite dense in 2-D. A similarly-designed mesh in 3-D would be so large (yield so many nodes or degrees of freedom) that it will be impractical to utilize for a solution, even with the computer betty.ornl.gov; a 128 core, 768 GB RAM cluster, especially designed for utilization by HFIR COMSOL analysts. While this mesh did produce favorable results, it was necessary to investigate meshing schemes to reduce the element density.

COMSOL offers three different types of meshing schemes: 1) FM, 2) boundary layer mesh (BLM), and 3) mapped mesh (MM). FM, being an unstructured mesh and based purely on the geometry, has the most versatility of all meshing schemes. FM consists of either triangular or quadrilateral elements in 2-D and tetrahedral or rectangular prismatic (brick) elements in 3-D. The triangular FM meshing scheme can easily be adapted to any type of 2-D geometry. This meshing scheme results in excessively high DOF for accurate models of high aspect ratio geometries such as the HFIR fuel plate and flow channel as demonstrated in the CY 2009 model previously mentioned. The FM is restrictive in that high element densities in one direction yield high element densities in the other directions due to the triangular structure of the element. Since the FM is based purely on the geometry, the goal being high element quality as defined by the geometry only, the high aspect ratio of the HFIR fuel plate will, in turn, naturally create very fine mesh structures. New in version 4.1 of COMSOL is a "physics generated" FM capability which allows for variation in the mesh design due to the physics being solved. This new capability was not investigated here, but is not expected to alter the primary dependence on the problem geometry.

The BLM uses quadrilateral elements in a layer type pattern along geometric boundaries chosen by the user. The user specifies the distribution and number of BLM layers to be used. Outside of these layers the domain is filled with a FM. This scheme benefits the user by allowing high element densities at a geometric boundary in the direction normal to the boundary, but the mesh is not restricted to high element densities in other directions like the FM.

The MM is a highly structured type mesh. It works well for regular quadrilateral geometries, but does not mesh complex geometries well, e.g. element overlap between adjacent domains is not uncommon. The user has control over distribution and element number as in the previous mesh types, however this meshing scheme can be restrictive in that, without using the more complex option of "parts and assembly" (similar to CAD packages), edge discretizations may require a match in each domain (i.e., opposing boundaries could require similar discretizations).

All meshing schemes were used in the final result of this reduced mesh study. In order to properly implement the MM, the model geometry was broken up into regular quadrilateral domains as shown in Fig. 2.8 (i.e., regions 1, 3, 4, 5, and 6). Since region 2, in Fig. 2.8, contains the curved leading edge of the HFIR fuel plate, it could not be made into a regular quadrilateral domain. As a result this region was meshed using BLM along the curved leading edge and FM in the remaining flow domain and solid domain of the fuel plate. The MM scheme was used in regions 1, 3, 4, 5, and 6. There exists a relatively small "buffer region" between regions 2 and 3 which is meshed with FM. This buffer region was necessary because the BLM and MM cannot share a common boundary.
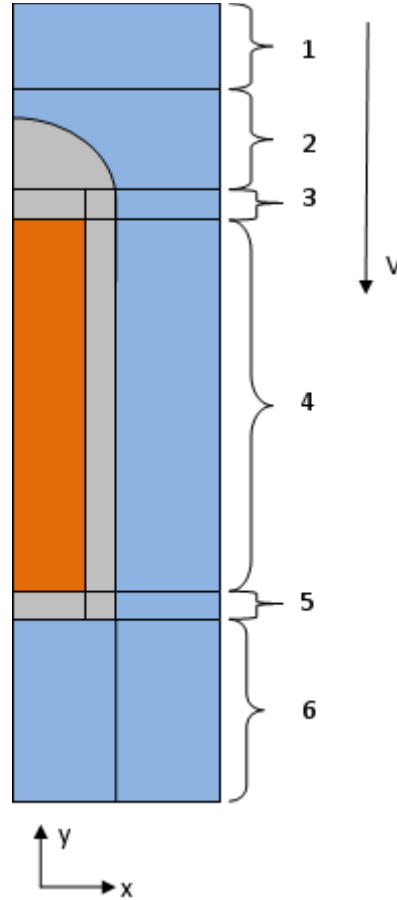
Fig. 2.8. 2-D HFIR fuel plate and flow channel model geometry.
The numbers are used to reference regions of different meshing schemes.
This drawing is not to scale, it is for visualization only. The orange section represents the $U_3O_8 - Al\ 1100$ cermet, or U-Mo for the LEU counterpart. The gray region represents the Al 6061 clad. The blue region represents the flow channel. Flow is from top down.

2.4.1   Simulation Physics

Before the meshing strategy is discussed, a few words regarding the physics of the model are in order. As previously stated, the model is 2-D with turbulent diffusive-convective heat transfer from a thermal energy source and temperature and pressure dependent material properties. The governing equations for the turbulent fluid can be written in invariant form as

$$\nabla \cdot \left(\rho \boldsymbol{u} \right) = 0 \tag{2.6}$$

$$\rho \left(\boldsymbol{u} \cdot \nabla \right) \boldsymbol{u} = \nabla \cdot \left[-p\underline{I} + \left(\eta + \eta_T \right) \left(\nabla \boldsymbol{u} + \left(\nabla \boldsymbol{u} \right)^T - \frac{2}{3} \left(\nabla \cdot \boldsymbol{u} \right) \underline{I} \right) - \frac{2}{3} \rho \kappa \underline{I} \right] + F \tag{2.7}$$

$$\nabla \cdot \left(-\left(\underline{k} + \underline{k_T} \right) \nabla T_f \right) = -\rho C_p \boldsymbol{u} \cdot \nabla T_f \tag{2.8}$$

13

where u is the velocity vector, ρ is the fluid density, p is the fluid pressure, η is the fluid dynamic viscosity, η_T is the apparent dynamic viscosity due to turbulence, $\underline{I}$ is the identity tensor, and κ is the turbulent kinetic energy in Equations 2.7 and 2.8. The thermal terms in Equations 2.6, 2.7, and 2.8 are as follows: $\underline{k}$ is the thermal conductivity tensor of the fluid, $\underline{k_T}$ is the apparent thermal conductivity tensor due to turbulence, T_f is the fluid temperature, and C_p is the specific heat of the fluid at constant pressure. The κ-ε closure model requires two more equations, one for the turbulent kinetic energy, κ, and the other for the dissipation of turbulent kinetic energy, ε. These equations can be found in references 3 and 6.

The governing equation for heat transfer in a solid, i.e. the clad and fuel, is formally represented as

$$\nabla \cdot \left(-\underline{k} \nabla T_s \right) = q'''$$ (2.9)

The difference in this general equation between the two solid domains is the value of the thermal energy source term, q'''. In the heat transfer equation for the clad $q''' = 0$, while the heat transfer equation for the fuel has $q''' = f(y)$. The COMSOL 3D model will include heat generation in both the clad and coolant due to gamma heating, but in this 2D development study only the predominant heat generation due to nuclear fission in the fuel is included. In equation 2.9, $\underline{k}$ is the thermal conductivity tensor of the clad or fuel, T_s is the temperature of the respective solid.

The default thermal boundary condition at the interface between the solid domains is continuity, i.e. the fuel-clad interface has a common temperature and heat-flux distribution. This condition assumes perfect thermal contact at the fuel-clad interface. While this condition is an idealization, it is appropriate in that the natural convection and surface to surface radiation of any gaps at this interface are not necessary to solve since the results obtained with a continuous boundary are reasonably accurate in a global sense.

The remaining boundary conditions deal with the global inlet where fluid enters the system, the global outlet where fluid exits the system, the left and right global boundaries and the solid-fluid interface. Thermal conditions for these boundaries are given in Table 2.1.

Table 2.1. Thermal boundary conditions for the CY 2010 reduced mesh model.

Boundary	Condition
Global Inlet	Temperature (T_f) = 321.9 K
Global Outlet	Convective Outlet
Global Left Side	Symmetry
Global Right Side	Symmetry
Solid-Fluid Interface	Continuity

The convective outlet condition set at the global outlet is described in the COMSOL documentation by the equation

$$-n \cdot \left(-\underline{k} \nabla T_f \right) = 0$$ (2.10)

This equation states that the conduction of heat in the fluid in the direction normal to the global outlet is zero. The symmetry condition set at the left and right global boundaries is described in the COMSOL documentation by the equation

$$-\boldsymbol{n} \cdot \left(-(\underline{\boldsymbol{k}} + \underline{k_T})\nabla T_f\right) = 0 \tag{2.11}$$

which also states that the conduction of heat is zero at these boundaries.

The fluid conditions at the boundaries given in Table 2.1 are given in Table 2.2.

Table 2.2. Fluid flow boundary conditions for the CY 2010
reduced mesh model

Boundary	Condition
Global Inlet	Velocity (v_0) = (15.89/2) m/s
Global Outlet	Pressure (p) = 0 Pa
Global Left Side	Symmetry
Global Fluid Right Side	Symmetry
Solid-Fluid Interface	No Slip

The initial guesses for the turbulent kinetic energy (*nitf.kinit*) and the turbulent dissipation rate (*nitf.epinit*) were set to default COMSOL values. The default turbulence intensity value of 0.05 is justified in the COMSOL documentation which states that "Fully turbulent flows usually have intensities between five and ten percent."[3] The turbulence length scale at the global inlet boundary was set to the value 8.89×10^{-5} m. The COMSOL documentation recommends, for fully developed flows, a turbulent length scale of 7% of the channel width.[4] Both the default turbulence length scale, 0.01 m, and the 8.89×10^{-5} m value were used to observe the effect of this parameter on the simulation results. These findings will be discussed later in this document. The Low Reynolds number (LRN) formulation for the simulation of turbulent flow was chosen to model the fluid domain due to reasons mentioned in the LRN section of this paper.

2.4.2   Meshing Strategy

All coordinates discussed in this section have the same orientation as that depicted in Fig. 2.8 unless otherwise specified. The mesh images shown below are taken from the CY 2010 best estimate model which uses 107,152 total elements. This is a 65 % decrease in the number of finite elements from the CY 2009 best estimate model.

Region 1 of Fig. 2.8 uses a MM with 10 evenly distributed elements in the x-direction and 8 elements in the y-direction with an element ratio of 35. The element ratio describes "the ratio in size between the last element and the first."[4] Therefore, as the element ratio increases, the element size decreases from one boundary to the other; e.g., in this instance the last element will be 1/35 the size of the first element. This feature is used in region 1 in anticipation of upstream deviations in the flow field due to the presence of the fuel plate. The mesh structure of region 1 is shown in Fig. 2.9.
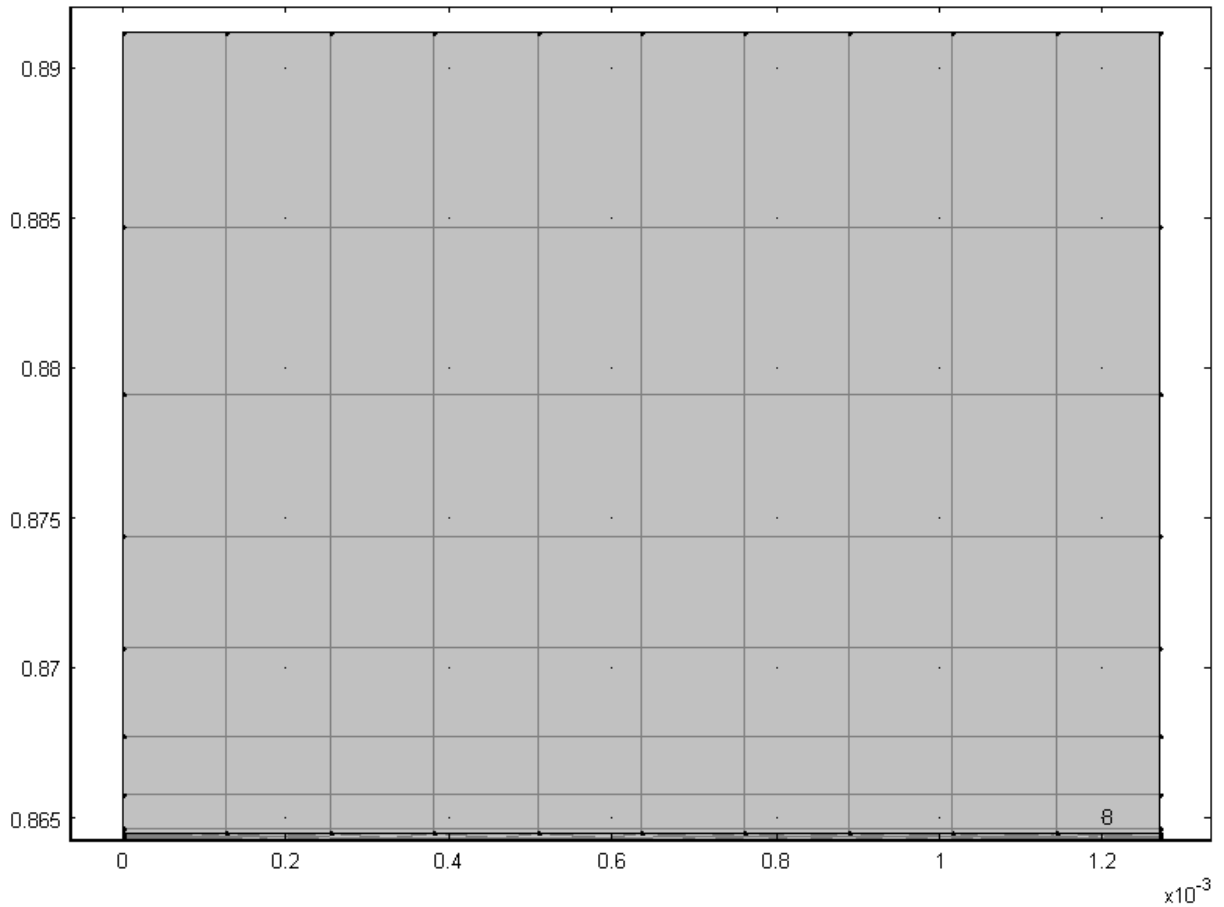
Fig. 2.9. Mesh structure of region 1.
Under the boundary Number 8, in the bottom right of the image there exists another row of elements.

Region 2 is discretized with BLM and FM as shown in Fig. 2.10. The lower portion of region 1 is shown at the top of Fig. 2.10 while the buffer region is shown below region 2.

The BLM resides along the curved leading edge, while both the remaining fluid domain and the clad in this region are discretized with FM. There are 30 BLM layers normal to the clad surface in the fluid domain. The stretching factor was set to a value of 1.1. This value of the stretching factor increases the thickness of the layers by 10% with respect to the preceding layer in the outward normal direction. The thickness of the first layer was set to the default automatic value, which is 1/20 of the local domain element height as stated in the COMSOL documentation.[4]
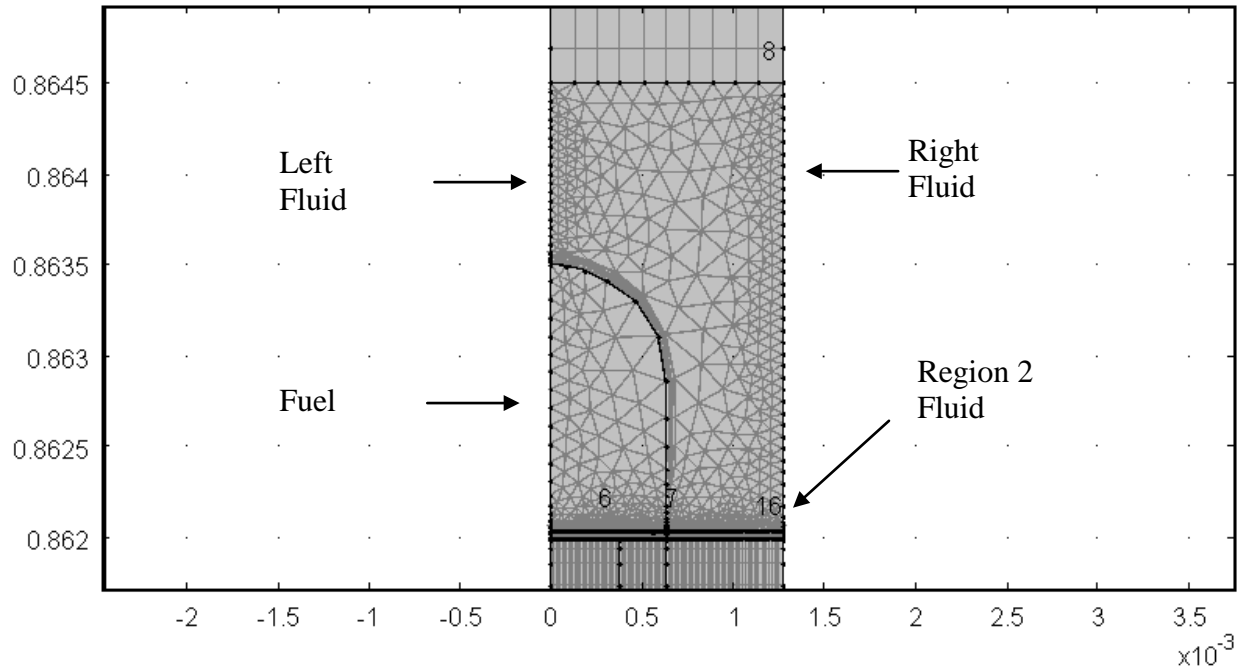
Fig. 2.10. Mesh structure of region 2.
The lower portion of region 1 and the buffer region are shown here.

Before the BLM was created, the FM was placed as a foundation for the BLM. Again, the element density increases in the downstream direction. All boundaries in region 2 have a specific discretization. FM was set up along the surface of the curved leading edge of the fuel plate with 100 boundary elements along the clad-coolant interface. This procedure is used to control the number of BLM elements along a boundary in the arclength direction. The FM distribution along the clad-coolant interface is a result of the user defined FM distribution along the fluid exit boundary of region 2.

The FM element distribution along the fluid exit boundary of region 2 fluid exit is 80 elements with an element ratio of 15 with the elements decreasing in size as one approaches the fuel plate. This distribution was necessary due to the MM that exists downstream of this region. More specifically the edge discretization restriction of the MM dictates this distribution. The region1-region2 interface, of course, has 10 elements. The right fluid boundary has an evenly distributed 40 element discretization, while the left fluid boundary of region 2 has 20 elements. The higher element density on the left fluid boundary was created to provide better resolution for the upstream flow disturbances that would be present due to the fuel plate.

The FM element structure on the interior of the plate's leading edge does not need to be as refined as the fluid FM element structure due to the relatively simple physics to be modeled in that region, i.e. conduction heat transfer. Due to the shared leading edge boundary, the element structure along this boundary is the same as that mentioned previously. The symmetry boundary of the plate in region 2 has 20 elements. The interface region between region 2 and the buffer region, however, has a more specific structure due to the downstream MM restrictions. This boundary has 100 evenly distributed elements.

The buffer region contains only FM, as shown in Fig. 2.11. This region was necessary because MM and BLM cannot share a common boundary. The element distribution in the x direction is dictated by the region 2 and region 3 boundaries. The element distribution in the y direction is governed by the solid-fluid interfacial boundary in the buffer region. This boundary has 40 evenly distributed elements.
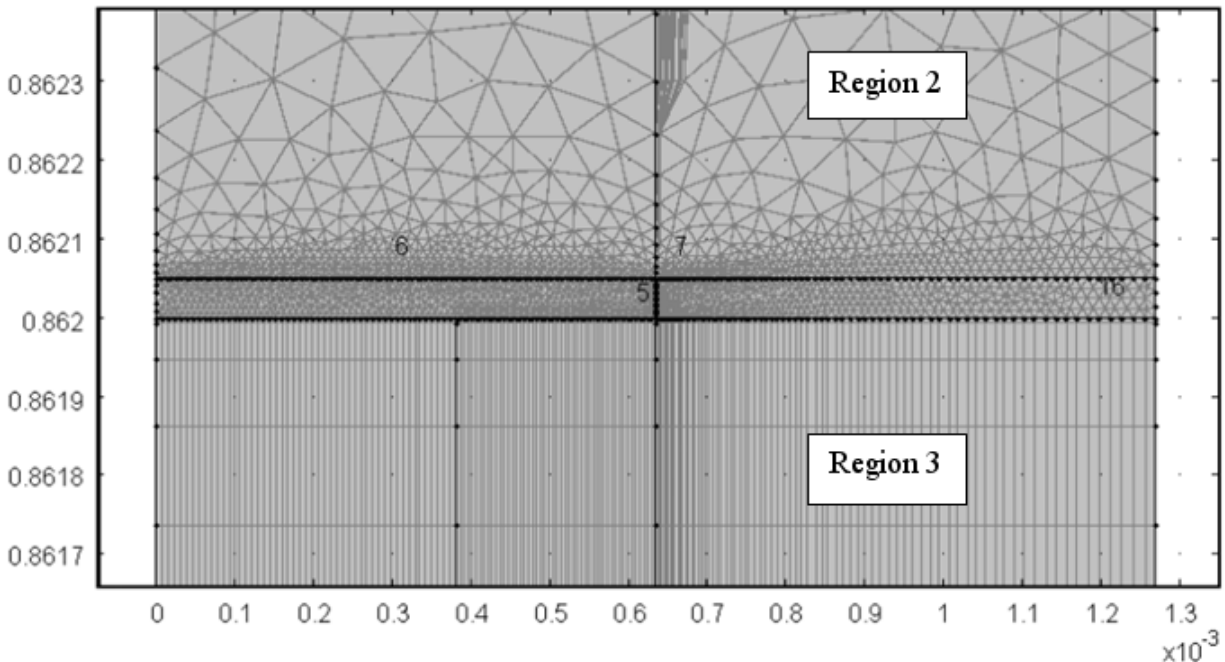
Fig. 2.11. The buffer region is the thin densely meshed region shown.
Region 2 and region 3 are depicted above and below the buffer region respectively.

Region 3 uses a MM with high element density at the entrance of the region from the buffer region which decreases into a significantly lower element density at the exit passing into region 4. Region 3 represents 97 % or 1.94 inches (4.93×10⁻² m) of the upstream 2 inch (5.08×10⁻² m) unfueled clad section of the fuel plate and coolant channel. The region 3 mesh is shown in Fig. 2.12.

The solid portion of region 3 (i.e., the two leftmost domains) has 50 evenly distributed elements in the x direction per domain. The distribution in the y direction is 50 elements with an element ratio of 355 with element size decreasing in the upstream direction. The distribution in the y direction was chosen to create a smooth transition in the mesh structure from the high element density regions to the reduced element density region of the fueled portion of the fuel plate. Due to the MM restriction of matching edge discretizations, the fluid domain in this region shares the same distribution in the y direction.

Due to developing velocity boundary layers and thermal boundary layers in region 4 (see Fig. 2.8) , the mesh in the fluid domain of region 3 is dense at the clad-coolant interface and becomes less dense at the right global boundary of the model. The element distribution in the x direction in the fluid domain has 80 elements with an element ratio of 15 with size decreasing toward the clad-coolant interface.
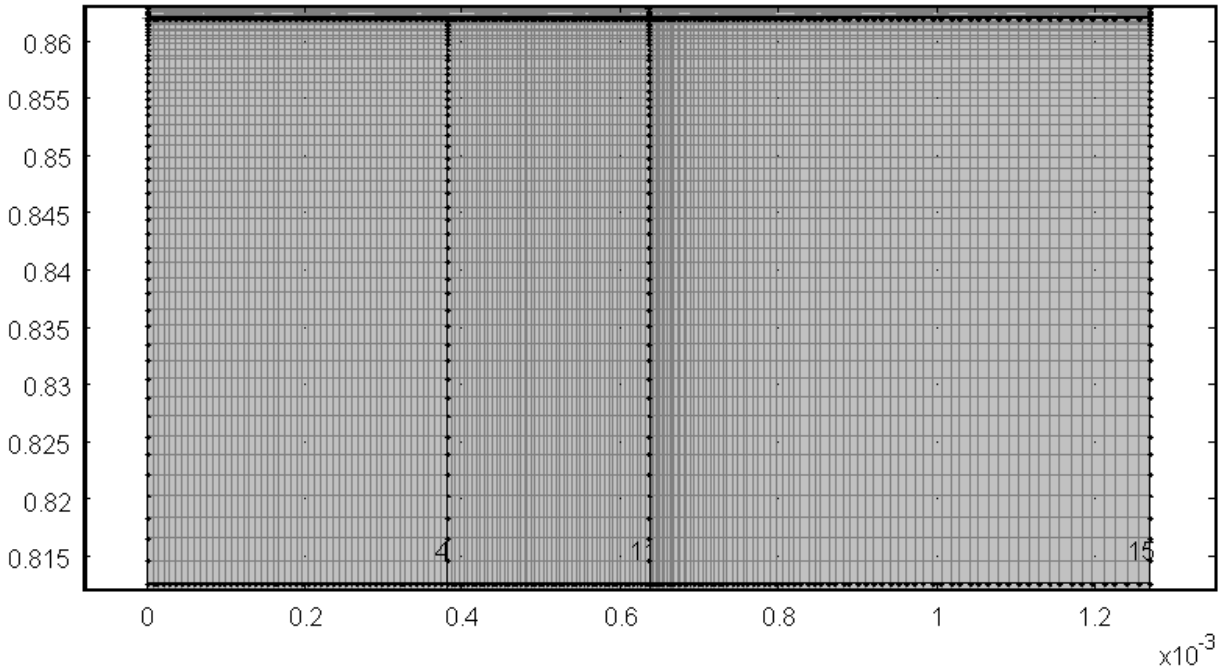
Fig. 2.12. Region 3 mesh.
The two leftmost domains are the solid clad, while the domain on the right is the coolant channel.

The length of the fueled section of the plate is 20 inches (5.08×10^{-1} m). The fueled section is represented by region 4 (see Fig. 2.8) in Fig. 2.13. While slight amounts of heat are deposited in the coolant upstream of this region, most of the heat transfer from the nuclear fuel to the coolant occurs in region 4. Thus it is very important to model this region as accurately as possible.

Since the dominant portion of the flow field is in the axial or negative y direction (shown vertically), as depicted in Fig. 2.8, the element density of the flow domain in the axial direction could potentially be significantly reduced in this region relative to CY 2009 model element densities in this same region. However, there exists a lower limit on the element density which is dictated by the power density profile. The power density profile in the fuel is described, in the SSHTC, by 27 evenly distributed axial points. The minimum axial element density to obtain proper power density resolution is 1.35 elements per inch or 27 evenly distributed axial elements in region 4. Region 5 has a similar element density. In region 5, the element density is rounded up to the nearest integer density value.

The element densities in region 4 and 5 were iterated by integer multiples of the base density to achieve a grid independent solution. The details of this element density parametric sweep will be discussed later.

The mesh structure of region 4 and region 5 (defined by Fig. 2.8) is shown in Fig. 2.13.
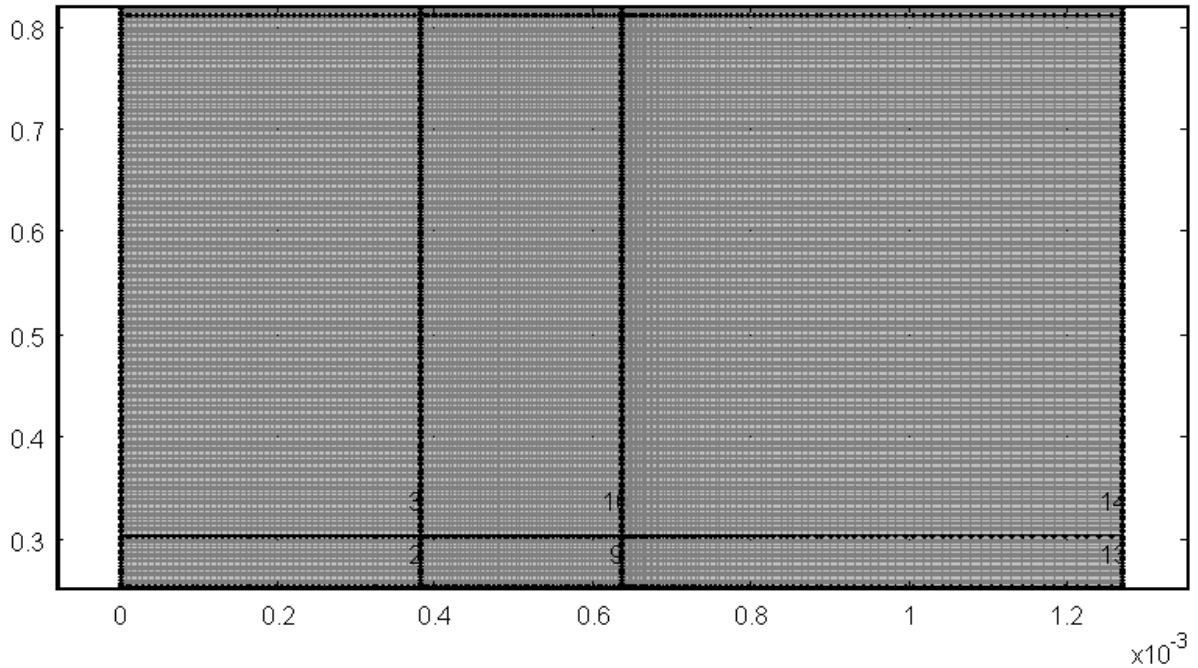
Fig. 2.13. Mesh structure of region 4 and 5. Region 4 is between 0.3 m and 0.8 m.
Region 5 is below region 4.

Region 6 again employs the MM. The element density at the trailing edge of the fuel plate is very high due to the need to resolve the strong vortex that resides there. This vortex contributes to the relatively high temperatures that are observed at the trailing edge of the fuel plate through the recirculation of the warm fluid.

The distribution in the x direction is dictated by the shared boundary between region 5 and region 6 and thus has the same distribution as region 4 in that direction. The axial distribution is set to 270 elements with an element ratio of 2000. This configuration was chosen to bring the L_c^* value below 1, as stated and shown in the discussion regarding the LRN formulation for turbulent flow. As the flow redistributes itself after expansion past the fuel plate, it settles and the effects of the plate on the momentum of the fluid are no longer observed. Thus the element density decreases downstream from the plate. The relatively long exit region downstream of the plate was created to satisfy the uniform pressure distribution boundary condition along the global exit of the system. The mesh structure of region 6 is shown in Fig. 2.14.
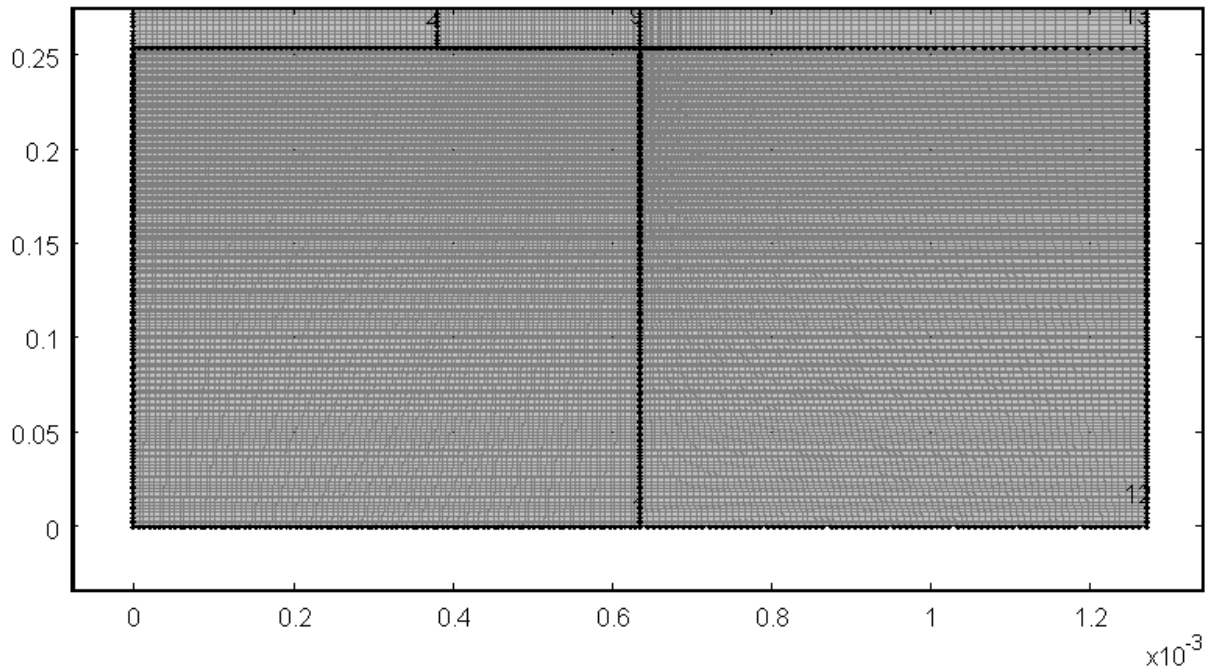
Fig. 2.14. Mesh structure of region 6.
Region 5 is shown at the top.

2.4.3   Model Analysis

The simulation physics has been described previously. All model analysis was conducted with COMSOL v. 4.0a. This section reports the results of the simulation and the analysis of error with respect to conserved quantities, i.e. energy and mass.

Two sets of models were executed. Both use the element density of region 4 and 5 (refer to Fig. 2.8) as a parameter. The axial element number in region 4 was increased by integer multiples of 27. As stated previously, 27 was the minimum element number needed to properly resolve the power density profile. The axial element number in region 5 was increased by determining the element density, i.e. elements per unit axial length, in region 4, multiplying this element density by 2 inches, i.e. the axial extent of region 5, then round to the nearest integer value. All other mesh characteristics remain unchanged.

The error in energy conservation is calculated by

$$\epsilon_{energy} = \left[\frac{(Energy_{out} - Energy_{in}) - Energy_{gen}}{Energy_{gen}} \right] 100 \tag{2.12}$$

where $Energy_{out}$ is the energy advected out of the global exit of the system, $Energy_{in}$ is the energy advected into the system at the global inlet, and $Energy_{gen}$ is the energy that is generated in the fuel region due to the fission process.

The advected energies per unit depth are calculated by the integral

$$Energy_{adv} = \int_0^L \rho C_p uT \, dx \tag{2.13}$$

The limits on the integral represent the spatial extent of the simulation geometry at the global inlet or global outlet of the system, 0.05 inches (1.27×10^{-3} m). The total energy generated per unit depth in the fuel is found by

$$Energy_{gen} = \iint_0^A f(y) \, dA \tag{2.14}$$

where *A* is the cross-sectional area of the fuel meat.

The relative error in the conservation of energy as a function of element number is shown in Fig. 2.15. The turbulent length scale, L_T, is used as a parameter. Both models are mesh converged at 107,152 elements; however, for $L_T = 0.01$ m, the simulation is mesh converged at 85,552 elements with respect to energy conservation. This, however, does not represent an accurate simulation as no eddies are resolved in the flow. It is interesting that an order of magnitude difference in the energy conservation error occurs as smaller eddies are resolved in the flow field.

The effect of L_T on the energy was investigated. The inlet energy is affected, since L_T is set at the inlet, and was decreased by 0.0442 %. It is not understood why L_T had this effect on the inlet energy; investigation into this result is ongoing. Assuming that the COMSOL recommendation for L_T is correct, the simulation still conserves energy rather well with a relative error value of 0.38 %.

The error in the conservation of energy in the solid, i.e. the fuel and clad, was calculated to be 0.0175 %. Thus the difference in the energy per unit depth generated in the fuel and the energy per unit depth leaving the plate is in good agreement. Since the turbulent length scale applies only to the fluid, L_T had negligible effect on the quantity of energy diffused through the plate.
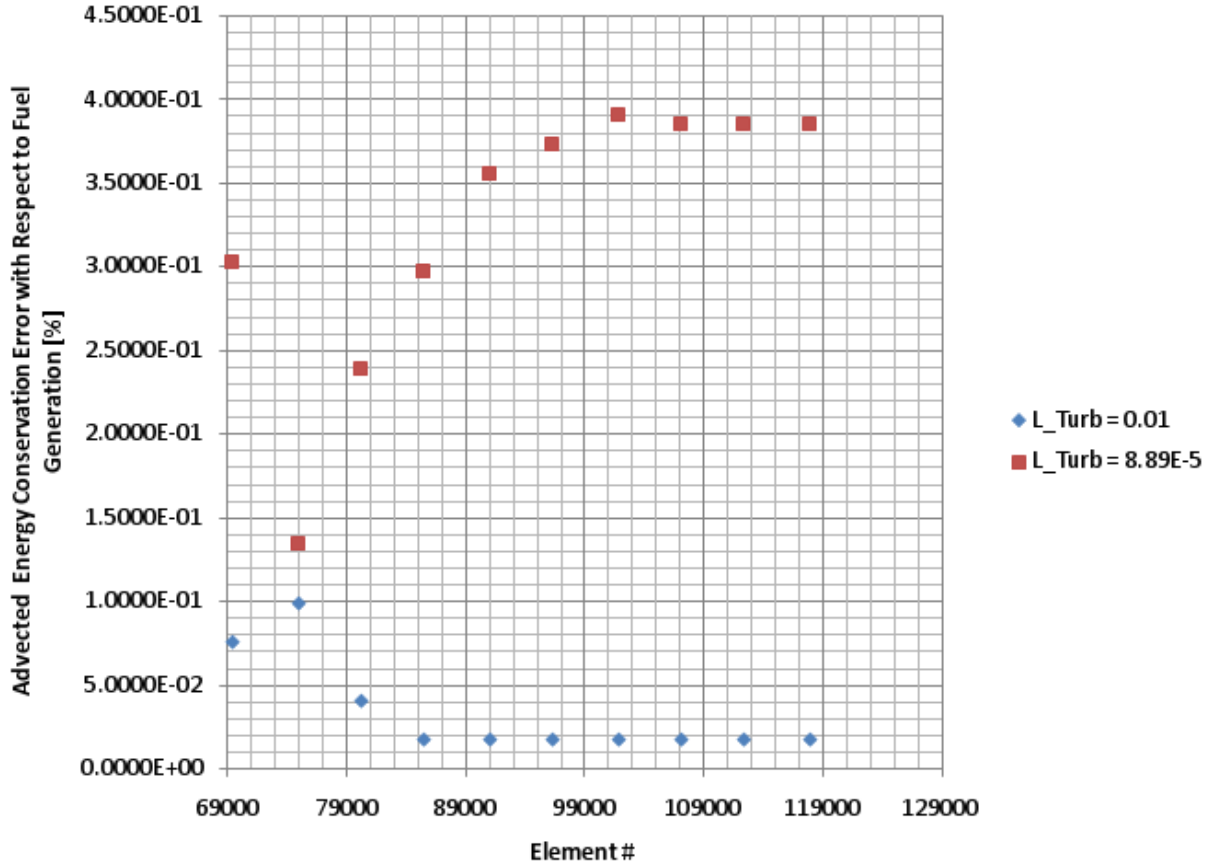
Fig. 2.15. Global energy conservation error as a function of element number with the turbulent mixing length as a parameter.

The relative error in mass conservation is calculated in a similar way to the energy error given in Equation 2.12. The relative error in mass conservation is formally represented by

$$\epsilon_{mass} = \left[\frac{mass_{out} - mass_{in}}{mass_{in}}\right] 100 \qquad (2.15)$$

where $mass$ is the mass flow rate into or out of the system and is given by

$$mass = \int_0^L \rho u \, dx \qquad (2.16)$$

The limits on the integration are the same as those for the advected energy. The mass was conserved to a very high degree in both sets of models; in fact no deviation in the mass was observed.

Although the energy error was affected by the change in the turbulent length scale, no other characteristics of the simulation seemed to change. The clad surface temperature was identical in both of the 107,152 element models as shown in Fig. 2.16.

23
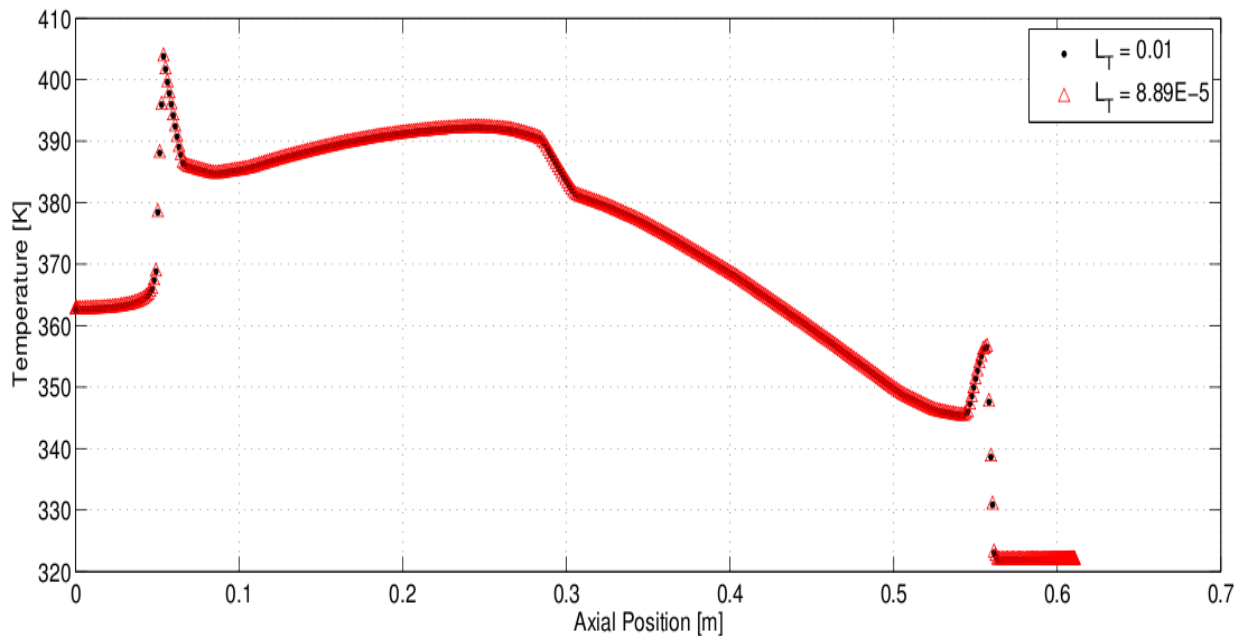
Fig. 2.16. Comparison of clad surface temperature with the turbulence length scale as a parameter.
The flow direction is from right to left.

Other quantities including the integrated exit energy, the clad surface energy, mass flow, and exit temperature were compared and no change was observed. Since the models show such similarity, one can make the claim that the effect of the turbulence length scale as it is defined in COMSOL does not carry much influence on this type of model.

It is conjectured here that L_T provides a method to specify inlet boundary conditions on the κ-ε model. As the flow becomes fully developed in the flow channel, adjacent to the plate the effect of the turbulent inlet conditions become negligible. Thus the models discussed henceforth will be those that employ $L_T = 0.01$. The clad surface temperature exhibited only slight deviations as the element density changed in the parametric study. Fig. 2.17 shows this qualitatively. While deviations do exist at the leading edge of the fuel plate the most notable changes occur at the trailing edge.
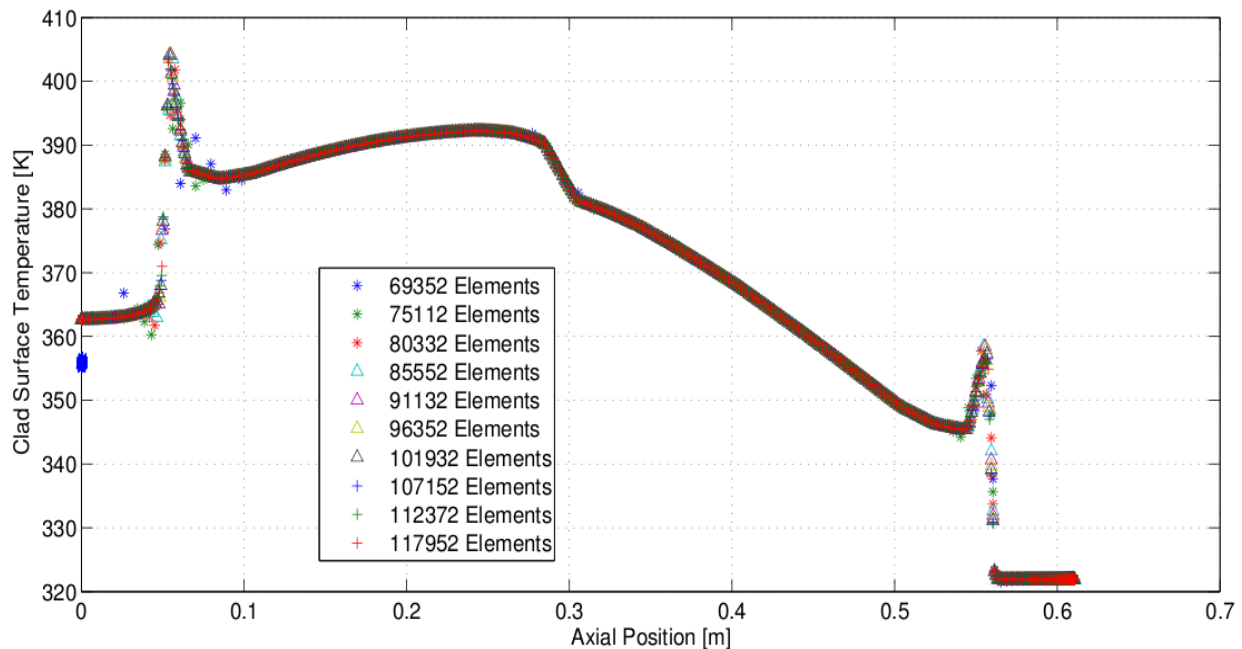
Fig. 2.17. Comparison of clad surface temperatures with varying element numbers.
Flow is from right to left.

The deviations at the trailing edge of the fuel plate are a direct consequence of the changing mesh in region 5 of Fig. 2.8. The local peak temperatures show minimal deviation with changes in element number and no observable deviations in the clad surface temperature are present in the fueled section of the fuel plate. Therefore, relatively accurate surface temperatures can be generated with a coarse mesh, however, it is important to recall that energy conservation errors may be significant for lower element density models.

The LRN model was compared with the SSHTC output for the clad surface temperature. Reference 6 outlines the procedure for determining the power density profile (PDP) from the SSHTC output of the clad heat flux. This same power density profile was used in the CY 2010 models, thus a direct comparison can be made regarding the effect of an isotropic thermal conductivity tensor relative to the unidirectional nature of the thermal conductivity used in the SSHTC, as well as other additional conservatisms incorporated through the "U factor" inputs of the SSHTC.

The clad surface temperature comparison is shown in Fig. 2.18. The red data represents temperatures from the LRN simulation. The black data represents temperatures from a modified PDP LRN simulation, the details of which are described at the end of this section. The difference in temperature is remarkable between the LRN simulation and the SSHTC. An approximate 20K difference exists in the downstream portion of the fuel plate.
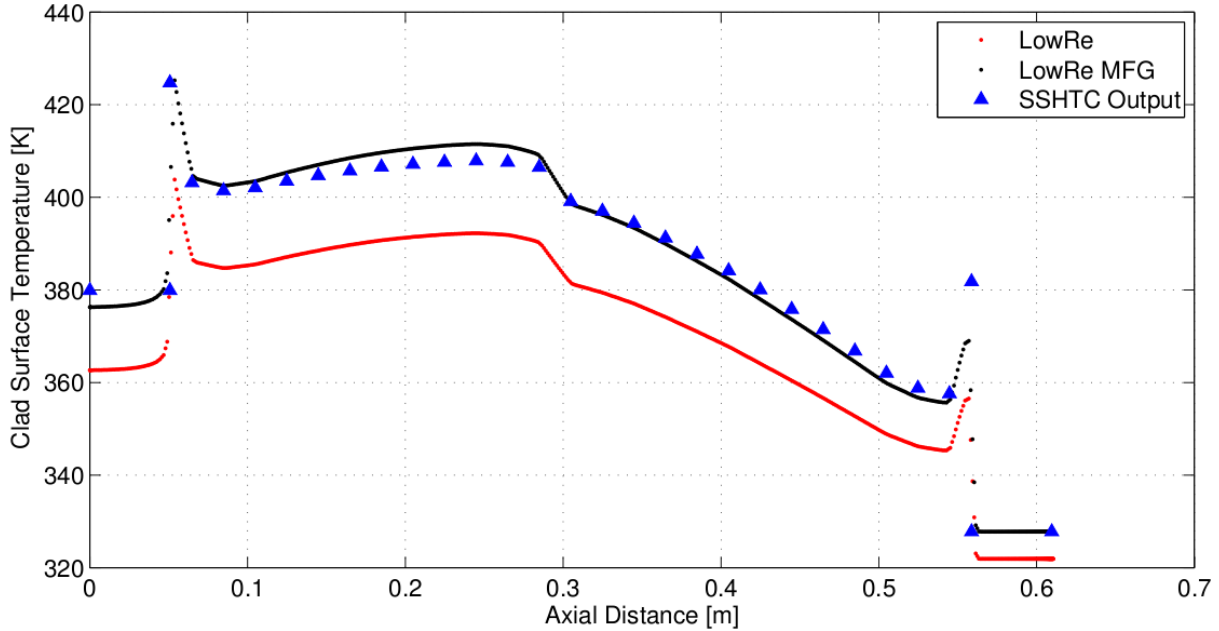
Fig. 2.18. SSHTC clad surface temperature compared with the LRN and the modified PDP LRN.
Flow is from right to left.

The difference decreases as one approaches the leading edge of the fuel plate, i.e. increasing axial distance in the figure. This difference is representative of "built in" conservatisms in the SSHTC to ensure safe operation of the HFIR. The artificially high temperatures associated with the SSHTC simulation are an artifact of the uncertainty in the power density of the fuel. The multiphysics-multidimensional capabilities of COMSOL allow the analyst to "relax" conservatisms to create a more physically accurate model.

The LowRe MFG data represents the clad surface temperature profile found from the LRN simulation with a modified PDP magnitude. The modification to the PDP magnitude was conducted to determine the necessary increase in power generation magnitude to produce temperatures similar to the SSHTC. This increase was calculated by taking the ratio of the outlet temperatures, i.e. COMSOL outlet temperature to SSHTC outlet temperature, and the result was subtracted from one. This calculation yielded a value of 19%. Thus a 19 % increase in the power magnitude is necessary to bring the clad temperatures to match up to that reported in the SSHTC.

2.4.4 Planned Investigation on Mesh Reduction

As stated earlier, version 4.0a of COMSOL was used in this part of the research. Since the majority of this work was done, version 4.1 was released which includes several improvements in mesh generation and other important areas related to this research. It is planned to verify the current results with version 4.1 (or the current released version whichever is later). The present edge matching requirements of the mapped mesh (MM) are not required in the "parts and assembly" form of the geometry generation within COMSOL. The "parts and assembly" form of geometry generation also allows for complete independence of mesh design across domains. Using these features of the present release of COMSOL, additional significant reduction in mesh density, hence, degrees of freedom and computer resources, are achievable. These issues are to be resolved prior to a final mesh design for the 3D analysis.

2.5   INVESTIGATION OF PERIODIC BOUNDARY CONDITIONS VERSUS EXTRUSION COUPLING BOUNDARY CONDITIONS

One of several tasks performed in the work documented by ref. 6 included a study to determine the adequacy of using periodic boundary conditions to simplify the modeling of hundreds of HFIR fuel plates arranged azimuthally around the cylinder that forms the HFIR core. This study was made using version 3.5a of COMSOL. In version 3.5a, the *extrusion coupling variables* boundary condition is recommended to be a more general method of coupling, which includes the periodic boundary condition as a subset. In particular, if there is a question about whether the flux at the surface specified by the periodic boundary condition is non-zero (specifically, non-adiabatic for the case of heat flux), then it is beneficial to use the *extrusion coupling variables* boundary condition. However, particularly in version 4 and later, it is considerably more difficult to properly implement the extrusion coupling variable boundary condition than the periodic boundary condition (which is easily implemented).

Starting with version 4 of COMSOL, the periodic boundary condition was apparently improved. Further, the implementation of the *extrusion coupling variables* boundary condition is not as straightforward, nor necessary, in order to achieve periodic boundary conditions that include periodicity of both the quantity conserved, and the companion flux (or derivative) at the periodic boundary. A new study was subsequently conducted and it has been verified that, indeed, the periodic boundary condition was sufficient to utilize in the COMSOL model and conserve both the quantity and derivative (or flux) of the quantity at the periodic boundary. Figure 2.19 demonstrates this finding with a 2D model of a representative HFIR fuel plate. The plate includes flowing coolant on each side of the plate. The coolant width is not equal on each side, but the sum of the width of each side is equal to a single coolant channel width (0.050"). In the case of an equal coolant width on each side, the derivative of both the velocity and temperature should be zero which is shown in Fig. 2.19. However, for an unequal coolant channel width, the monitored derivatives should be nonzero, but equal, and the quantities (velocity and temperature) should also be equal. This is indeed the case as shown from the test case result of Fig. 2.20. Therefore, the periodic boundary conditions will be used for this boundary condition type.
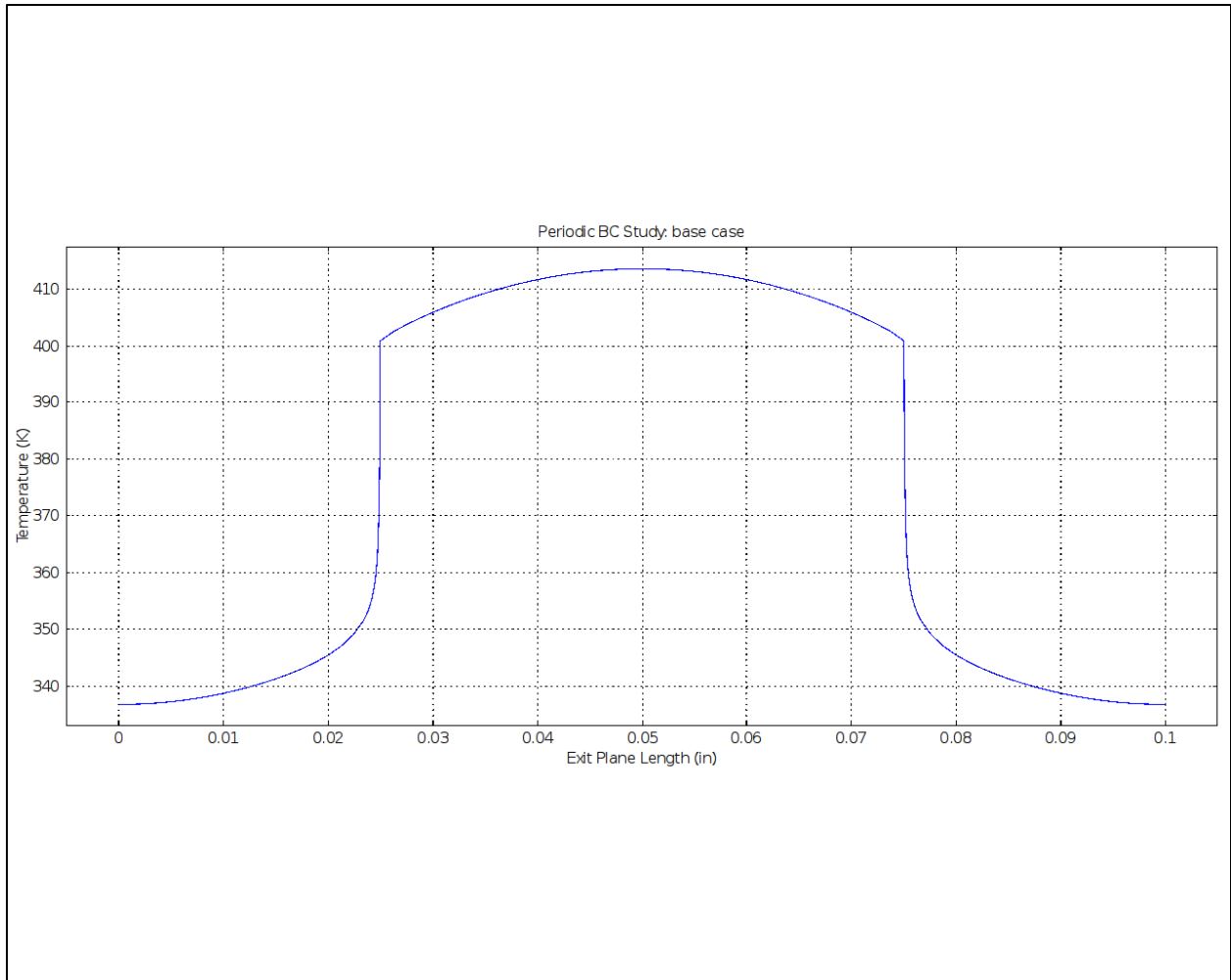
**Fig. 2.19. Periodic boundary condition HFIR fuel plate test base case
with equal coolant channel width.**
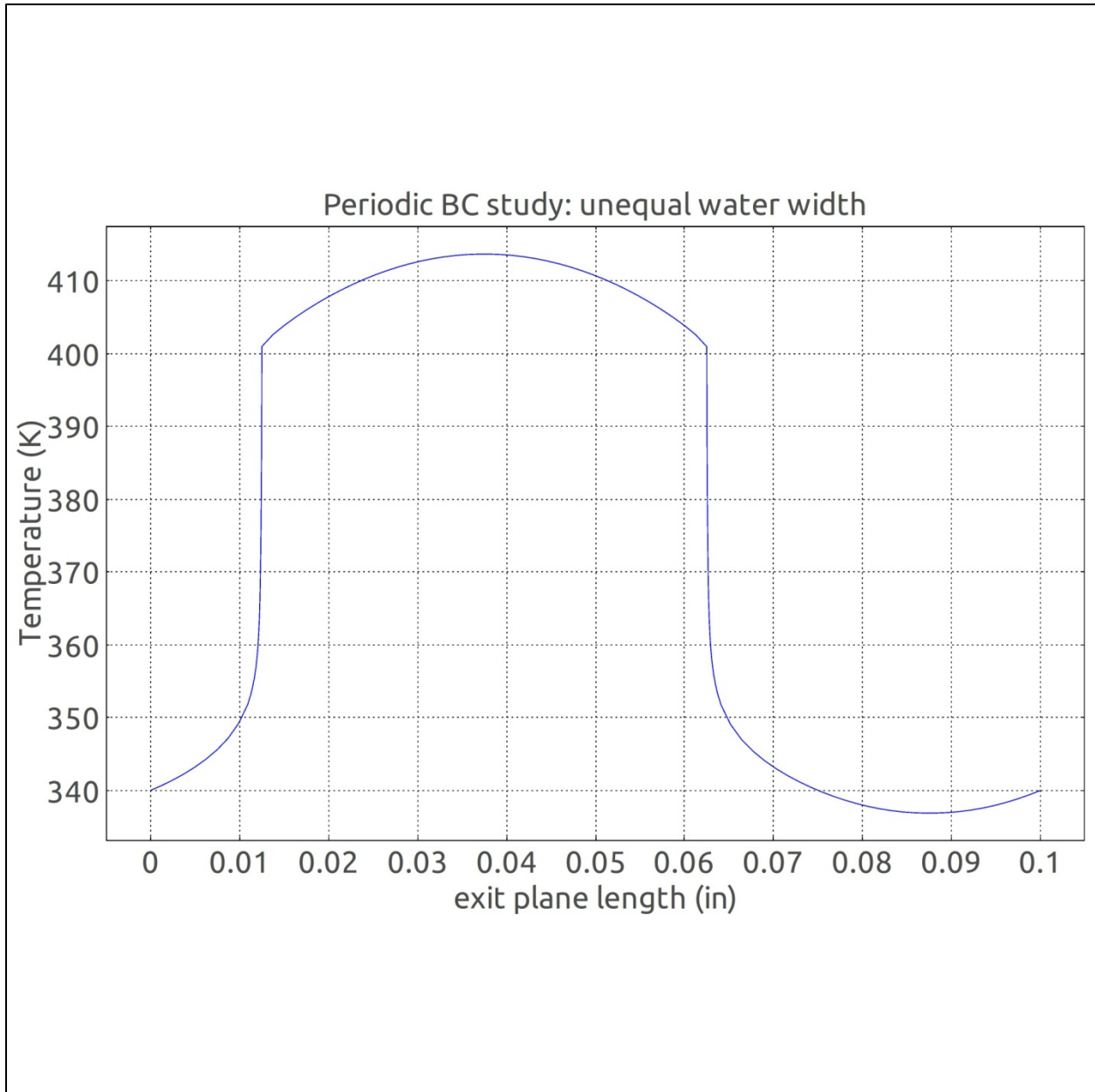
**Fig. 2.20. Periodic boundary condition HFIR fuel plate test altered case
with unequal coolant channel width.**

3.0   3D THERMAL-HYDRAULIC MODEL DEVELOPMENT

There are several aspects to creating a three-dimensional (3D) model of the HFIR fuel plate that one must consider regardless of the simulation tool utilized. With respect to COMSOL, the order of the model builder tree is a natural way to consider the tasks that need to be performed, including (1) specification of constants, variables, equations, functions that are either global or specific to a domain or surface, (2) geometry creation, (3) assignment of materials and associated material properties, (4) creation of the mesh, (5) specification of the physics equations to be solved, (6) specification and performance of the solution, and (7) examination of the results through reports, plots, and tabulations. Most of the items listed above are common to computational fluid dynamics (CFD) codes or other large analysis codes that are similar in some respects to COMSOL. Perhaps the most unique item that is specific to COMSOL is listed above as item 5, whereby the physics solved by the model requires specification in COMSOL. Most other engineering analysis codes of various types are designed specifically for a certain class of physics, such as fluid dynamics, heat transfer, structural mechanics, etc. COMSOL, on the other hand, is designed from the base level up to be a multiphysics code that will, theoretically, solve an unlimited number of physics equations simultaneously. At the present time, the Research Reactors Division (RRD) of ORNL is using COMSOL to solve models simulating heat transfer, fluid flow, structural mechanics, and nuclear-reactor physics.

Since the release of version 4.1 of COMSOL last October 2010, the main task associated with the 3D model development of the HFIR fuel plate until the end of CY 2010 has been on the geometry, or item 2 above. Section 3.1 will give a brief discussion of attempts made thus far to create an accurate geometry and mesh using commercial CAD packages. Section 3.2 will include an explanation of the significance of the version 4.1 release and the impact this release has had on the geometry creation. Section 3.3 below will also present some discussion of the meshing associated with geometry presented herein. Since the start of CY2010, we now have completed most of the other items listed above to some extent, and are now into the problem-solving mode. We will document these non-geometry associated tasks in the CY 2011 reporting. The reader should be able to see preliminary reporting of the current results at the RERTR bi-annual meetings and/or copies of the presentations from these meetings provided by the LEU conversion project management team at ANL.

3.1   DEVELOPMENT OF 3D INVOLUTE GEOMETRY WITH CAD PACKAGES

RRD has been using COMSOL since FEMLAB-3.0 in early 2004. Even in these early versions years ago, the code accepted certain CAD formats as input to create geometries. The general capability was crude by current standards, and found to be quite limited in application. However, even in this early version, the support for Solidworks CAD input was available; perhaps due to the parasolid CAD standard provided with Solidworks. Then on 9/6/2005, version 3.2 was released that also included the CAD Import module, which was much improved over the previous offerings. This was about the same time that the code was renamed from FEMLAB to COMSOL. The initial offering supported many more commercial formats including separate additional add-on modules for importing CATIA® V4, CATIA® V5, Inventor, Pro/E, and VDA-FS. The v3.2 Solidworks collaboration also included a "live connection" interface, which is very similar to the present-version called "live-link" interface.

The "live-link" feature for CAD with COMSOL creates a computing environment whereby the GUI of both packages are active and communicating with each other. A change in the geometry on one side is reflected on the other side essentially simultaneously. For the Solidworks-COMSOL live-link, a change made on the Solidworks geometry screen, is seen on the COMSOL screen and vice-versa; with certain restrictions of course (must be in the geometry mode, not solving, etc.). This feature is very powerful, and is quite useful for design optimization, parametric sweeps, etc.

Then on 4/23/2010, version 4.0 of COMSOL was released. Along with many new features and changes, further improvements were made to the CAD import module and Solidworks live-link as well as additional CAD live-link modules for Pro/E and Inventor. Now, at the present time (5/18/2011), version 4.2 of COMSOL has been released with additional live-link modules for AutoCAD and SpaceClaim. There obviously has been an ongoing level of emphasis on CAD connectivity and many improvements to the CAD interface for COMSOL.

Early on, we had made a concerted effort to gain support from our local engineering drafting staff in RRD to utilize their expertise to provide fuel plate CAD files for import into COMSOL. The local CAD staff have standardized on Microstation, which is currently not directly supported by COMSOL. However, Microstation can export into formats that are readable by COMSOL. However, even after repeated attempts, we were unable to gain additional support to provide an iterative working relationship between the COMSOL analysts and the Microstation professionals. For example, we must have a representation of the internal geometry of the fuel plate which was not in the Microstation drawings we were provided. At the time, we were still using the 3.5a version of COMSOL, so we decided to pursue the more directly-supported Solidworks CAD.

In addition to the COMSOL code, there are other analysis codes that are particularly compatible with Solidworks; most notably, the ATILLA code (also one which we are licensed for, and have a goal to test for HFIR applicability). Therefore, a single Solidworks license was obtained, and one of our staff twice received basic training on Solidworks. Nevertheless, it was realized that Solidworks was too complex for the average engineering analyst to master, so no internal expertise exists yet for 3D CAD within RRD which we can interact with to develop COMSOL geometries.

We did receive some Solidworks CAD files developed by Wade Marcum of OSU specific to the HFIR fuel element design. These design files included a representation of the entire HFIR inner and outer fuel element with individual fuel plates modeled. However, neither the fuel plate internals nor the fuel-plate rounded top were included in these models. Since these are vital components that we must include in our models, we were not able to use these Solidworks model files without further work with the CAD design files.

We were able to find an ORNL professional CAD engineer who was experienced with Solidworks and was available part time. We were running version 3.5a of COMSOL at the time, and we got quite a bit done. We were able to create the HFIR fuel plate, and create the radial contour shape of the fuel-plate internals, and we started to make some progress on the rounded top entrance of the HFIR fuel plate. However, COMSOL had a great deal of difficulty in meshing the Solidworks-generated internal geometry, and the shapes were difficult to visualize and manipulate; even with the live-link activated. Competing priorities with other project goals brought this effort to a halt. We did have some success with this effort. The figures below show the HFIR inner fuel plate top side from the inside and outside respectively as meshed by COMSOL v3.5a using the Solidworks-generated geometry file as input.   If we could have gotten over the difficulty with fuel-plate internals, this method may have worked out. Ultimately, the dual expertise in both mathematics and Solidworks CAD operability is what was missing.
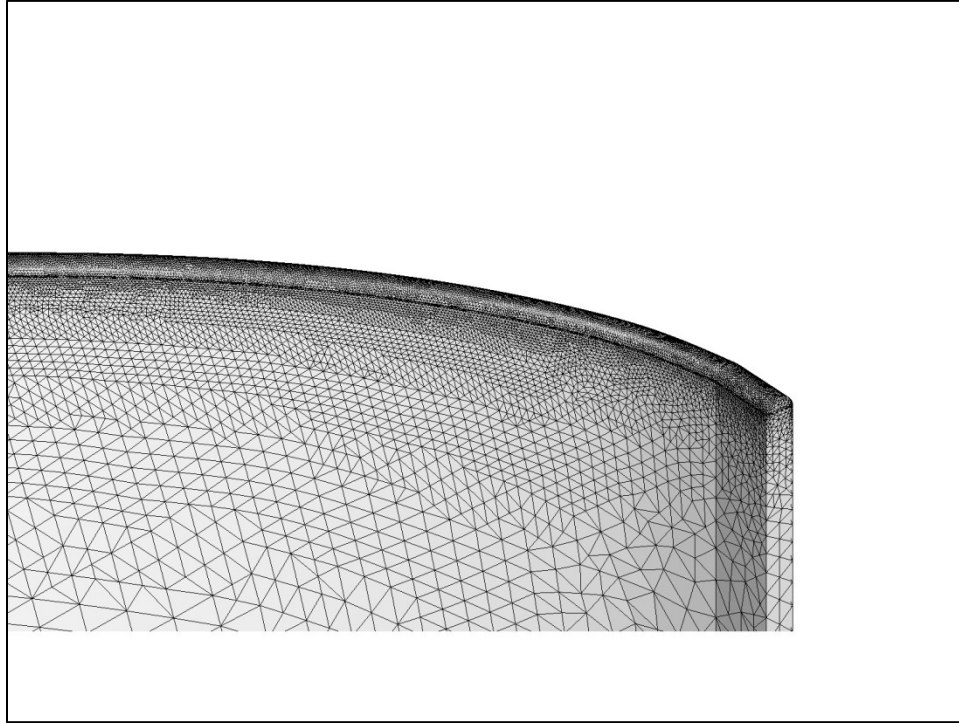
**Fig. 3.1. Solidworks Import of the HFIR inner fuel plate, top view, inner side plate,
meshed by COMSOL version 3.5a.**

After working with the improved native COMSOL capability (see Section 3.2 below), the COMSOL technical support suggested that the external CAD program method of geometry creation is superior for complex geometries. This makes sense, of course, because the CAD software has been designed to perform this task to the ultimate detail. The problem is that we have neither obtained the key person whom we need to do this task, nor taken the time to learn one of the supported CAD packages ourselves. There are many CAD software packages available which are supported by COMSOL and vice versa. The most logical thing to do is to utilize the local CAD mechanical designers to perform this task. It is a matter of obtaining the appropriate level of priority to secure their time or learn it ourselves.

Another option is to find a CAD software package that is easier to learn and use with COMSOL. The Spaceclaim package is supposed to fit this role in the market. COMSOL has also recently added a live-link for Spaceclaim. Spaceclaim does appear to be much easier to use than Solidworks. We have added a task to re-investigate the external CAD option for geometry creation.
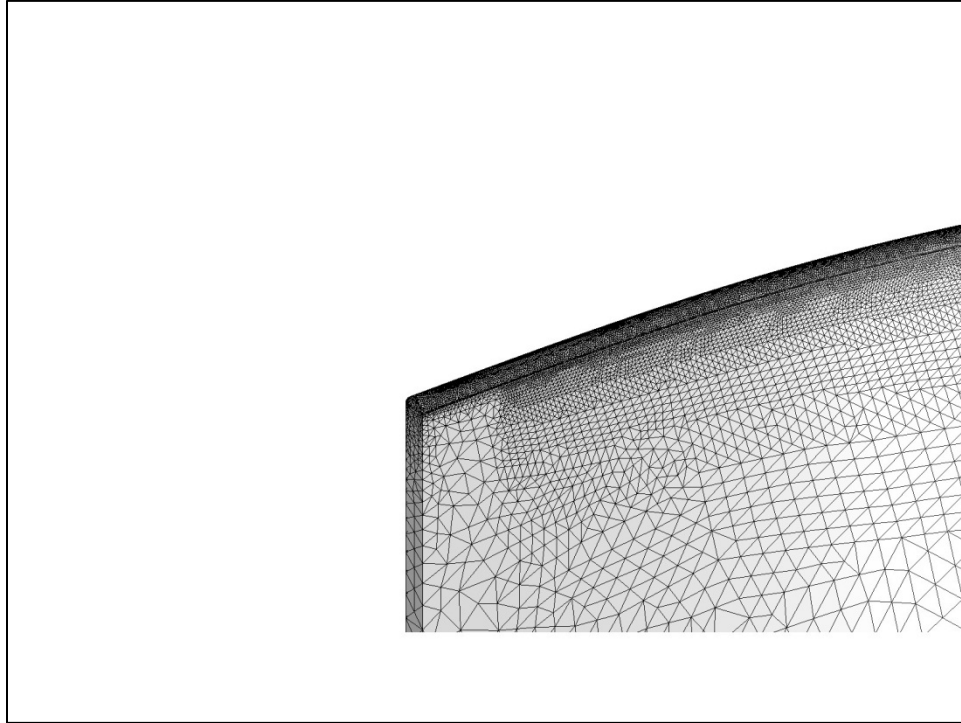
Fig. 3.2. Solidworks Import of the HFIR inner fuel plate, top view, outer side plate, meshed by COMSOL version 3.5a.

3.2   DEVELOPMENT OF 3D INVOLUTE GEOMETRY WITH NATIVE COMSOL CAD

Prior to the release of version 4.1 of COMSOL, in order to create the HFIR fuel-plate geometry with native COMSOL CAD, the root geometry creation is performed by connecting multiple points to create the involute curve shape. Ultimately this would cause the creation of multiple surfaces to track, specify, initialize, and activate in order to examine or manipulate. Furthermore, the results were corrupted by streaklines along lines created by extruding the original point values of the involute approximation. The 3D flow distribution was actually altered at the intersection of the planes at these same point-valued lines where eddies were formed by the simulation as if the flow might actually behave in such a manner if the involute plate were not smooth. This form of geometry creation was therefore, not acceptable for the high-quality of solution we demand for this project. It should also be noted that if the geometry were created using the external CAD software, as described by Section 3.1, then this solution corruption would not exist because the geometry is defined by single surfaces wherever possible.

Upon the release of version 4.1 of COMSOL, a new feature was made available called the "parametric curve" which allowed for an arbitrary curve to be specified in equation form and placed in 3D space. This opened up the opportunity to input the expression for an involute directly into COMSOL as a geometry entity. From this fundamental involute curve, additional surfaces and volumes can be created through extension and extrusion into 3D space. This, in turn, eliminates the problem of multiple surface tracking (and flow simulation corruption), such that, the surfaces of the involute-shaped fuel plate can be specified by a single specification (mouse click) rather than multiple, and possibly hundreds of, individual specifications as it was prior to this new feature.

This new parametric curve feature proved to be very effective and has become the foundation for the geometry of the current working model of the HFIR LEU fuel plate with COMSOL. Even with the

success of this new feature (parametric curves), not all is perfect however. Because the HFIR fuel plate is so long axially relative to the radial direction, and even greater in the plate thickness direction (aspect ratio = 480), persistent difficulties arose when trying to combine the individual parts of the geometry to create the combined model. It became necessary to utilize the "assembly" feature rather than the more-desirable "union" feature when combining all parts together in the last process of the geometry creation. This was necessary because of slight imperfections and inaccuracies in representing the geometry mathematically to the computer. These imperfections can be thought of as "round-off error" in comparison to what we as analysts might think of when explaining why these imperfections exist in the model.

There are several tradeoffs between the "union" and "assembly" methods for forming the geometry:

a.   The union method executes the finite-element assembly and solver faster than the assembly method. Apparently, this is because the node values along the boundaries between the parts of an assembly must be interpolated to provide for the correct flux quantities to be incorporated; continuity by default. On the other hand, a continuous flux is provided by default using a union method. This is the primary advantage of the union method: speed.

b.   The union method requires that identical nodes be shared across the boundaries between domains (or parts of an assembly). This will yield higher accuracy at the expense of less flexibility. This is taken care of automatically by the software when a union geometry is meshed by COMSOL. We think of this as a disadvantage of the union method since the result is less flexibility.

c.   The assembly method allows for each domain (part) to be meshed independently. In turn, having more control over the mesh improves the quality of the solution. This is the primary advantage of the assembly method.

d.   As a 3D model becomes larger in size (greater number of degrees of freedom to be solved), an extensive amount of cpu time is required to perform the finite-element assembly process. Indeed, the cpu time required for the finite-element assembly process can become so extensive, that it can surpass the solver cpu time and become the dominant resource load and time consumer to solve the problem. This is the primary disadvantage of the assembly method.

e.   The formation of a geometry using the union method is more difficult to achieve than the assembly method. Further, it may not be possible to create the geometry by the union method, in which case, the assembly method is the only option.

f.   The assembly method requires the specification of identity pairs for each boundary internal to the model coupled to an adjacent part. For the union method, these internal boundaries are automatically established without user intervention as a continuity boundary condition. In version 4.2, it has been stated that the setup of the identity pairs is somewhat automated for the assembly method also. This will be tested soon, but for now this is another disadvantage of the assembly method because setting each identity is time consuming and prone to error.

For version 4.1 of COMSOL and later, the assembly method does, indeed, work well to create the geometry of the HFIR fuel plate and fuel internals. It is desirable for the union method to also work so that the computation time of the solution process might be shortened. Therefore, we intend to re-check

the applicability of the union method for this geometry with the new version 4.2 (and probably should check at each major version thereafter).

A close examination of all the details of the geometry creation is not necessary for this report, but a brief introduction will help to understand what is involved and the level of input required. Figure 3.3 shows the input menu page required to create the parametric curve of the root involute curve in 3D. The right side of Fig. 3.3 shows the result of building this curve as visually shown in 3D on the computer screen. This single involute curve is the foundation for the creation of the remaining parts to the HFIR fuel plate geometry. All the remaining parts are built-upon or extruded from this root involute parametric curve.
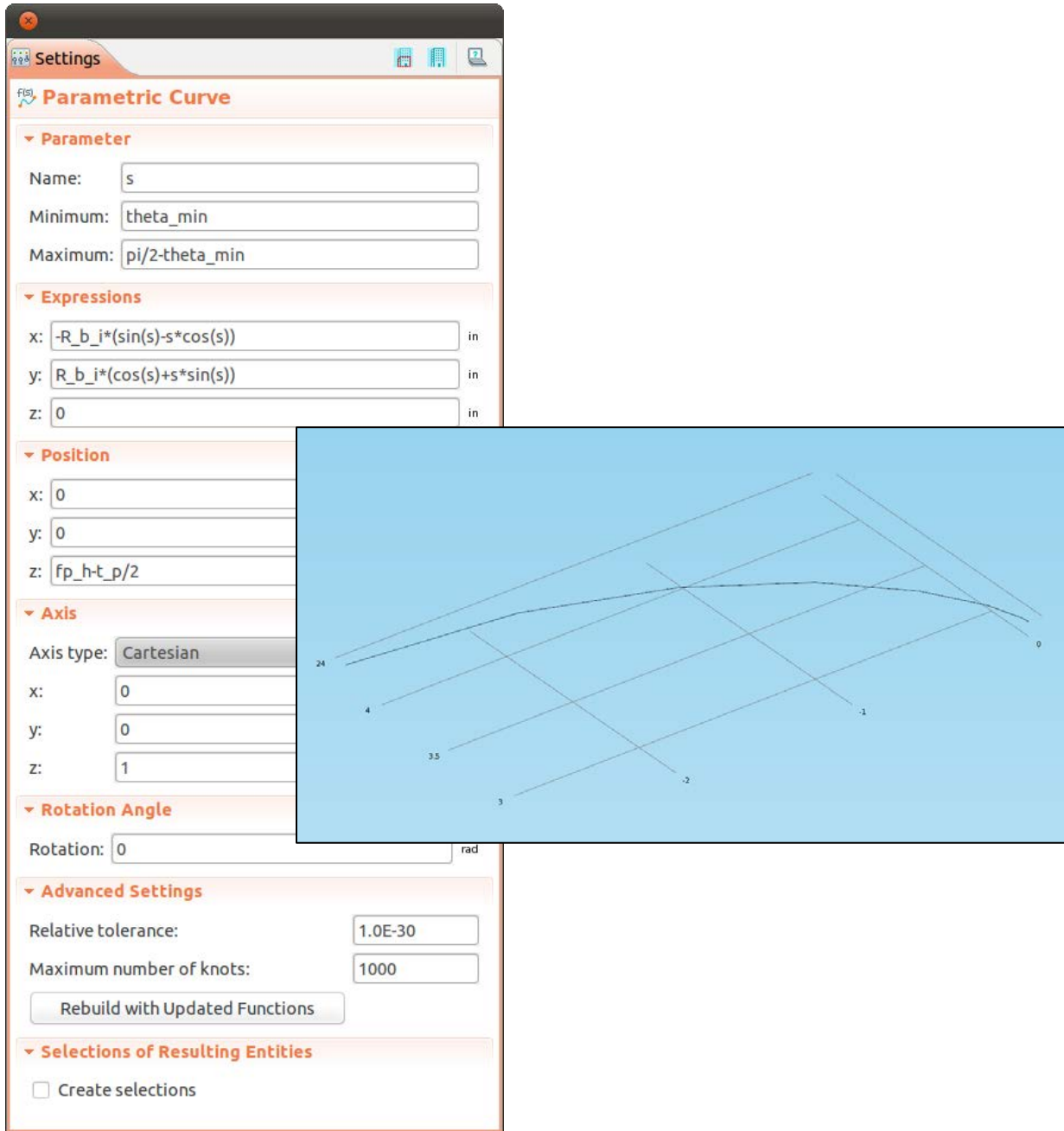
**Fig. 3.3. COMSOL input menu and parametric curve result for the root involute shape
of the HFIR inner fuel plate.**

Conceptually, one can create the remaining parts by either extruding axially, or extruding in the direction of the involute curve itself. After trying both methods of extrusion, and after consultation with COMSOL tech support, it was decided to extrude along the involute curve itself to have the greatest level of success in preserving the intended geometry. Figure 3.4 shows the model builder tree input on the left side of the figure, and the resulting extruded fuel-plate rounded top geometry shape on the right side of the figure.
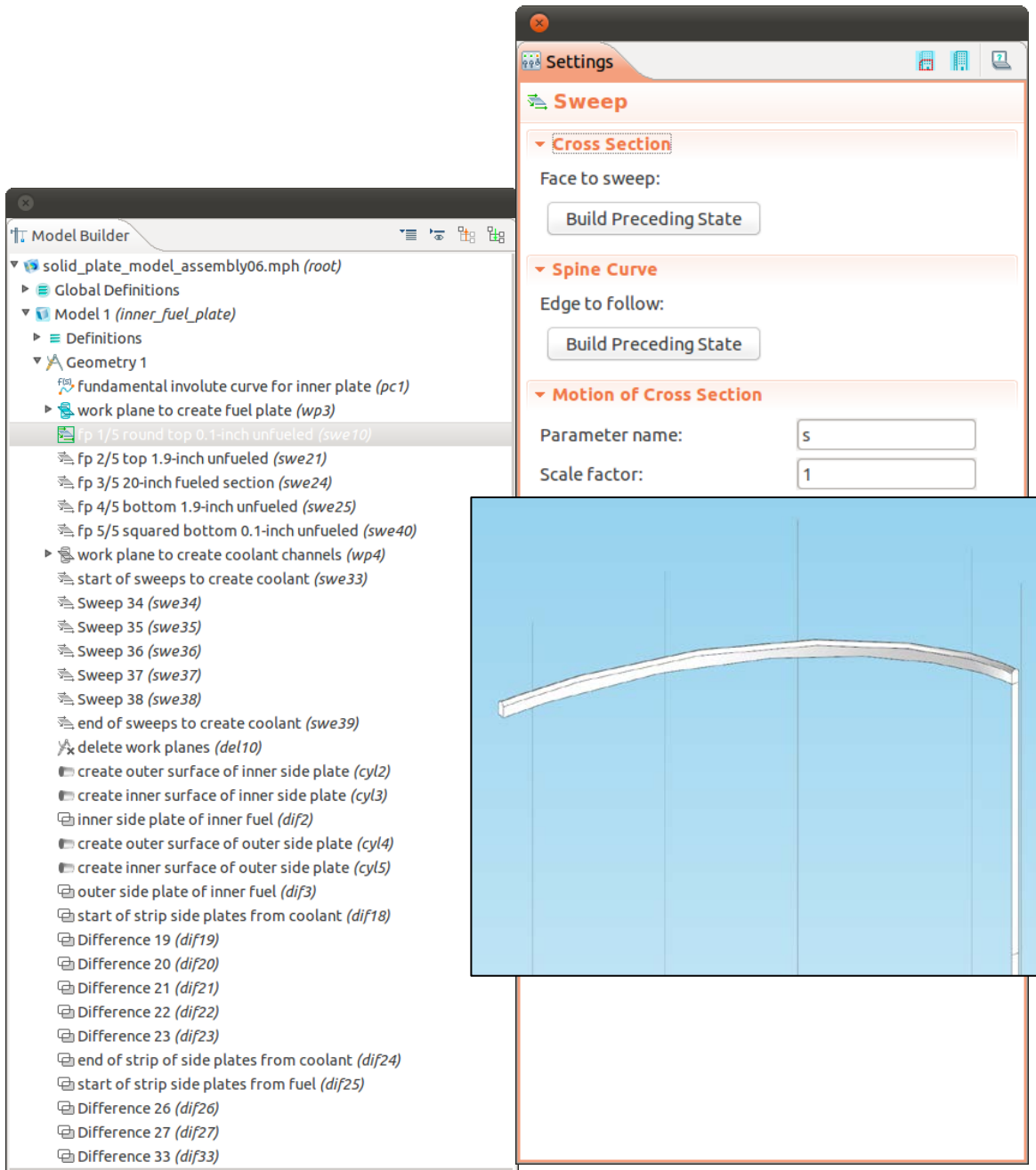
Fig. 3.4. Sweep or extruded HFIR inner fuel plate rounded top shape as shown by the model builder tree entry (left side) and graphical result (right side).

The remaining parts are similarly created by extrusion and subsequent difference and union Boolean operations on the parts to ultimately arrive at 18 separate parts to be assembled to create the completed geometry. The 18 individual part numbers and names are shown as Table 3.1 below. The assembled HFIR fuel plate model includes the fuel plate, fuel internals, coolant, and side plates. Figure 3.5 shows the complete assembled HFIR fuel plate model. The part numbers are labeled with reference to Table 3.1 for the part name. Note that convex coolant parts 9, 7, and 5, and additionally, fuel parts 12-17 inclusive are not visible in Fig. 3.5.

Table 3.1. List of Parts that form an assembly for the COMSOL model of the HFIR inner fuel plate

Part type	Part name	COMSOL tag	Part number
Side plate	Outer	Ext5	1
Side plate	Inner	Ext6	18
Coolant	Entrance	Dif18	11
Coolant	Rounded top	Dif4	10
Coolant	Top 2" unfueled concave	Dif5	8
Coolant	Top 2" unfueled convex	Dif5	9
Coolant	20" fueled concave	Dif6	6
Coolant	20" fueled convex	Dif6	7
Coolant	Bottom 2" unfueled concave	Dif7	4
Coolant	Bottom 2" unfueled convex	Dif7	5
Coolant	Squared bottom	Dif8	3
Coolant	Exit	Dif24	2
Fuel	Round top unfueled	Dif25	16
Fuel	Top 2" unfueled	Dif26	15
Fuel	20" filler unfueled	Dif34	14
Fuel	Bottom 2" unfueled	Dif28	13
Fuel	Squared bottom unfueled	Dif33	12
Fuel	Fuel meat	Ext7	17
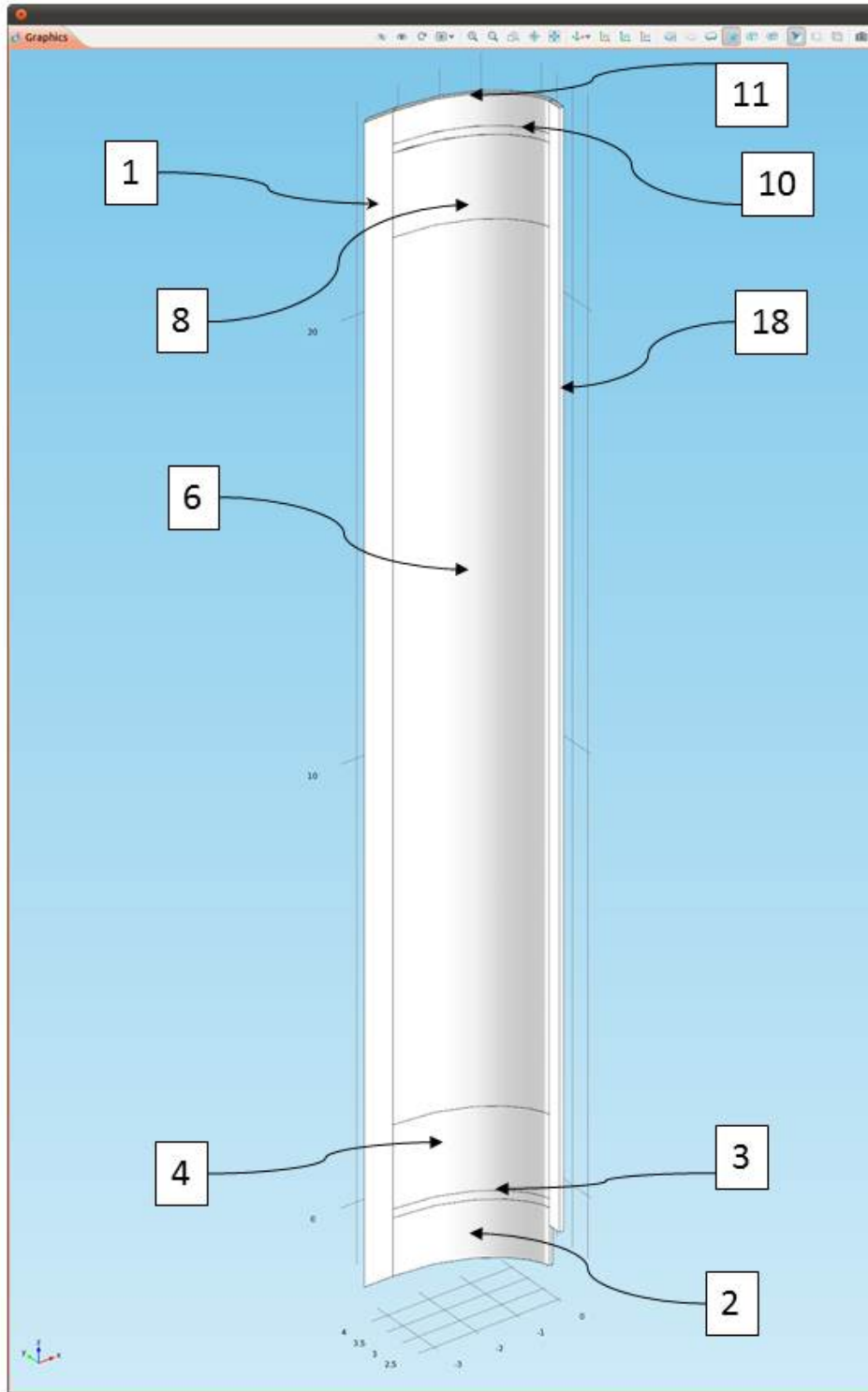
Fig. 3.5. Assembled HFIR inner fuel plate COMSOL model geometry.

3.3 INVESTIGATION OF 3D FUEL-COOLANT ASSEMBLY TECHNIQUES

The difference between performing a union and an assembly of the final geometry representation in the HFIR fuel plate COMSOL model is rather simple from the user's perspective as shown in Fig. 3.6. Certainly, internal to the COMSOL code, the difference between the union and assembly is quite complex, but the explanation of these details is out of the scope of this report. The default setting is to perform a union operation on the geometry parts. The performance of a union operation will result in an error for this model, so no further discussion is made of this option since it is not possible to complete with the current HFIR fuel plate model.
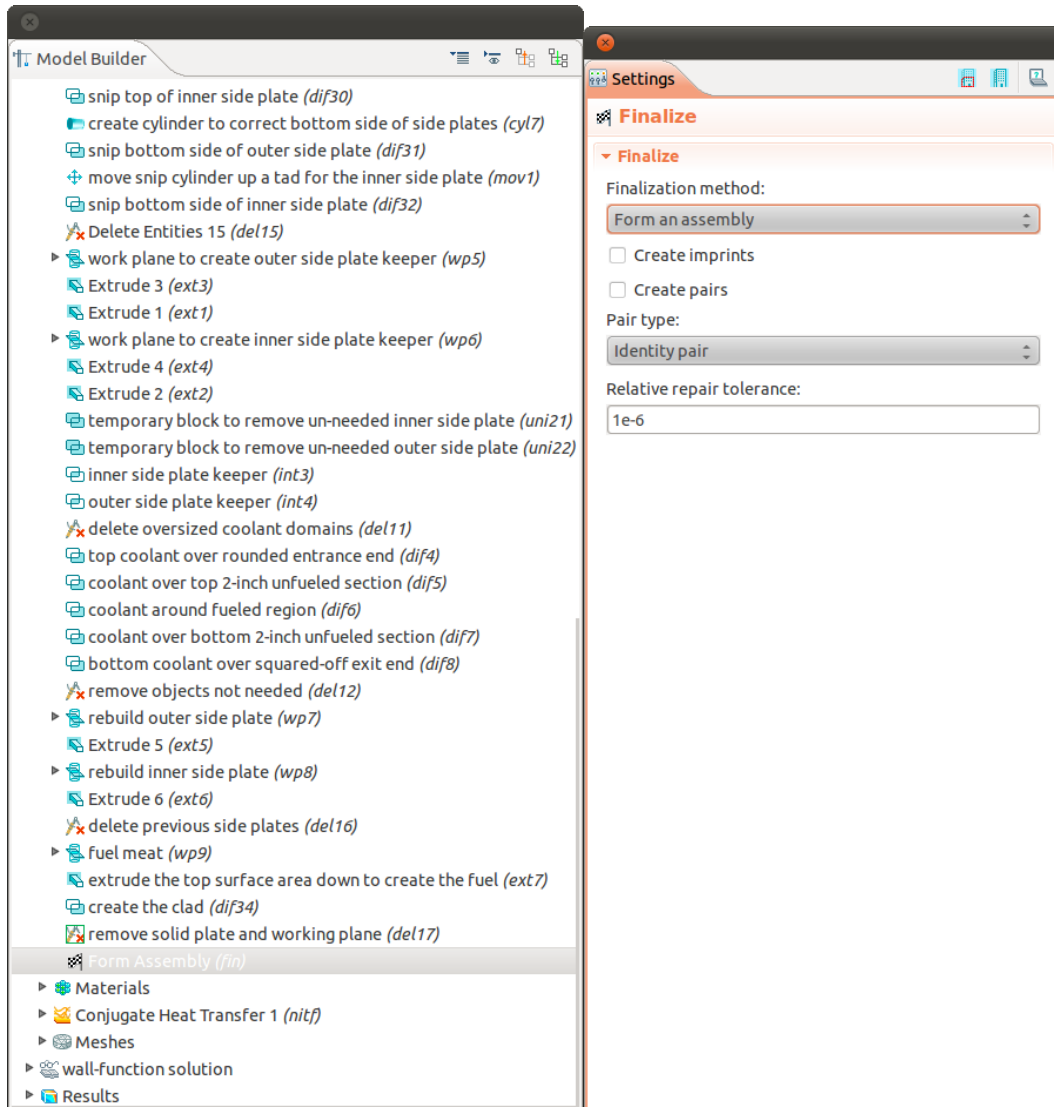
Fig. 3.6. COMSOL model builder tree input for the final geometry assembly step for the HFIR inner fuel plate.

The user must deliberately change the final step in the geometry creation from a union to an assembly in order to complete the HFIR fuel plate geometry creation. This assembly step is indeed successful using a value of 1.0e-6 for the relative repair tolerance. This is a normal and expected adjustment step required for a geometry model of this complexity.

In addition to performing the assembly operation, a long set of identity pairs needs to be defined in order to provide the coupling of the physics between the several parts of the assembly (18 in the present model of the HFIR fuel plate). Figure 3.7 shows the list of identity pairs defined for the HFIR inner fuel plate model. Adjacent to the list is a typical menu listing of input requirements for each of the identity pairs. A total of 25 sets of identity pairs are required for this model. Note that separate identity pairs are required for the "flow equation" and the "energy equation". An identity pair is not required for those boundaries that are already defined in order to create the problem; for example, inlet temperature, exit pressure, inlet flow, periodic boundaries, etc. For the special boundary case where the wall function turbulence model is defined, these surfaces also do not require an identity pair. Even with all these exclusions from the list of boundaries for the 18 parts, there are still a considerable number of surfaces that need to be defined with identity pairs. The process of creating the identity pairs can be quite cumbersome and time consuming, but once done, the model geometry is completely defined by the completion of this step. Furthermore, with the availability of the new parametric curve feature of COMSOL, the total number of identity pair input surfaces has been significantly reduced, hence, providing a significant improvement in the input requirements and lower the probability of error by the user.
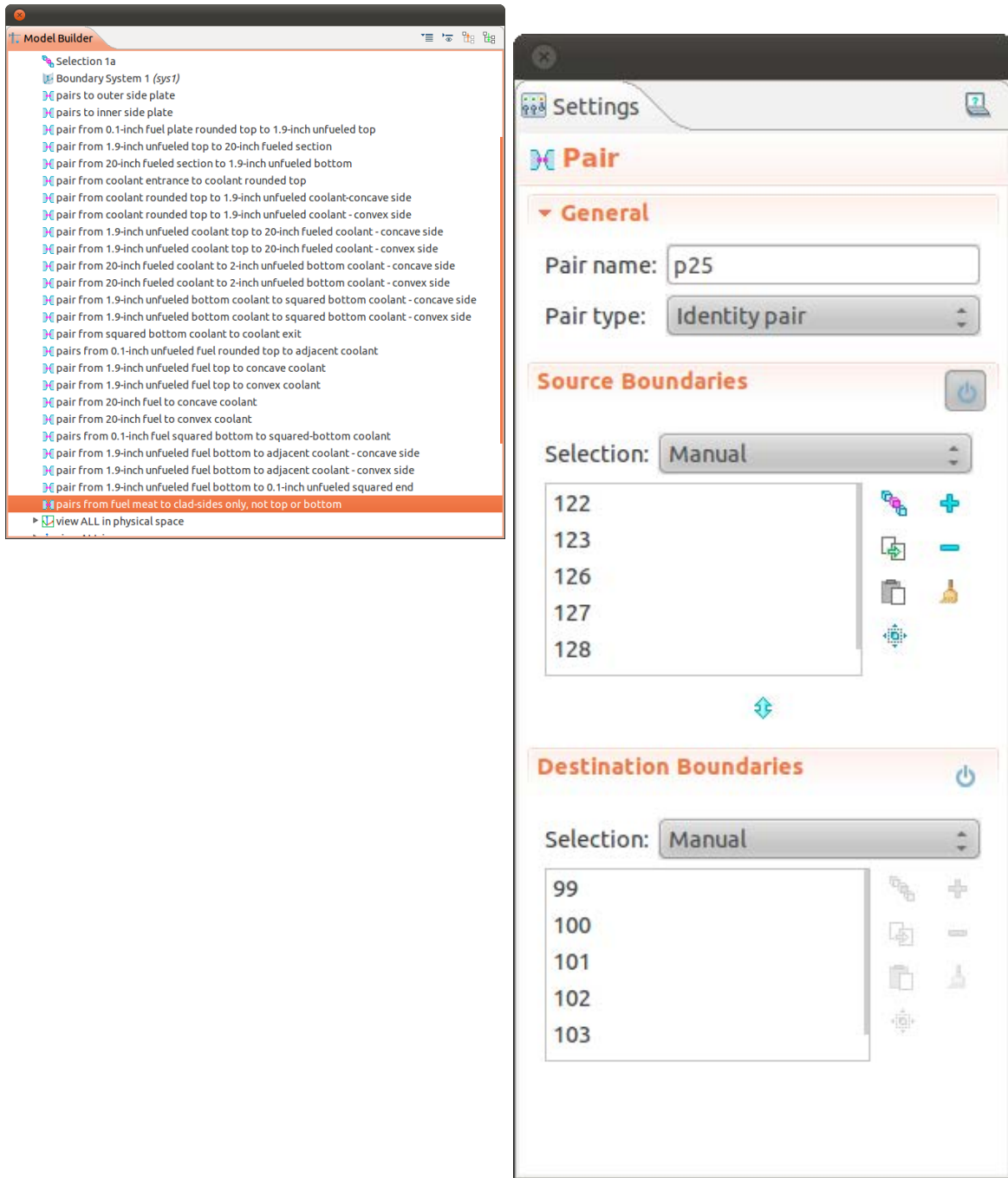
Fig. 3.7. List of identity pairs (left) and typical input requirements (right) for the HFIR inner fuel plate COMSOL model.

The next step in the process is to create the mesh upon the geometry. The present model takes advantage of the full array of meshing techniques available with the native COMSOL meshing tools. The shorter, stubby parts that make up the fuel plate top and bottom end pieces, and the adjacent coolant domains around these two parts are meshed entirely by free-meshed tetrahedral finite elements. These four domains, particularly the coolant domains, contain perhaps the highest element density of the entire model. This is the primary reason why these four parts were segregated from the rest of the model. Figures 3.8 and 3.9 show the fuel-plate top region and fuel-plate bottom region meshed entirely by free-mesh tetrahedron elements. The entire 3D geometry could be meshed using the free-mesh tetrahedron method, but would then result in a model very difficult to solve due to the massive number of degrees of freedom created by the large number of nodes.
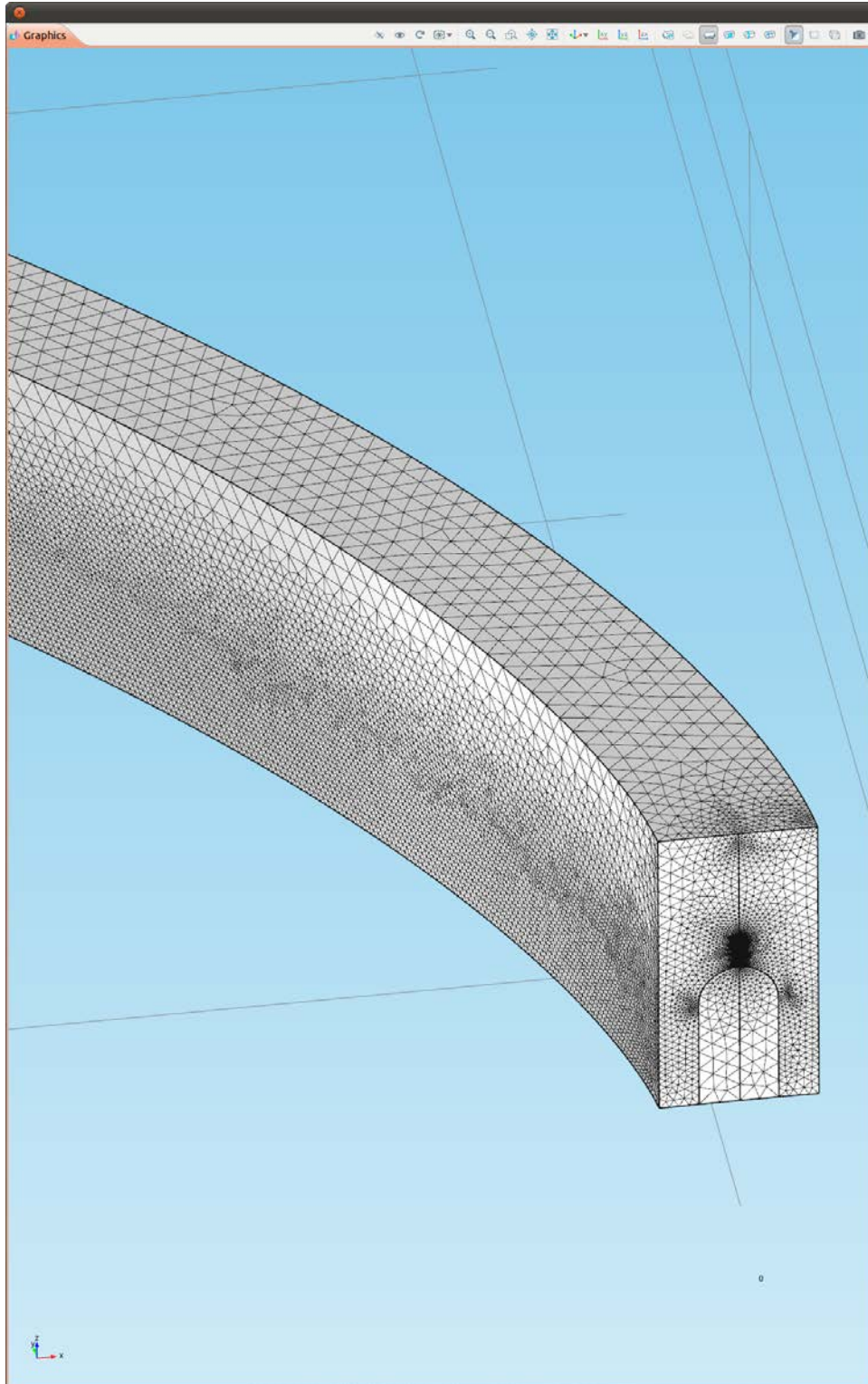
Fig. 3.8. HFIR inner fuel plate rounded top region typical free-mesh tetrahedron design showing coolant over the fuel plate.
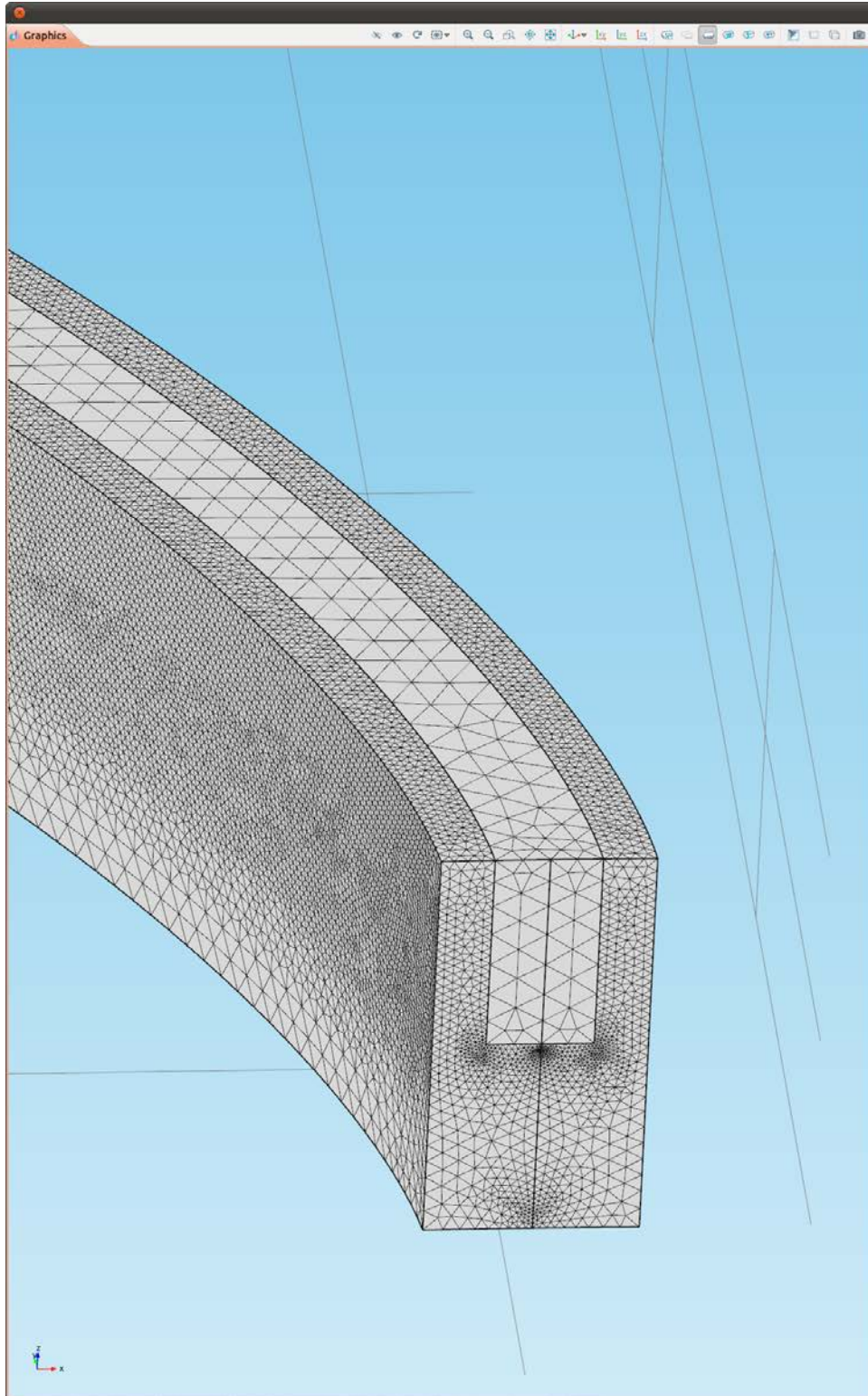
Fig. 3.9. HFIR inner fuel plate rounded bottom region typical free-mesh tetrahedron design showing coolant under the fuel plate.

The remaining parts of the model are meshed by sweeping (or extruding) the mesh from one surface to another surface in the axial direction. This design approach saves a considerable amount on the number of elements, while still preserving the accuracy needed to obtain a quality solution. This is possible because of the dominant flow (w) in the axial direction. The source surface mesh is defined by one of two ways: 1) creating a triangular or mapped mesh on that surface, or 2) copying the existing mesh from the adjacent surface. Method 2) (by copying) is the preferred way because it will create an identical nodal pattern (node-to-node mesh) between the adjacent surfaces which optimizes the accuracy of the flux (usually continuity) between the adjacent parts (similar to what would be done for the union method of geometry creation). However, if method 1) is used, there is not a great deal of loss in accuracy since the finite element mesh will be refined to produce a small residual in the flux continuity across the boundaries.

We will not present all details of every part meshed in this report since it is not necessary to do so. However, we will present an example of each of the two types of sweep meshes (triangle generation and/or copied surface mesh). Figure 3.10 shows the copied mesh from part #10 (coolant adjacent to the fuel-plate rounded top) top surfaces to part #11 (coolant entrance region) lower surfaces. The mesh is swept (or extruded) from the bottom surface to the top surface. Figure 3.11 shows a view from the triangular mesh created at the top surface of the fueled portion of the inner fuel plate. This triangular mesh is then extruded (or swept) from this top surface down the 20-inch length of the fuel to the bottom of the fueled-section of the fuel plate. The axial node lines are specified identical to the node lines given in the MCNP calculation of the power density provided as external input to the model.
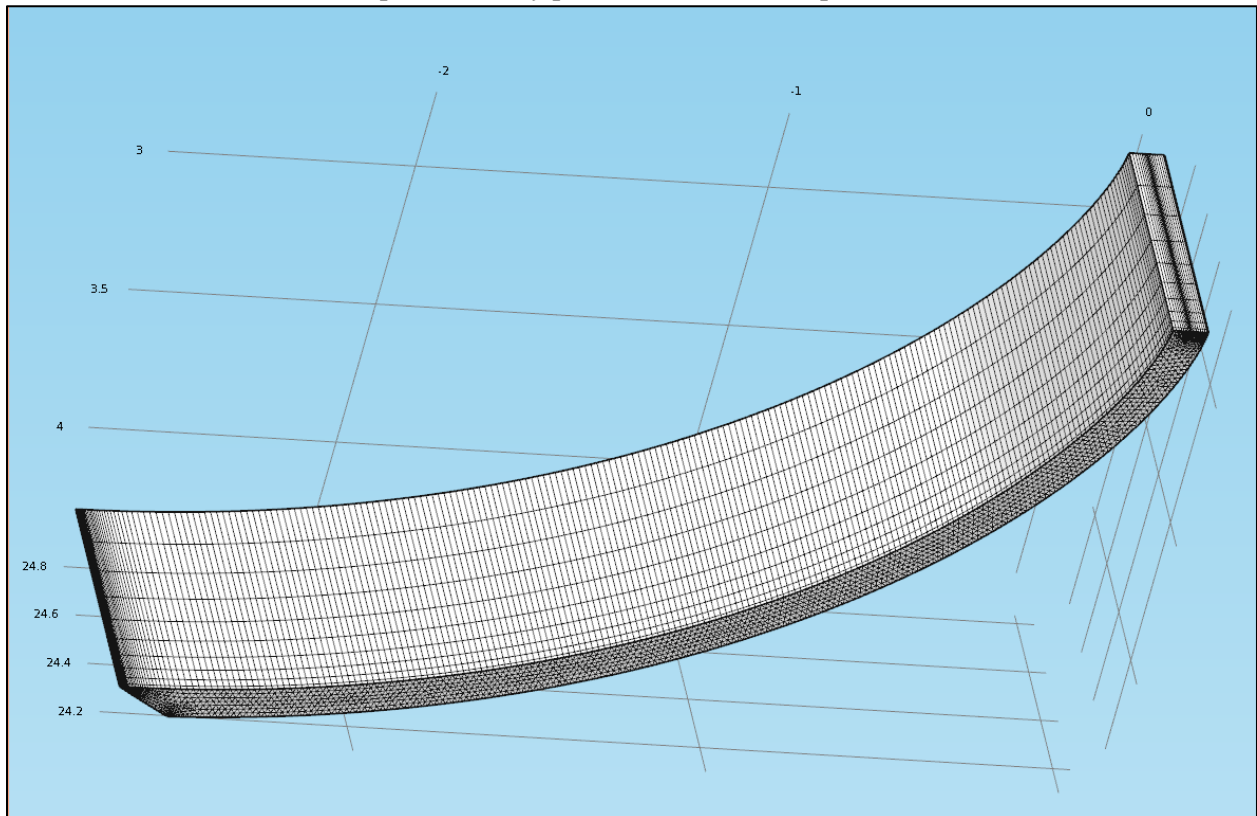
Fig. 3.10. Extruded mesh of the HFIR inner fuel plate coolant entrance region using a copied mesh as the extrusion source surface.
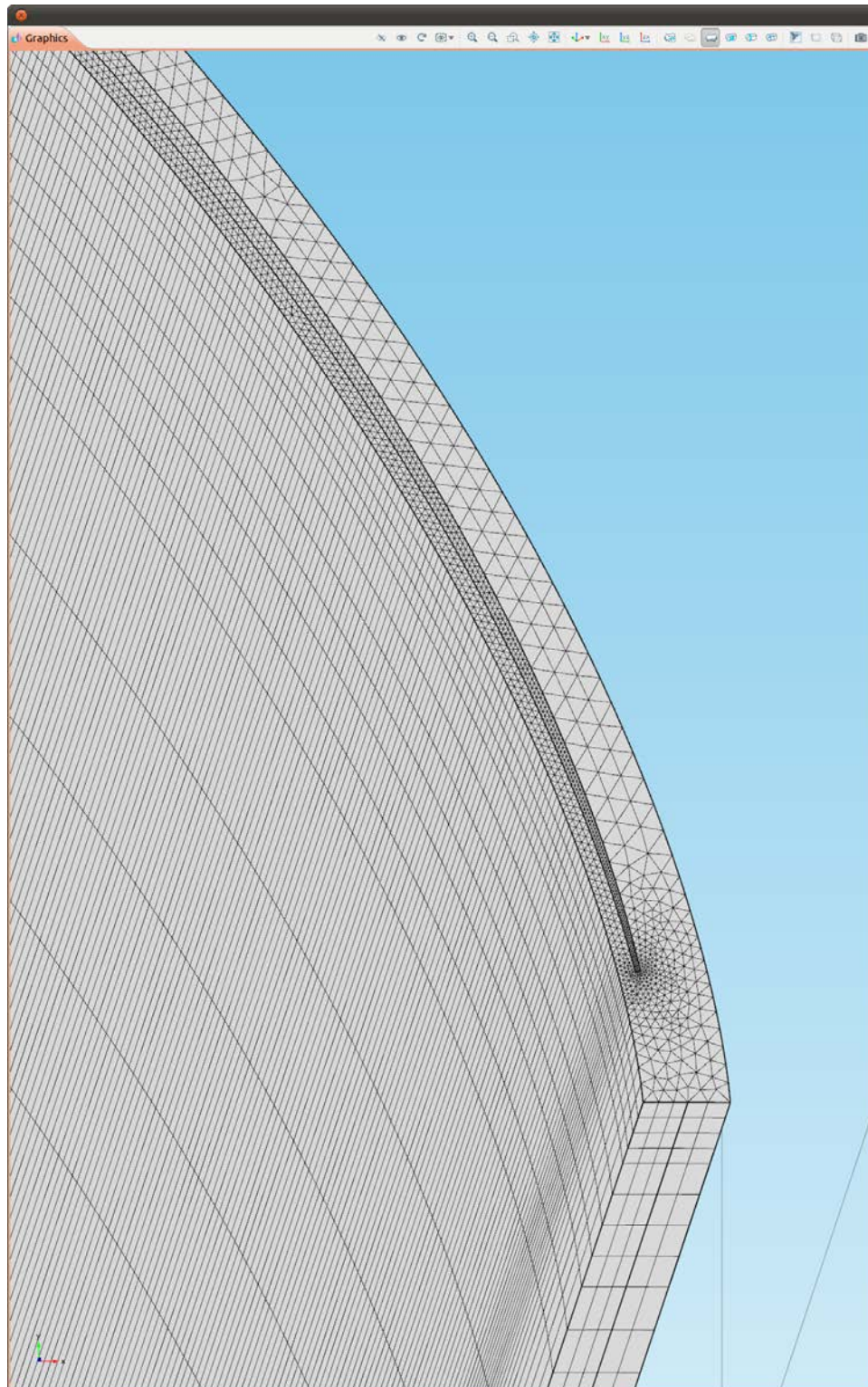
Fig. 3.11. Extruded mesh of the HFIR inner fuel plate fueled section using a triangular mesh as the extrusion source surface.

As a final step in the meshing process, a thin boundary layer mesh is added over all the wetted surfaces in the model. The process of creating a boundary layer mesh is provided by special tools within the COMSOL meshing options just for this purpose in 3D. The model builder tree is designed in a manner in which the boundary layer mesh may be enabled/disabled as needed in order to create a sequence of mesh densities leading up to the inclusion of the boundary layer mesh as the last step in achieving a converged solution that satisfies our error criteria. As it turns out, only 4 of the 18 parts require the creation of a separate boundary layer mesh step. Two other parts, the entrance and exit coolant region, include the boundary layer mesh by copying the mesh surfaces from the adjacent top and bottom regions of the coolant over/under the fuel plate. Figure 3.12 shows the detail of a completed boundary layer mesh on the underside corner of the coolant over the fuel top.
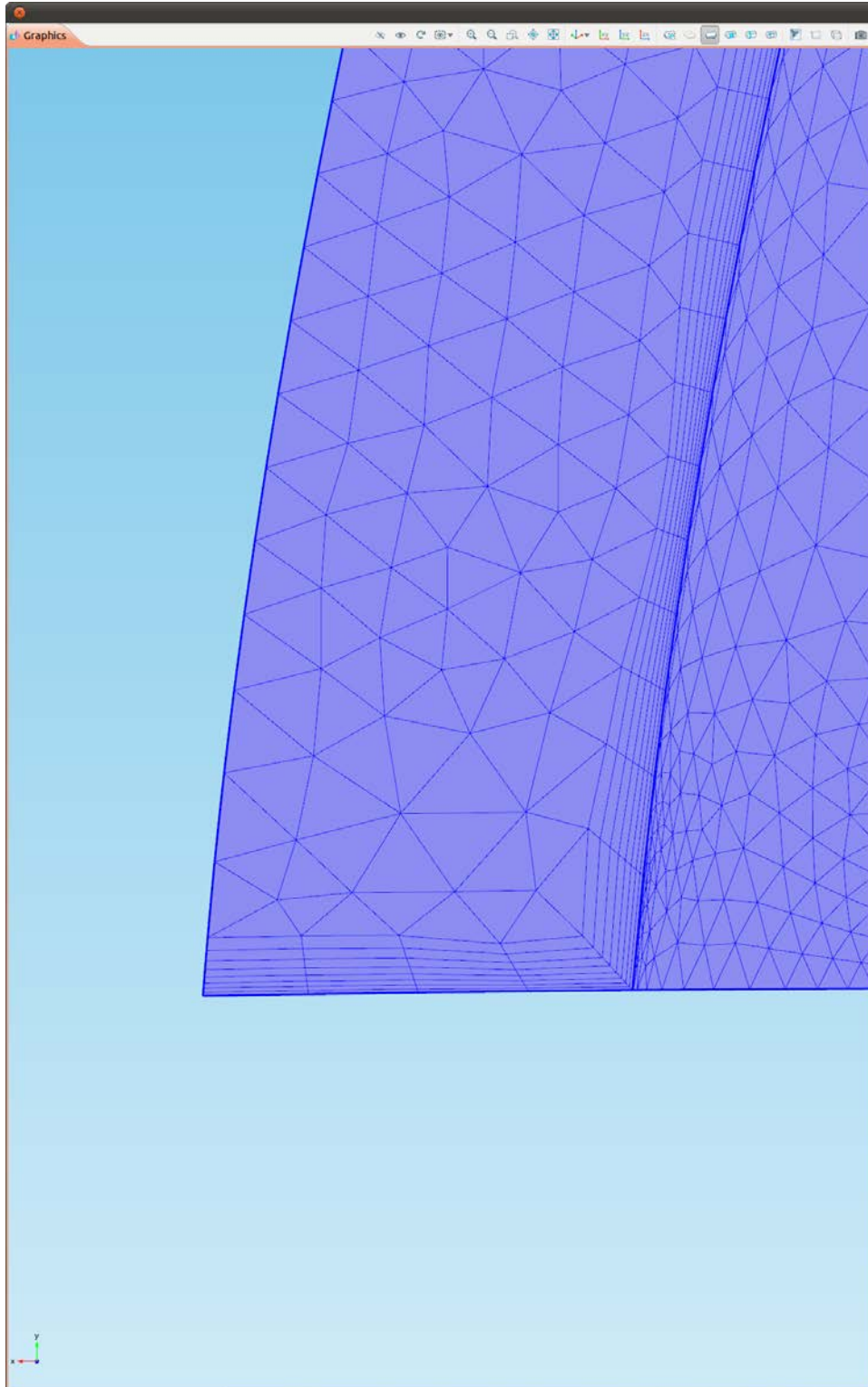
Fig. 3.12. Detailed examination of a typical COMSOL boundary layer mesh added to the coolant region over the HFIR inner fuel plate top.

And finally, it would be beneficial to have a figure showing the entire meshed image of the HFIR inner fuel plate. However, such a figure is not provided here because it would just appear as a solid black image with no detail. Complete details of the final model, including images of all meshing details, will be included in a formal calculation performed under the QA process within the Research Reactors Division of ORNL.

4.0   STRUCTURAL MECHANICS METHODS AND MODEL DEVELOPMENT

4.1   FLUID STRUCTURE INTERACTION (FSI) METHODS DEVELOPMENT

The performance of this task has undergone a major shift in personnel and priority as this fiscal year has progressed. One graduate student started on the project in January, 2010 and left the project for full-time employment by the end of July, 2010. Several of the preliminary FSI results from this student were presented at LEU meetings. All of his work was preserved as is, and made available for a new student to take his place on the project.

For example, the figure below shows a COMSOL velocity solution obtained for flow over a flat plate typical of HFIR thin plate and flow conditions (flow left to right). This problem demonstrated the ability of COMSOL to obtain the FSI solution, including Arbitrary Lagrangian-Eulerian (ALE) adaptive meshing techniques, which are required to solve a problem of this type. Many questions remain unanswered regarding this solution, however. For example, why did the plate deflect in a preferred direction when all conditions should be symmetrical with respect to this problem? Therefore, no conclusions have been reached with any of these initial solutions at this point.
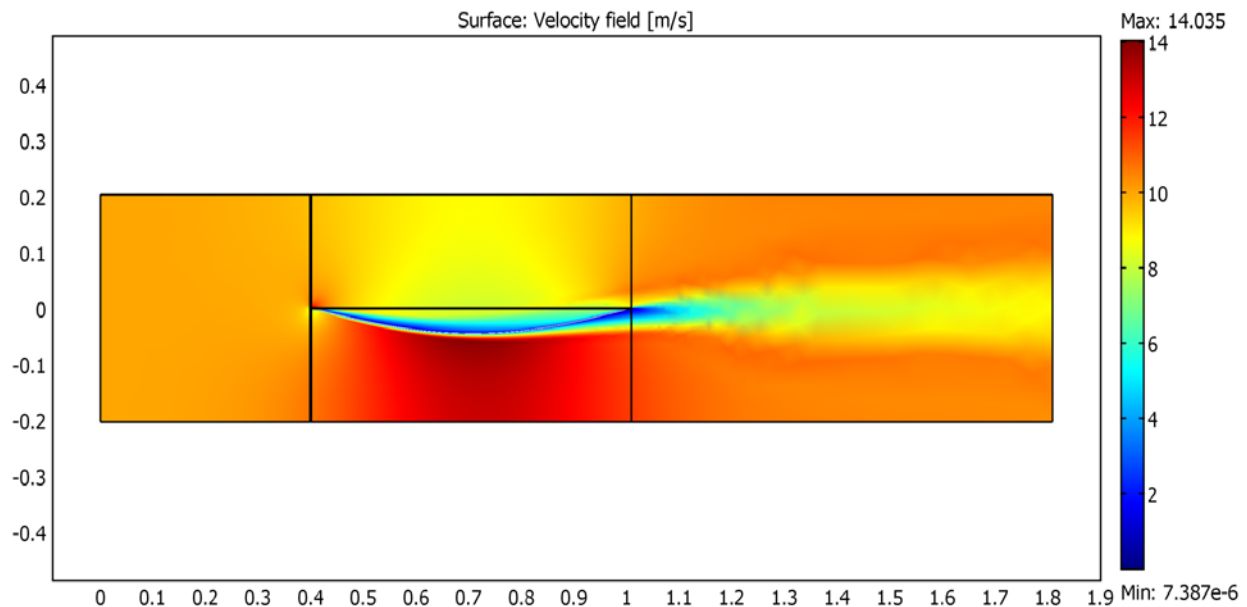
**Fig. 4.1. COMSOL velocity solution obtained for flow over a flat plate typical of
HFIR thin plate and flow conditions.**
(Flow left to right).

Starting in late September 2010, a new graduate student, Franklin Curtis, along with his major professor, Dr. Kivanc Ekici, joined the project under the existing contract with UTK-MABE. We have realized since the first student left the project that we were lacking in direct guidance for the student involved in this part of the work. Furthermore, Dr. Ekici brings a wealth of knowledge in this technical area since his area of expertise is aeroelasticity, which fits perfectly with our need for increased technical expertise in this area of the project.

In addition to recovering the work from the previous student, the new team of Curtis and Ekici has focused their early involvement on performing validation cases that are related to the HFIR fuel-plate FSI problem. Both Curtis and Ekici are new users of COMSOL, so they have also been learning how to use the code.

A complete Fluid-Structure Interaction (FSI) analysis of the HFIR plates involves the solution of both fluid dynamics and structural dynamics problems, which need to be coupled through the use of the ALE in COMSOL. Validation of COMSOL for each individual problem (fluid dynamic and structural dynamic) should be the first step in ensuring the validity of the coupling mechanism in a much more controlled environment. The structural dynamics module of COMSOL was the first component of the FSI problem to be explored. The goal of the exploration was to validate the accuracy and verify the use of a linear structural solver in COMSOL.

Two recent validation problems are noteworthy and are reported here. The analytical solutions for the cases presented herein can be found in *Analytical Methods in Vibrations*, by Leonard Meirovitch.[9] These solutions were compared to the computational results obtained using COMSOL's "Eigenfrequency analysis" module. The first test case involves the eigen-analysis of a uniform cantilevered beam with transverse vibration.

Consider a uniform cantilever beam of length L fixed at $x = 0$ and free at the other end, as shown in Fig. 4.2. The general equation, which describes harmonic transverse free vibrations of this cantilever beam is given by

$$\frac{d^2}{dx^2}\left[EI\frac{d^2Y(x)}{dx^2}\right] = \omega^2 m\, Y(x) \tag{4.1}$$

where *EI* is the bending stiffness, ω is the natural frequency of vibration, and *m* is the mass per unit length.
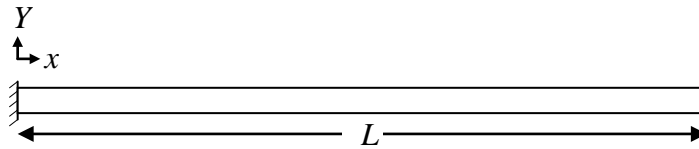
Fig. 4.2. Schematic of the cantilevered beam analyzed.

The solution of Eq. 4.1 requires zero deflection and slope at the fixed end and zero moment and shear at the free end. Therefore, the boundary conditions can be written as

$$Y(0) = 0, \quad \frac{dY(0)}{dx} = 0 \tag{4.2}$$

and

$$\frac{d^2Y(L)}{dx^2} = 0, \quad \frac{d^3Y(L)}{dx^3} = 0 \tag{4.3}$$

The differential equation governing the motion of the beam can be further simplified as

$$\frac{d^4Y(x)}{dx^4} - \beta^4 Y(x) = 0$$

where (4.4)

$$\beta^4 = \frac{\omega^2 m}{EI}$$

As can be seen, Eq. 4.4 is a fourth order linear ordinary differential equation for which the generalized solution is given by

$$Y(x) = C_1 \sin(\beta x) + C_2 \cos(\beta x) + C_3 \sinh(\beta x) + C_4 \cosh(\beta x) \qquad (4.5)$$

where the constants C_1, C_2, C_3, and C_4 are determined from the boundary conditions.
Equation 4.5 along with the boundary conditions determines the natural frequencies of vibration through

$$\cos(\beta L) \cosh(\beta L) = -1 \qquad (4.6)$$

An investigation of the solution above reveals that there are an infinite number of values for β, which determine the natural frequencies based on the parameters given in Eq. 4.4. As an example, the natural

frequency for the first bending mode would be $\omega = 1.875^2 \sqrt{\frac{EI}{mL^4}}$. As the next step in the analysis, this

and subsequent bending modes were computed in COMSOL and the numerical results were compared to the analytical solutions given by Eq. 4.6. The COMSOL analyses were performed for a three-dimensional beam for the following variables:

Length (L)	1 m
Width (w)	0.1 m
Thickness (t)	0.01 m
Density	2780 kg/m^3
Young's Module (E)	70 GPa
Poissais Ratio (v)	0.33

where w is the width of beam, t is the thickness of the beam, E is the elastic modulus, and v is the Young's modulus of the beam. The results of the analysis are provided below in Table 4.1. It can be seen that the agreement between the analytical and computed eigenfrequencies is very good with a difference no larger than 0.9%.

Table 4.1. Natural frequencies for the first four bending modes

	Analytical values, Hz	COMSOL, Hz	% Difference
Mode 1	8.106005293611	8.176084907221	0.8645
Mode 2	50.799468041394	51.206255349876	0.8008
Mode 3	142.239981469321	143.410069368738	0.8226
Mode 4	278.733593766735	281.241079959632	0.8996

Having determined the natural frequencies of free vibrations, we now turn our attention to the eigenmodes of the solution. Figure 4.3 shows the solution for the third eigenmode as provided by COMSOL for the transverse solution. It must be noted that, although not shown here, the eigenmode computations from COMSOL agree well with the analytical eigenmodes given by Eq. 4.5.
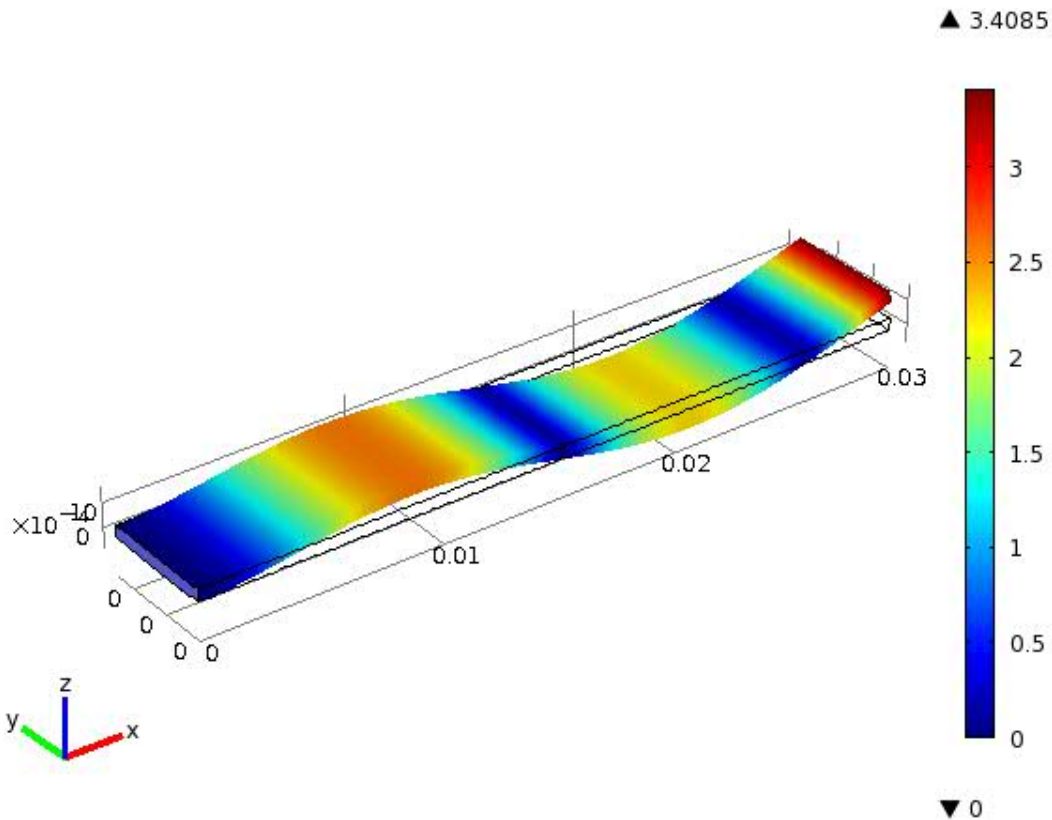
Fig. 4.3. Modeshape for the third eigenmode solution of a cantilever beam undergoing free vibrations.

Since the Eigenanalysis module of COMSOL involves finite element solution of the structural dynamics problem for a more generalized form of the governing equations, the numerical results include all possible modes (bending, torsion, etc). The cantilevered beam has many other analytical solutions for frequency; for further verification, torsional vibrations were also explored and compared to analytical solutions provided by Meirovitch. The solution for the beam in torsion fixed at one end follows the same steps as shown for the transverse vibrations and yields the frequency equation given by

$$\tan(\beta L) = \frac{1}{\beta}, \beta^2 = \frac{\omega^2 I}{GJ} \tag{4.7}$$

Similar to the transverse problem, there are an infinite number of solutions to the equation given above each corresponding to a different eigenmode. The analytical and COMSOL values for the first four modes are given in Table 4.2. Similar to the transverse analysis, the torsional frequencies agree well with the analytical solution, with a maximum error of 1.6%.

Table 4.2. Natural frequencies for the first four torsion modes

	Analytical Value, Hz	**COMSOL, Hz**	**% Difference**
Mode 1	155.86767693068	153.42017927161	1.5702
Mode 2	467.60303079204	465.39015705743	0.4732
Mode 3	779.33838465341	779.53697579606	0.0255
Mode 4	1091.07373851477	1108.50023918975	1.5972

Although the results presented up to this point give confidence in the eigenanalysis calculation capabilities of COMSOL, a cantilevered beam is not an accurate representation of the geometry used for HFIR. The geometry that most resembles the HFIR plates is a flat plate pinned along its edges parallel to the flow direction. To perform this analysis, COMSOL was run using the shell analysis module together with the eigenfrequency module. The flat plate has the same parameters as the cantilevered beam with the exception that $w = L$.

The analytical results can be obtained by solving the governing equation of a flat plate undergoing free vibrations given by

$$\nabla^4 W(\text{x,y}) - \beta^4 W(\text{x,y}) = 0 \, , \beta^4 = \frac{\omega^2 \rho}{D_E}. \tag{4.8}$$

where $D_E = \frac{Eh^3}{12(1-v^2)}$ is constant for a plate of uniform density. The boundary conditions for a plate with a pinned edge can be written as

$$W = 0 \text{ and } M_n = \frac{\partial^2 W}{\partial n^2} = 0. \tag{4.9}$$

leading to the frequency equation for the general system given by

$$\omega_{mn} = \pi^2 \left[\left(\frac{m}{a} \right)^2 + \left(\frac{n}{b} \right)^2 \right] \sqrt{\frac{D_e}{\rho}}, \tag{4.10}$$

where a and b are length and the width of the flat plate and m and n are any positive integers (1,2,….). For the results presented here, a square plate geometry was used so that $a = b = L$. COMSOL computations were performed using a fine computational mesh consisting of 19,998 elements. The eigensolutions for the first 250 modes were obtained numerically and frequencies were compared to theoretical values obtained from Eq. 4.10. Table 4.3 presents these results, which demonstrate a good overall agreement between the analytical and numerical calculations. Note that for some of the modes, COMSOL computations yield less accurate results, which need further attention.

Table 4.3. Natural frequencies for a pinned flat plate

	COMSOL, Hz	Analytical values, Hz	% difference
m=1, n=2	74.4224963	75.7255658	1.7207786752
m=1, n=3	145.3374838	151.4511316	4.0367131534
m=1, n=4	258.5884021	257.4669237	0.4355815648
m=1, n=5	393.8707364	393.7729421	0.0248352008
m=1, n=6	577.2293649	560.3691869	3.0087625148
m=1, n=7	748.4518989	757.2556580	1.1625874257
m=1, n=8	1006.7561269	984.4323553	2.9932655376
m=1, n=9	1275.8647576	1241.8992790	0.5170754727
m=1, n=10	1546.2396948	1529.6564291	0.1854406185
m=1, n=11	1870.0211660	1847.7038054	0.0702146314
m=1, n=12	2240.4289436	2196.0414081	0.1061081849
m=1, n=13	2602.8151673	2574.6692370	0.1720152409
m=1, n=14	3041.2318956	2983.5872923	0.0285215235
m=1, n=15	3496.8459105	3422.7955739	0.0179422767

To ensure accuracy of the results from the mesh used, a mesh refinement study was performed. For the mesh refinement, the model was built with approximately 5,000 nodes and doubled for each consecutive mesh except for the last mesh, which was set to approximately 180,000 elements. The mesh refinement study, along with the computational times on the cluster compute node betty01 are provided in Table 4.4. In addition, Fig. 4.4 shows the percent difference between the predicted values and numerical results for the first frequency.

Table 4.4. Mesh refinement study

| Mesh #	Elements	Degrees of freedom	Computational time (s)
1	4998	122352	87
2	10080	245328	176
3	19998	484752	330
4	39754	960840	718
5	79992	1929384	2122
6	179982	4333920	3184
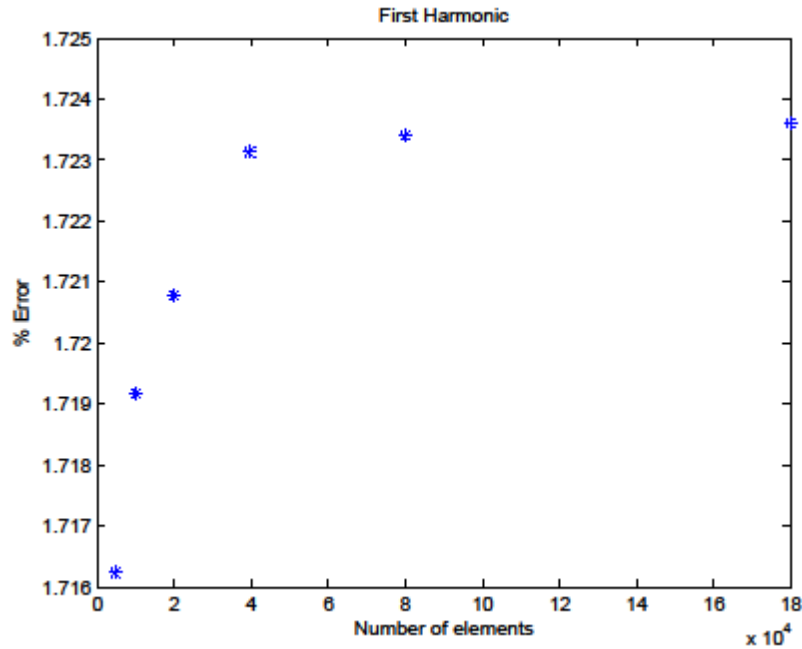
Fig. 4.4. Percent error for the first eigenfrequency solution.

As expected, the error approaches an asymptotic value as the mesh is refined. Strangely, the first two frequencies get progressively worse with mesh refinement. On the other hand, the third through fifth frequencies follow a pattern more representative of a numerical solution. The error exponentially decreases to an asymptotic value as seen in Fig. 4.5 for the third harmonic.
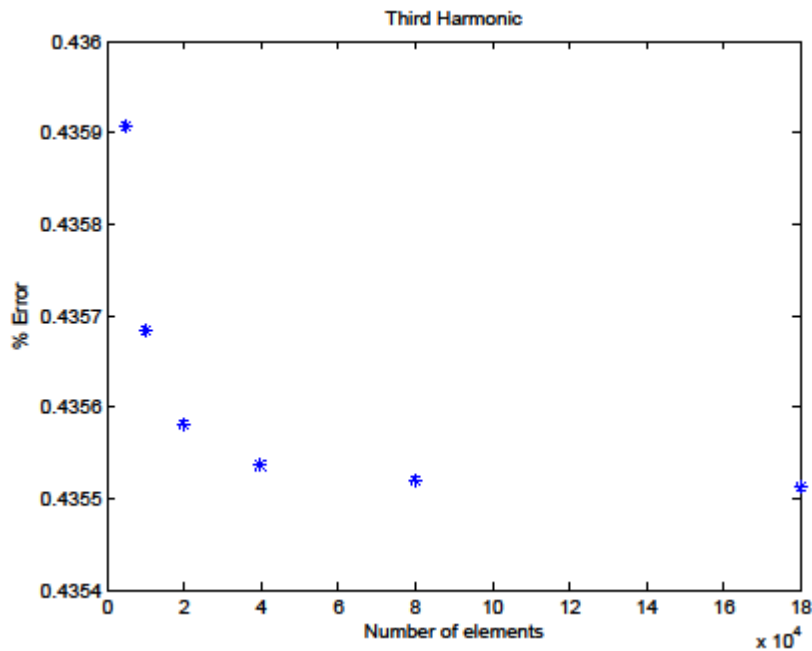

Fig. 4.5. Percent error for the third eigenfrequency solution.
The eigenfrequenices for each harmonic were also compared to the final mesh values. These values were plotted on a log scale with the percent difference plotted along the y-axis as shown in Fig. 4.5.
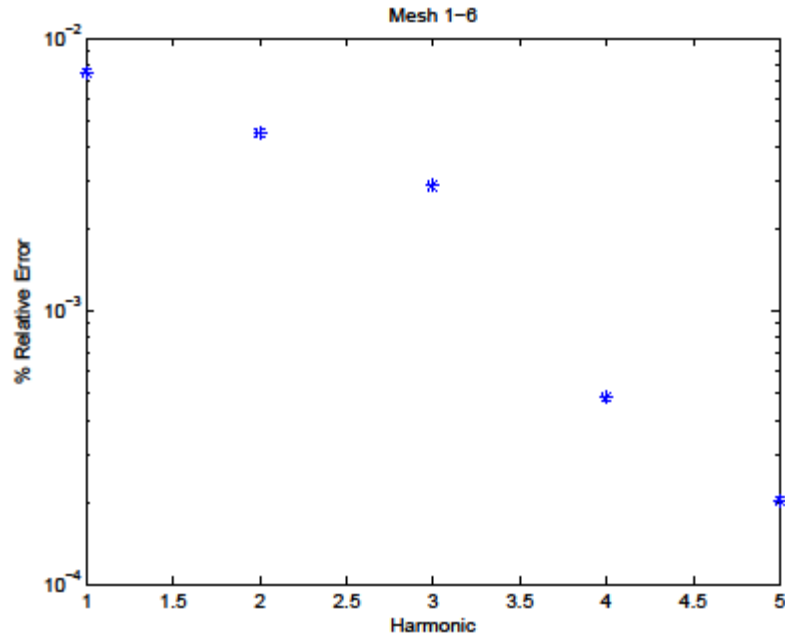
Fig. 4.6. Percent relative error of coarse mesh and finest mesh results.

Figure 4.6 follows the predicted linear relationship for the FEA analysis percent difference with the exception of the outlier point seen in the figure. The remaining eigenfrequencies follow similar trends and Table 4.5 provides the results.

**Table 4.5. Percent relative error for each harmonic and mesh
compared to the solutions obtained with the final mesh**

	Mesh 1-6	Mesh 2-6	Mesh 3-6	Mesh 4-6	Mesh 5-6
Harmonic 1	0.0075018562	0.0045052540	0.0028765574	0.0004830741	0.0002032999
Harmonic 2	0.0141913344	0.0084484391	0.0053406571	0.0009353541	0.0003922440
Harmonic 3	0.0003931207	0.0001705460	0.0000689780	0.0000236865	0.0000079895
Harmonic 4	0.0007057255	0.0002682391	0.0001012045	0.0000337348	0.0000110537
Harmonic 5	0.0014578905	0.0004655297	0.0001560335	0.0000488454	0.0000148849

Examining the analysis performed using COMSOL, one can be confident that the program numerically simulates the eigenfrequency analysis that will be used for the structural part of the FSI studies. This more rigorous approach has been welcomed by the project team as we now feel more comfortable that the FSI technical area will be investigated with a more traditional approach to this type of problem solving. A new statement of work for CY 2011 has been generated which clearly identifies the FSI tasks to be completed which include a direct simulation and comparison to the OSU tests for the generic plate tests.

4.2   Thermal-Structural Interaction

The HFIR fuel plate is mounted to the side plates of the fuel element by intermittent welds along its axial length. A full 3-D COMSOL model is able to simulate the effect of the welds on the behavior of the plate as a result of thermal stresses. A simpler 2-D model, as presented herein, will not be sufficient for all details. The present COMSOL 2-D model represents an axial slice at the center of the fuel plate extending out into the adjacent flow channel, as indicated by the red line in Fig. 4.7. COMSOL version 3.5a was used to model the thermal-structural interaction (TSI) due to its availability at the time this study was performed during CY 2010 and familiarity with this version of the software.

The decision to perform 2-D modeling of the TSI was made in an effort to become familiar with the processes involved in TSI modeling with COMSOL before attempting a full 3-D simulation. 2-D models are naturally less difficult to solve than 3-D, and they are less computationally expensive.
The 2-D model of the plate is taken at arc length position 6 of the involute geometry as outlined in the SSHTC. This position was chosen due to the minimal influence of the burnable poison at that position.
Figure 4.7 shows a top-down cross-sectional view of the fuel plate.
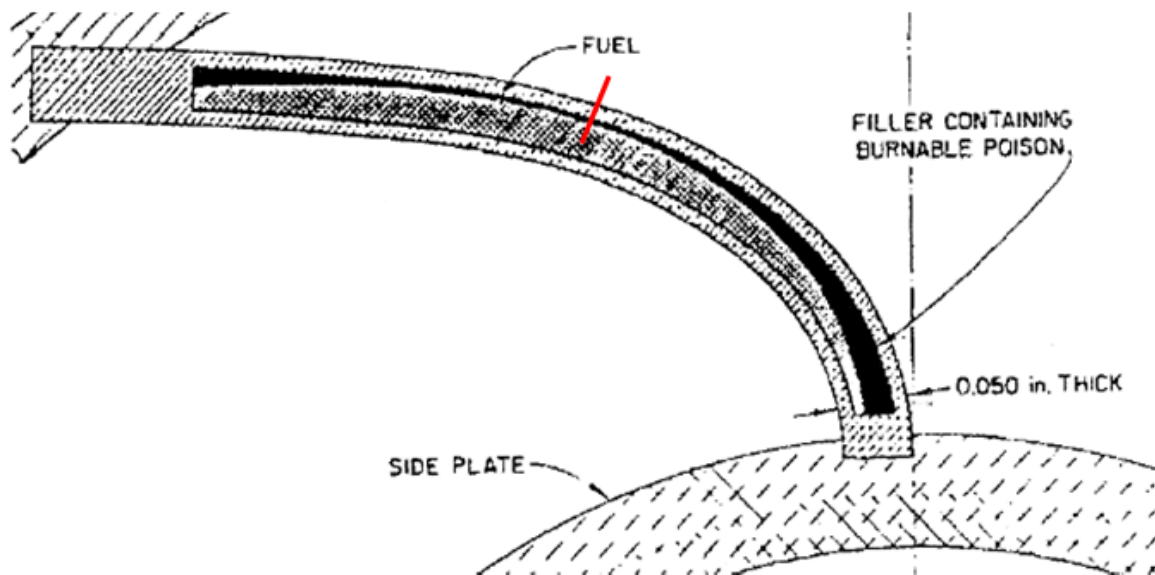
Fig. 4.7. Top view of HFIR fuel plate.
The red line represents the 2-D section of the fuel plate used in the model.
This section spans the entire 24 inch length of the fuel plate.

The physics modeled is that of plane stress coupled with heat transfer and fluid flow. The deformation of the plate due to normal stresses caused by the flowing fluid (fluid-structure interaction or FSI) is discussed in other sections of this report. In this TSI study no arbitrary Lagrangian-Eulerian Formulation (ALE) was used and, as a result, no mesh deformation was modeled. The fluid affects the simulation by removing heat from the fuel plate, and therefore, influencing the temperature distribution within the plate that causes the thermal stress.   The details of the thermal-fluid interaction (TFI) physics may be found in ref. 4. The subdomain data that were supplied to the software were material properties, constraints, and load. The details of the clad subdomain inputs are reported in Table 4.6.

Table 4.6. Clad subdomain settings for plane stress

Property	Value	Sources
Young' Modulus, E	68.9 GPa	Ref. 10
Poisson's Ratio, υ	0.33	Ref. 10
Coefficient of Thermal Expansion, α	2.43×10^{-5} 1/K	Ref. 6
Constraint	Free	
Strain Temperature	T_s	
Strain Reference Temperature	321.9 K	Ref. 7

The strain temperature, T_s, is the internal plate temperature determined from the TFI. The details of the fuel subdomain inputs are reported in Table 4.7.

Table 4.7. Fuel subdomain settings for plane stress.

Property	Value	Sources
Young' Modulus, E	70 GPa	Ref. 11
Poisson's Ratio, υ	0.33	Ref. 10
Coefficient of Thermal Expansion, α	2.4×10^{-5} 1/K	Ref. 11
Constraint	Free	
Strain Temperature	T_s	
Strain Reference Temperature	321.9 K	Ref. 7

In order to model the effects of the thermal stresses upon the structure of the fuel plate in 2-D, assumptions on boundary conditions are necessary. In a full 3-D model, stresses in the arclength direction are present as a result of the constraint due to the welds along the side plates. Since the leading and trailing edges and the clad-coolant interface are indeed free to move during thermal cycling, the most natural boundary condition is that of a surface that can move but is also restrained due to stresses set up in the adjacent material. These constraints cannot be represented in this simplified 2-D model representation. With the exception of the plate symmetry boundaries, all other boundaries are modeled in this 2-D representation as free. Thus the boundaries will deform more than physically possible. Therefore, it can be stated that these results are conservative with respect to maximum thermally-induced displacement normal to the fuel-plate thickness. The temperature and deformation results of this simulation are shown in Fig. 4.8.
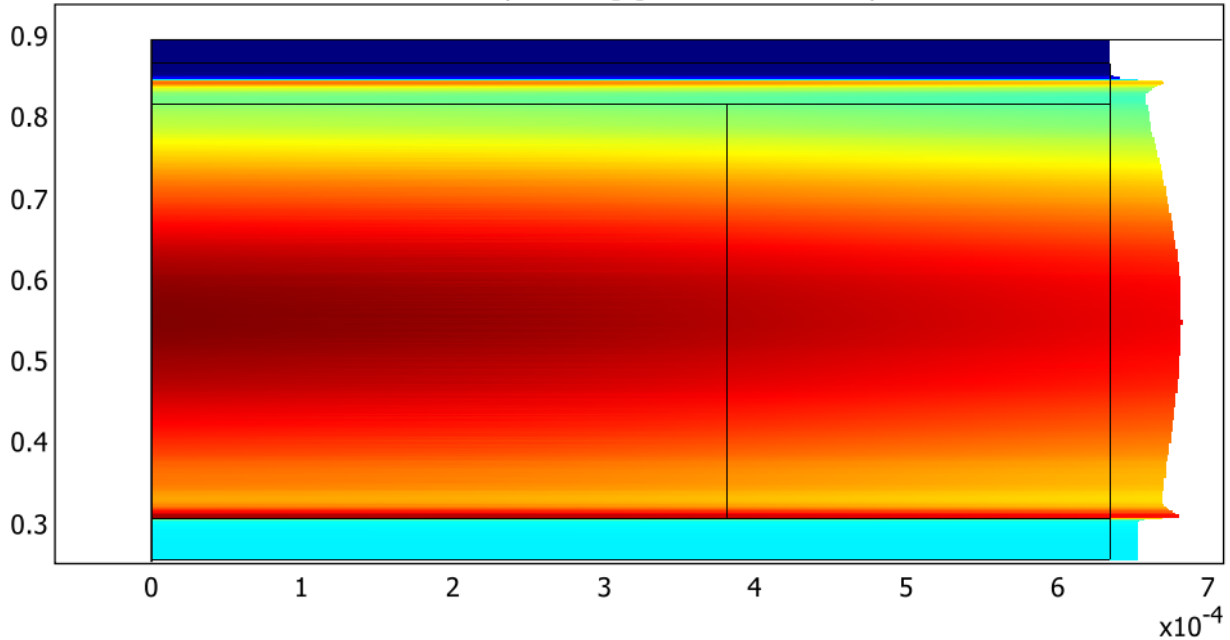
Fig. 4.8. Results of the thermal-structural interaction simulation.
The color scale is representative of temperature. The deformation, in units of meters, is shown relative to the solid lines with a scaling factor of 30.06. The x and y axis represent the fuel plate half-width (nominal 0.025") and height (24") as an unequal scale for visualization purposes in units of meters.

The maximum temperature (dark red) in the simulation is 428.38K and the minimum temperature (dark blue) is 321.9K. An input-scaling factor is imposed that increases the visualization of the deformation by 30.06, i.e. the visualized deformation seen in Fig. 4.7 is approximately 30 times larger than it truly is. Even though the deformation is small ($\sim 10^{-4}$ m) relative to the overall axial height of the plate, these results do demonstrate the potential for delamination of the LEU fuel plate if the solid layers within the plate (not modeled in this study) do not expand at similar rates.

The profile of the deformation matches that of the smooth power density profile in the fuel. This is intuitive when considering the aspect ratio of the HFIR fuel plate, i.e. the aspect ratio length to width is 480. Even though the heat is conducted in an isotropic manner throughout the plate, most of the heat will leave the plate through its long 24 inch (0.6096 m) face in a direction normal to that face. Considering Fourier's law of heat conduction

$$q = -kA\nabla T \tag{4.11}$$

one finds that the amount of energy conducted is proportional to the cross-sectional area. Therefore, since the long face of the HFIR plate has the larger surface area it stands to reason that the majority of the heat will pass out of the plate through this face. As a result, the power density profile will manifest itself in the temperature profile and the deformation shape shown.

It is important to reiterate that this model is not a complete representation of the all the physics associated with the full 3-D thermal-structural interaction that is present in the HFIR fuel element. This is primarily due to the lack of deformation constraints that can be simulated in this simplified 2-D model. The only way to obtain an accurate simulation of all the desired phenomena is to model a full 3-D plate where the weld constraints along the side plates can be represented appropriately. While the deformation shown in Fig. 4.8 is larger than what is physically allowable, the profile of the deformation is indeed correct and the general trend is appropriately demonstrated.

The deformation profile also provides insight into potential deviations of the flow field due to thermal stresses in the plate that may adversely manifest themselves due to the high rate of flow through the core. Regarding the transfer of heat, separation of flow may occur in the channel at local deformation peaks, which could establish eddies and thus decrease the efficiency of the transfer of heat to the fluid from the plate. Regarding scale build up and the decrease of clad integrity due to corrosion, the impingement of the fluid at the deformation peaks could increase the potential for spalling of clad material. These are just a few examples of phenomena that could occur due to the physical form of the clad during and after thermally-induced deformation.

More detailed and accurate simulations of the HFIR fuel plate are to be performed during FY 2011.

5.0   DEVELOPMENT OF SIMPLIFIED 3D MODELS

As discussed previously in Section 3.0, COMSOL has its own computer-aided design (CAD) interface and it also supports other popular commercial CAD packages (Pro-E, SolidWorks, etc.) for creating 3D geometry models. HFIR's fuel plate (both the inner fuel plate as well as the outer fuel plate) has a very specific shape—a mathematical involute—which must be correctly represented to capture the geometry and, consequently, the physics correctly. Using the equations of an involute for the convex and concave edges of the fuel plate, a representative 3D geometry has been created in COMSOL. Note that this capability (parametric curve) did not exist in COMSOL until version 4.1. Based on the single plate geometry, a strategy has been identified to automatically create <u>any</u> number of plates and their respective channels in a minimal number of user steps. This capability will be essential for multi-plate and multi-channel simulations.

In the following sub-sections:

*   Starting with the mathematical equation of a typical involute curve, we will describe the equations governing the involute curves for both the convex and concave edges of a HFIR fuel plate. Equations will be provided for both the inner as well as the outer plate of the HFIR core.

*   Using the abovementioned equations, steps to create the 3D geometry for one plate in the COMSOL CAD interface will be presented.

*   Using the 3D plate CAD geometry as the basis, steps will be presented for creating the geometry for multiple plates and channels in a minimal number of user steps.

5.1   MATHEMATICS OF AN INVOLUTE

An involute is defined as a mathematical profile obtained from a given curve (in our case, a circle) by attaching an imaginary taut string to the given curve, and tracing its free end as it is wound (or, unwound) onto that given curve. In Fig. 5.1 below, creation of a circle's involute is illustrated.


A simple cylinder and a string.

Wrap the string around the cylinder.

Pull

Pull the string tight and keep it tangent to the cylinder.

Involute curve

Trace the end of the string while un-wrapping it around the cylinder. The resulting trajectory is an involute curve.
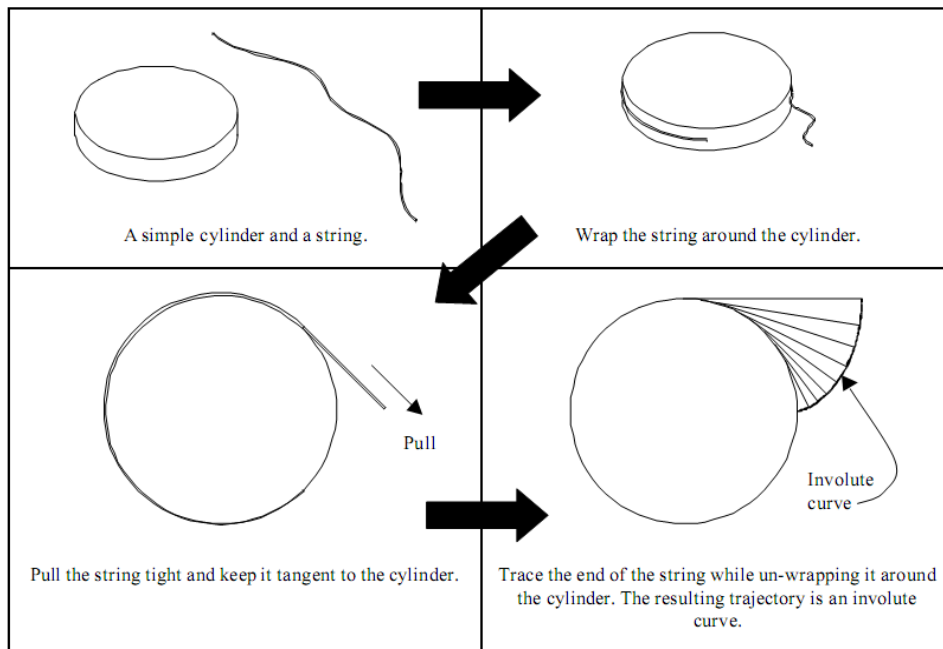
Fig. 5.1. An example for the generation of an involute curve from a circle.

There are two key parameters that control the involute curve of a circle: (i) the radius of the base circle, and (ii) the angle that the string is unwrapped around the circle. Notice that in the example shown in Fig. 5.1, the string is unwrapped 90° around the circle. Next, we will write the equations for this right-angle involute profile.

From Fig. 5.2, we can write the equation for the free end of the string ((x,y) point in the figure) which is the equation of the involute curve.
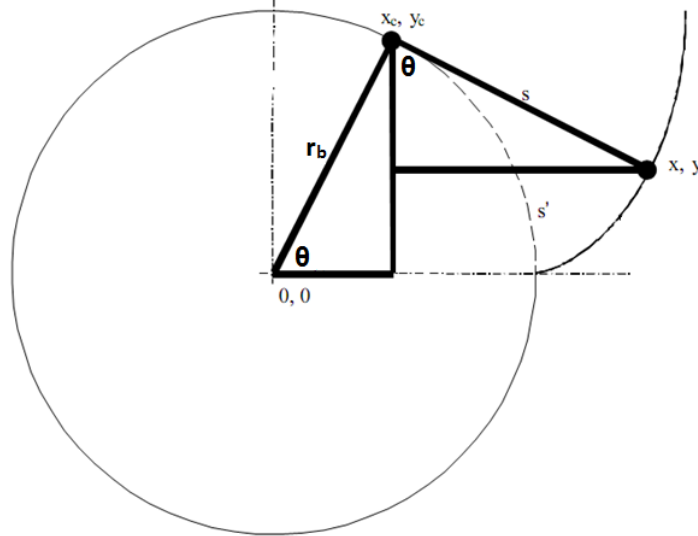

Fig. 5.2. Equations for a right-angle involute circle.

From Fig. 5.2, we can write:

$$x = x_c + s \sin \theta$$
$$y = y_c - s \cos \theta$$

where $x_c = r_b \cos \theta$, $y_c = r_b \sin \theta$ and $s = r_b \, \theta$.

Here, r_b is the radius of the base circle and θ is the angle of unwrapping (in the units of radians).

5.2   INVOLUTE EQUATIONS GOVERNING THE HFIR'S PLATE GEOMETRY

A top view sketch of HFIR's inner and outer fuel element is shown in Fig. 5.3 with all the necessary dimensions. Below we provide the governing equations for the convex and concave edges of the inner and outer fuel plate:

    i.   Inner plate – Convex side

For the convex side of the inner fuel plate, the equation of the involute can be written as:

$$x = r_b \left(\cos \theta + \theta \sin \theta \right)$$
$$y = r_b \left(\sin \theta - \theta \cos \theta \right)$$

where $r_b = 2.7215$ in., and θ varies from 0° to 89.233015^o.
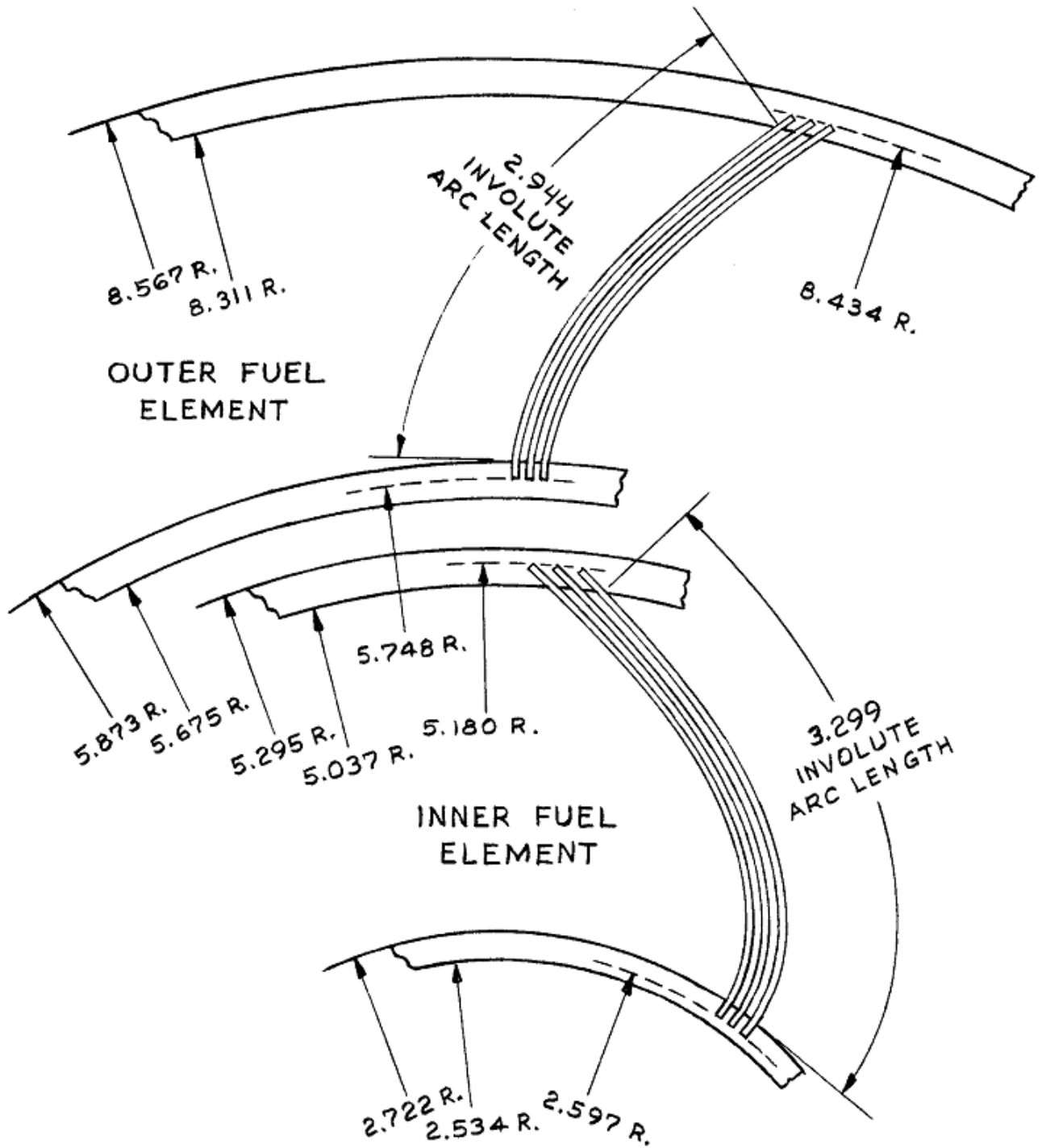
Fig. 5.3. Geometry and dimensions (in inches) for HFIR's inner and outer fuel element plates (R: radius).

ii. Inner plate – Concave side

For the concave side of the inner fuel plate, the equation of the involute can be written as:

$$x = r_b \cos\theta + (r_b\theta - t)\sin\theta$$
$$y = r_b \sin\theta - (r_b\theta - t)\cos\theta$$

where r_b = 2.7215 in., and θ varies from $1.05271°$ to $90.28567°$. Here, t is the thickness of the fuel plate (= 0.05 in.).

iii. Outer plate – Convex side

For the convex side of the inner fuel plate, the equation of the involute can be written as:

$$x = r_b \ (\sin\theta - \theta\cos\theta)$$
$$y = r_b \ (\cos\theta + \theta\sin\theta)$$

where r_b = 5.873 in., and θ varies from $0°$ to $57.3666°$.

iv. Outer plate – Concave side

For the concave side of the inner fuel plate, the equation of the involute can be written as:

$$x = r_b \sin\theta - (r_b\theta - t)\cos\theta$$
$$y = r_b \cos\theta + (r_b\theta - t)\sin\theta$$

where r_b = 5.873 in. and t is the thickness of the fuel plate (= 0.05 in.).

Note that, in HFIR's inner and outer elements, the involute fuel plates are assembled such that their corresponding convex or concave faces are opposite to each others' (see Fig. 5.3 and observe the opposite facing of the inner and outer fuel elements). This is the reason that, in the above equations for the outer plate, equations for the x and y coordinates are different from their inner plate counterparts (equation for the outer plate's x-coordinate corresponds to the inner plate's y-coordinate equation, and so on).

5.3   3D CAD MODEL DEVELOPMENT FOR HFIR'S FUEL PLATE IN COMSOL

Using the new Parametric Curve feature of COMSOL, introduced in version 4.1, one can now build CAD geometry in COMSOL using parametric equations defining the coordinates of the curve. Internally, the software represents the parametric curve by a B-spline, which is computed to approximate the mathematical curve defined by the x, y, and (in 3D) z expressions. The number of knot points in the spline increases automatically until the curve approximation satisfies the tolerance specified in the Relative tolerance edit field of COMSOL or until it reaches the number of knots specified in the Maximum number of knots edit field of COMSOL.

Several steps to successfully create CAD geometry for the involute fuel plate in COMSOL are outlined below and also, shown in Fig. 5.4:

i. Involute curve generation for the convex and concave sides of the plate using the equations described earlier.

ii. Generation of 2D involute-shape surface by connecting the ends of both the curves (Fig.5.4, part 2).

iii. Taking the difference of the above involute surface with the side-plate circles (Fig. 5.4 [parts 2 and part 3]).

iv. Extrusion of the surface in the z-direction to produce the 3D involute plate (Fig. 5.4, part 4).
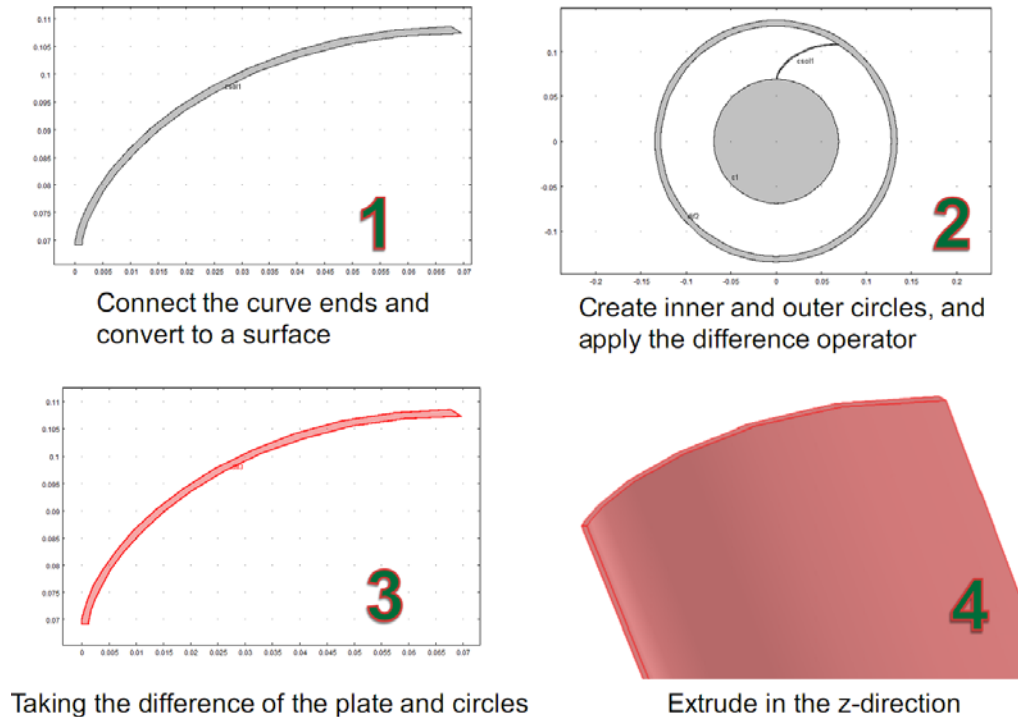
Fig. 5.4. Steps to create CAD model of HFIR's fuel plate in COMSOL.

5.4   CREATING MULTIPLE PLATES AND CHANNELS IN COMSOL

Once the CAD model for a single plate is developed in COMSOL, we can now rotate this plate to create multiple plates which are adjacent to each other. Because the plates and channels are of the same shape and size, this task can be performed in a single step using the COMSOL's Rotate feature. As shown in Fig. 5.5, the angle of rotation (theta in the figure) can be defined as a global parameter and then used in the Rotate feature to create multiple plates. For example, in Fig. 5.6, five adjacent plate regions are created in 2D. Also notice that because of rotating a single plate to create multiple side-by-side plate regions, we now have two interfacial curves loosely overlapping each other (leaving gaps and overlaps, the lower panel in Fig. 5.6). Since, in reality, we only have a single interface in between a fuel plate and its adjacent coolant channel, we have to merge these two interfacial curves with a relative tolerance using the Union operator of the COMSOL, as shown in Fig. 5.7.

In Fig. 5.8, the significance of using the Difference operator with the side plate circles is illustrated. In the absence of this operation, there will be very short edges left at the interfacial boundaries ultimately leading to the meshing difficulties. Resulted multiple 2D regions from Fig. 5.8 can now be extruded in the z-direction to create multiple plates and channels in 3D.

Fig. 5.5. Rotation of a single involute plate in 2D to create multiple plates and channels in COMSOL.

Fig. 5.6. Multiple adjacent plates in 2D are created using the rotate feature of COMSOL.

As shown, the interface between any two adjacent plates is now composed of two loosely overlapping curves, which has to be merged together for generating a single interface boundary between two adjacent domains.
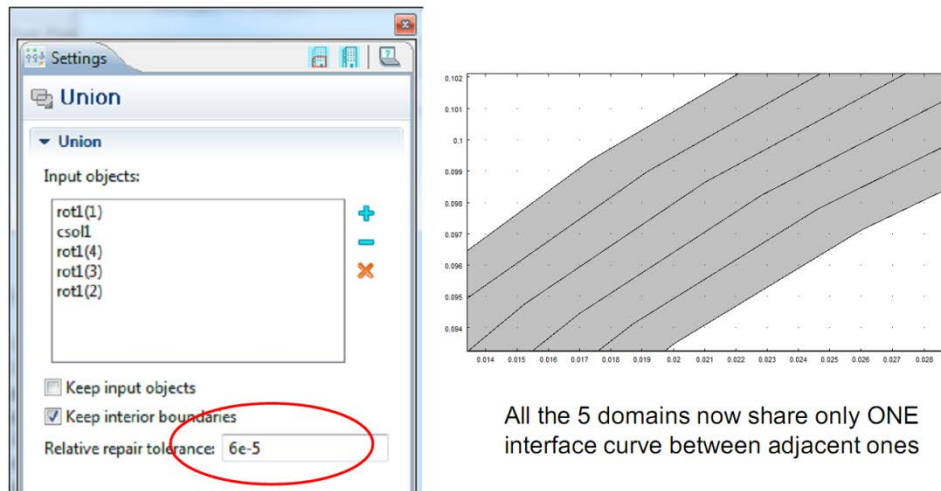
Fig. 5.7. Union operator of COMSOL is used for merging the two interfaces between the adjacent plate regions.
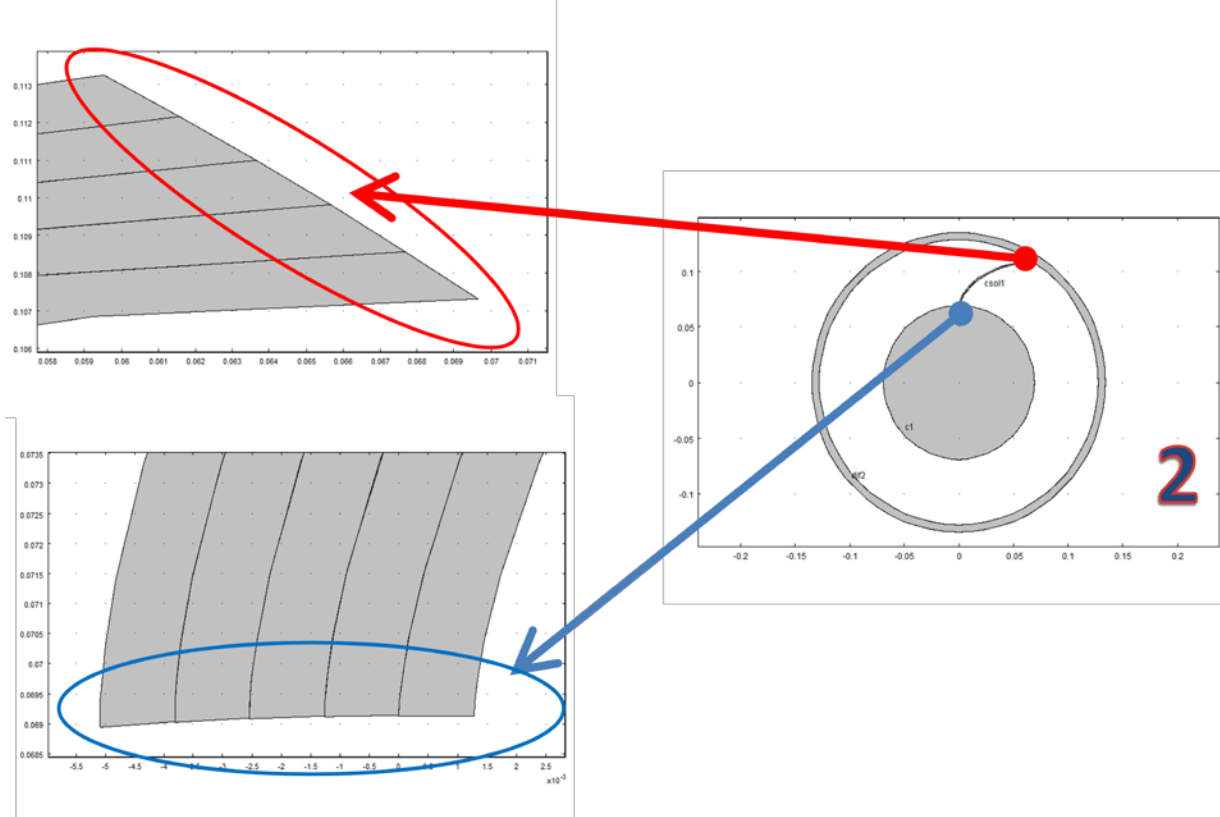

Fig. 5.8. Using the difference operator with the side plate circles (see also, Fig. 4 #2), artificial short edges at the interface boundaries can be avoided.
If present, these short edges usually lead to meshing difficulties.

5.5   FULL-CORE HFIR GEOMETRY DEVELOPMENTS IN COMSOL

Using the earlier described Rotate feature of COMSOL, we can now duplicate a 2D plate region 341 times (172 plates + 172 channels – 1 original plate = 341), as shown in Fig. 5.9, to produce the full inner core region of the HFIR. After extruding the 2D regions for 24 inches in the z-direction, we can build the full inner core of HFIR in 3D, as shown in Fig. 5.10. Also listed in the left panel of the figure are the operations needed to build the full 3D inner core starting from the equations of the involutes for the convex and concave edges of the fuel plate.
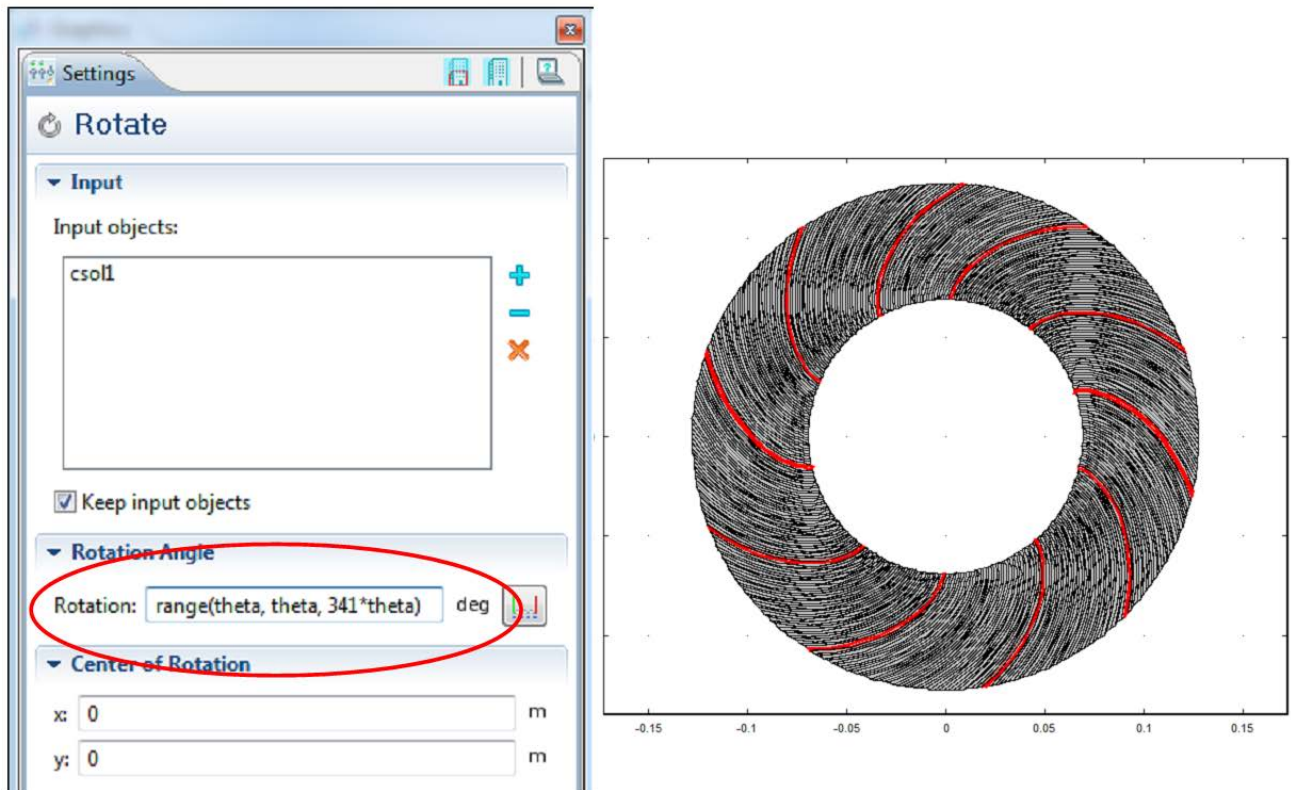

Fig. 5.9. Rotate operation in COMSOL can be robustly performed to automatically generate the full-core 3D geometry for the HFIR core.
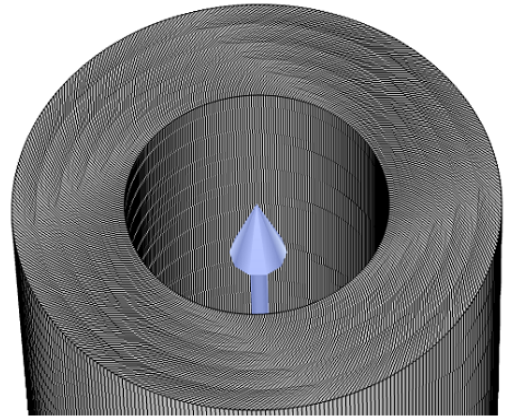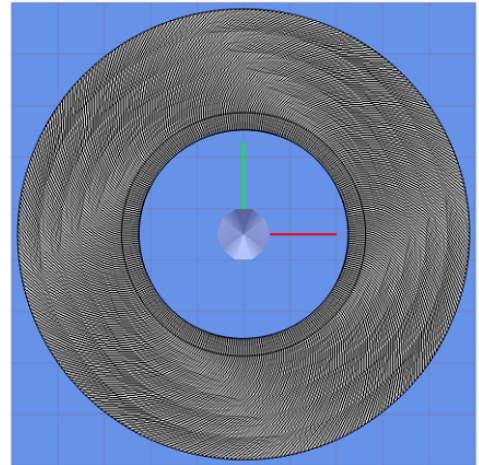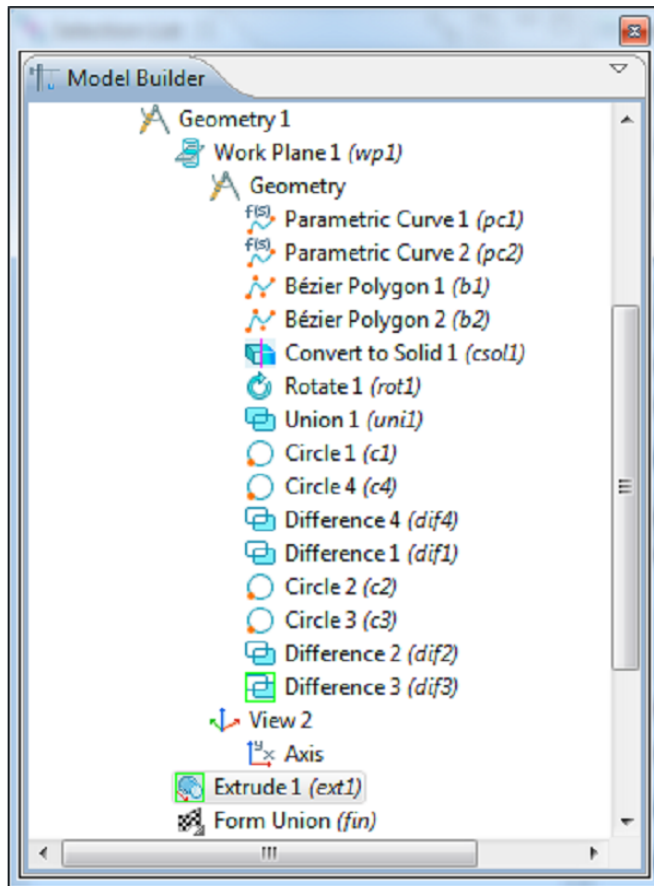
**Fig. 5.10. Full 3D inner core of HFIR with 171 fuel plates
and their adjacent channels as modeled in COMSOL.**

5.6   CREATION OF OFF-DESIGN NARROW AND WIDE COOLANT CHANNELS

For thermal safety analysis of HFIR, we are interested in investigating heat transfer behavior of narrowchannels sandwiched among the fuel plates and the regular sized channels in HFIR's core. Based upon the earlier discussed steps, we have identified a strategy to create narrow channels in COMSOL. These steps are described in Fig. 5.11, and shown in Fig. 5.12 using the COMSOL viewgraphs.
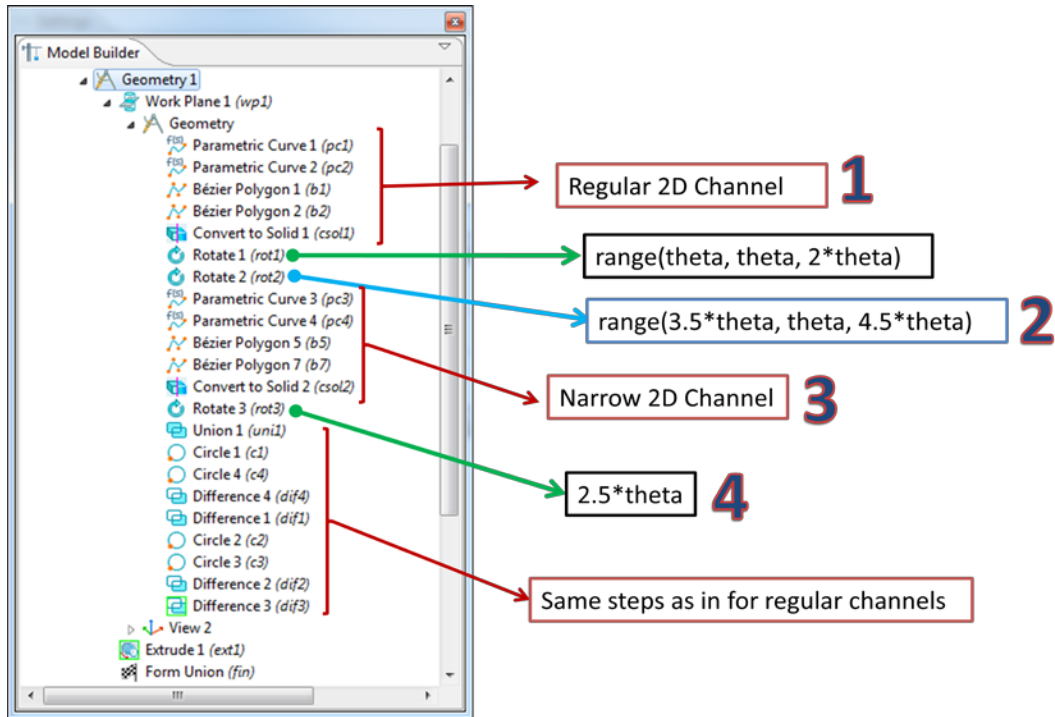
Fig. 5.11. Step-by-step guide for building sandwiched narrow channels in COMSOL for safety analyses purposes.
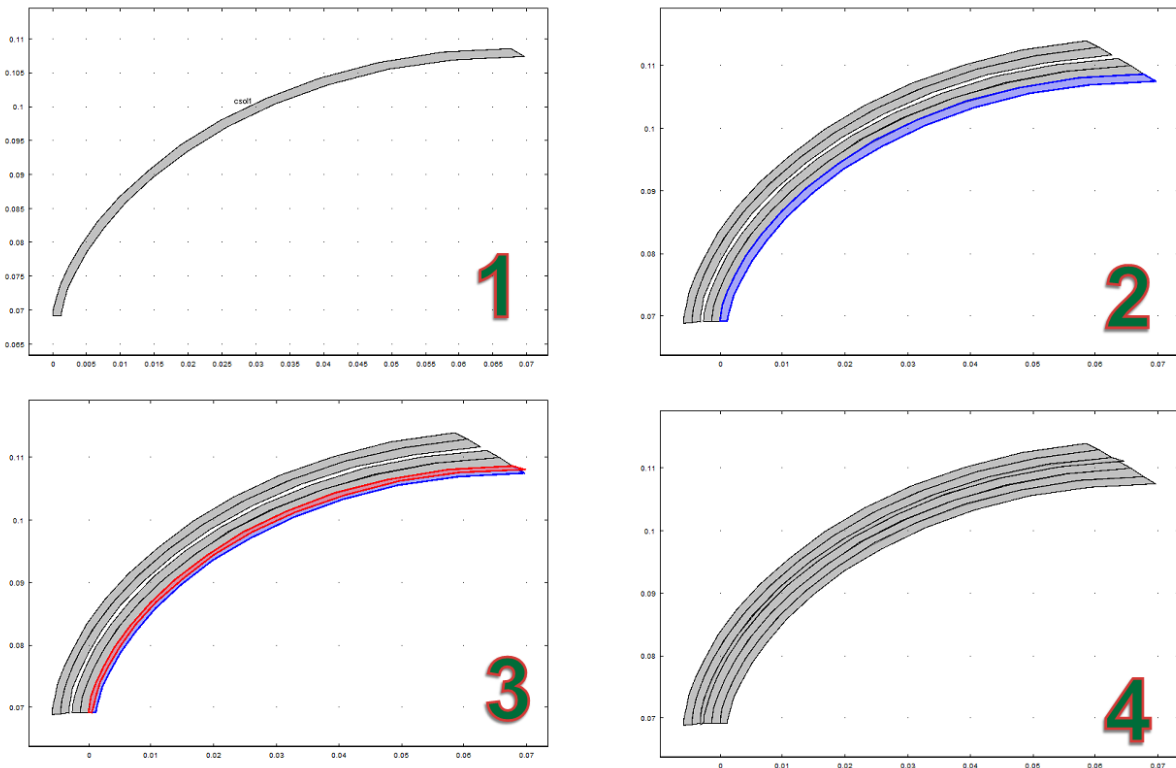
Fig. 5.12. Numbered steps in Fig. 5.11 are shown here for illustration.

6.0   INVESTIGATION OF OXIDE GROWTH MODELING IN HFIR FUEL

The topic of oxide growth upon the HFIR fuel surface during normal operation has been studied and documented previously. These documents are readily available and the determination of the oxide thickness and composition anywhere on the fuel plate as a function of fuel cycle time can be recovered from these documents. Furthermore, the resulting flow degradation, pressure drop, and increased heat transfer resistance that occurs due to the oxide growth is also well known. This data can certainly be compiled and the proper physics incorporated into a global COMSOL model of the HFIR fuel plates currently being developed for this project.

The original idea for this task was proposed by one of the students working on the project to not just incorporate the existing data but to expand the modeling effort to include the actual chemical reactions taking place including all details associated with the formation of the oxide along with transformation of the clad material in combination with the water to form the oxide. This level of detail is certainly possible given the capabilities of the chemical reaction engineering module available as a standard product from COMSOL. The idea was to provide a time-dependent model that would include the HFIR cycle length as the duration of the transient to be simulated. The student had hoped that this idea might become a Ph.D. dissertation topic that he would pursue as a part of this project.

As the student participated more on this LEU conversion project, he decided this task (chemical reaction modeling of the oxide formation process) was not something he wanted to pursue for his PhD, so this task has been put on hold. It is anticipated that the more simplistic approach of using existing correlations for oxide growth will be put into the model after all the more difficult challenges of heat transfer, thermal-structure interaction, and fluid-structure interaction are completed, or at least matured to the point where this task will make sense to spend time on.

7.0 SOFTWARE QUALITY ASSURANCE, INCLUDING AN INVESTIGATION OF DISTRIBUTED PARALLEL PROCESSING

On July 17, 2009, at version 3.5a of COMSOL, the code was qualified and inserted into the catalog of computer codes that could be used for nuclear safety-related calculations for HFIR. In addition to global requirements per ORNL procedures as set forth by DOE, the code qualification followed RRD procedure SBP-1300/R1 to complete this task. The primary effort to complete this qualification was to perform a set of verification calculations which compared COMSOL sample results to model results as shown in the documentation that is delivered with COMSOL at the time.

It was anticipated that with each new major release of COMSOL, this software quality assurance step (SQA) would be repeated and the current version would always be in the catalog as the project moves along. What we discovered upon the release of version 4.0 of COMSOL was that the model library, from which the sample problems were obtained, was not as complete as it was in version 3.5a. As a consequence, the task of SQA verification was not sufficiently diverse in the problem application with respect to the documentation, so this task was deferred until a later time. With each subsequent release (4.0a, 4.1, 4.1a) the model library documentation has been checked and a judgment made as to the adequacy with respect to SQA for purposes of this project. Up until this point, the cost/benefit of the SQA step has been determined to weigh on the side of deferral until a later time.

With the upcoming release of v4.2 (indeed, we are using an early release of v4.2 at the present time on our betty cluster) in late May 2011, the general consensus from the COMSOL code developers is that all the features and documentation level from version 3.5a will be present in version 4.2. In other words, with all the new and improved features in the version 4+ series of COMSOL, the documentation and several "nice" features from version 3.5a were left out (for example, the report generator, and the convergence history plot) or not complete. Therefore, it is anticipated that version 4.2 could be a good point to "freeze" the code version and perform some SQA and generate formal reports and/or calculations with the code for RRD and the LEU conversion project.

Another recent finding from the COMSOL development team is that an ISO-9001 SQA certificate is in the works for a future release of COMSOL. COMSOL has been considering this for some time, and several of the competing software packages already include an ISO-9001 certificate as an integral part of their product. The COMSOL Corporation has come to realize that if they want to expand their market into more industries, such as nuclear, they will find it beneficial to include the ISO-9001 option. If this were to happen, then the SBP-1300 procedure provides a waiver of the verification step since the ISO-9001 certificate guarantees that the software package is verified as part of the installation step. Therefore, there is a tradeoff between taking the time and cost to verify proper code installation for the SQA of the code now prior to the actual creation of the final design/safety analysis documentation for the LEU conversion, versus the promise of an ISO-9001 certificate in the future in time to complete the final calculations.

The COMSOL team has disclosed to us that most of the technical requirements to meet the ISO-9001 certificate are already met with their present code development practices and procedures. The primary holdout on going ahead with the ISO-9001 qualifications is the additional cost associated with obtaining a legal team to provide for the formal certification with ISO. These additional costs would ultimately have to be passed on to the customer. So, it becomes a matter of how to price, and whether it makes good business sense in the long run. At the present time, one advantage that COMSOL offers to their customers for comparable software is their lower price.

One of the verification problems that was included in SQA verification of the 3.5a version of COMSOL was the parallel processing performance for a representative conjugate heat transfer problem typical of what might be encountered on this LEU conversion project. At version 3.5a, only shared-memory parallelism was supported. However, starting with version 4 and later, distributed parallel processing is also supported. This same representative problem was repeated with version 4.1 and the performance is shown below:
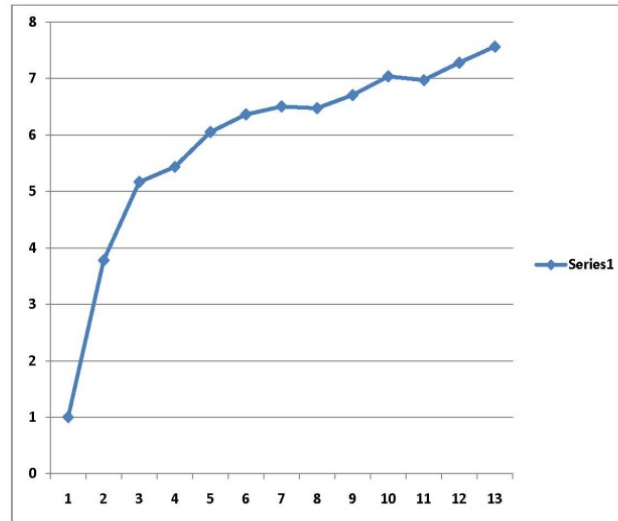

Fig. 7.1. Distributed parallel processing speed-up as a function of Betty Cluster Compute Node Number (+1) for a representative conjugate heat transfer problem for HFIR LEU conversion.

Note that each compute node activates 8 cores so that a total of 12x8=96 cores are used for the last point on the curve. The final 4 compute nodes (9-12) of the betty cluster are 16-core compute nodes, but only 8 cores of these compute nodes are utilized in this benchmark. The detailed core distribution between 1-2 compute nodes agrees closely with the speed-up associated with version 3.5a. This benchmark clearly demonstrates that the speedup does not roll over with this cluster. Therefore, it is certainly true that the speedup potential for COMSOL has not been achieved in this benchmark. Note also, that this benchmark includes a recent upgrade to infiniband communications between the compute nodes that was not present in prior benchmarks of this kind with COMSOL on the betty cluster. Therefore, it is highly recommended to increase the number of compute nodes to realize the full speedup potential for COMSOL in a distributed parallel computing environment.

8.0   REFERENCES

1.   Ilas, Germina, Primm, R. T. III, "Low Enriched Uranium Fuel Design with Two-Dimensional Grading for the High Flux Isotope Reactor," ORNL/TM-2010/318, March 2011.

2.   COMSOL 3.5a Multiphysics Users Guide page 52.

3.   Kays, William, Michael Crawford, and Bernhard Weigand. Convective Heat and Mass Transfer. New York, NY: McGraw Hill, 2005

4.   COMSOL 4.0a Documentation.

5.   CFD Online (06/18/2010) Law of the Wall retrieved [12/2010] http://www.cfd-online.com/Wiki/Law_of_the_wall.

6.   Freels, James D., et al. 2D Thermal Hydraulic Analysis and Benchmark in Support of HFIR Conversion Using COMSOL ORNL/TM-2010/18, 2010.

7.   McLain, Howard A. HFIR Fuel Element Steady State Heat Transfer Analysis Revised Version ORNL-TM/1904, 1967.

8.   Kirkpatrick, John R. Calculations for HFIR Fuel Plate Non-Bonding and Fuel Segregation Uncertainty Factors K/CSD/TM--79, 1990.

9.   Meirovitch, Leonard, "Analytical Methods in Vibrations," New York, NY: Macmillan Pub., 1967.

10.   ASM Aerospace Specification Metals Inc. Aluminum 6061-T6 retrieved [10/2010] http://asm.matweb.com/search/SpecificMaterial.asp?bassnum=MA6061t6.

11.   MATBASE Material Properties of Al99,0(1100) retrieved [10/2010] http://www.matbase.com/material/non-ferrous-metals/wrought-aluminium/al99.0-1100/properties.

INTERNAL DISTRIBUTION

1. K. J. Beierschmitt (*beierschmitt@ornl.gov*)
2. G. I. Bell (*bellgi@ornl.gov*)
3. J. L. Binder (*binderjl@ornl.gov*)
4. I. T. Bodey (*bodeyed@ornl.gov*)
5. S. M. Bowman (*bowmansm2ornl.gov*)
6. S. E. Burnette (*burnettese@ornl.gov*)
7. D. H. Cook (*dhc@ornl.gov*)
8. R. A. Crone (*cronera@ornl.gov*)
9. F. G. Curtis (*curtisfg@ornl.gov*)
10. J. D. Freels (*freelsjd@ornl.gov*)
11. J. C. Gehin (*gehinjc@ornl.gov*)
12. S. R. Greene (*srg@ornl.gov*)
13. A. S. Icenhour (*icenhouras@ornl.gov*)
14. *G. Ilas (ilasg@ornl.gov)*
15. P. Jain (*jainpk@ornl.gov*)
16. J. H. Miller (*millerjh2@ornl.gov*)
17. C. V. Parks (*parkscv@ornl.gov*)
18. D. L. Pinkston (*pinkstondl@ornl.gov*)
19. D. G. Renfro (*renfrodg@ornl.gov*)
20. L. J. Satkowiak (*satkowiaklj@ornl.gov*)
21. J. D. Sease (*seasejd@ornl.gov*)
22. K. A. Smith (*smithka@ornl.gov*)
23. W. J. Toth (*tothwj@ornl.gov*)
24. K. Wong (*xw7@ornl.gov*)
25. S. J. Zinkle (*zinklesj@ornl.gov*)
26. ORNL Laboratory Records (*hamrindr@ornl.gov*)

EXTERNAL DISTRIBUTION

27. A. Adams, U.S. Nuclear Regulatory Commission, One White Flint North, 11555 Rockville Pike, Rockville, Maryland 20852-2738 (*axa@nrc.gov*)
28. R. A. Butler, Director, Research Reactor Center, 1513 Research Park Drive, Columbia, MO 65211 (*Butler-Ra@missouri.edu*)
29. G. S. Chang, Idaho National Laboratory, P.O. Box 1625, Idaho Falls, ID 83415-3885 (*gray.chang@inl.gov*)
30. J. Chamberlin, NA-212, U.S. Department of Energy, 1000 Independence Avenue SW, Washington, DC 20585 (***jeffry.chamberlin@nnsa**.doe.gov)*
31. D. Diamond, Brookhaven National Laboratory, P.O. Box 5000, Upton, NY 11973-5000 (*dia-mond@bnl.gov*)
32. D. Kutikkad, Assistant Reactor Manager-Physics, University of Missouri Research Reactor Facility, Columbia, MO 65211 (*kutikkadk@missouri.edu*)
33. C. Landers, NA-212, U.S. Department of Energy, 1000 Independence Avenue SW, Washington, DC 20585 (***Christopher.landers@nnsa**.doe.gov)*
34. J. Matos, Argonne National Laboratory, 9700 S. Cass Avenue, Argonne, IL 60439 (*jim.matos@anl.gov*)
35. C. McKibben, University of Missouri Research Reactor Facility, Columbia, MO 65211 (*mckib-benj@missouri.edu*)
36. J. Dwight, Idaho National Laboratory, P.O. Box 1625, Idaho Falls, ID 83415-3750 (*John.Dwight@inl.gov*)
37. T. Newton, MIT Nuclear Reactor Laboratory, 138 Albany St., Cambridge, MA 02139 (*tnewton@mit.edu*)
38. W. Richards, NIST Center for Neutron Research, 100 Bureau Drive, Stop 8561, Gaithersburg, MD 20899-8561 (*wade.richards@nist.gov*)
39. J. Roglans, Argonne National Laboratory, 9700 S. Cass Avenue, Argonne, IL 60439 (*roglans@anl.gov*)
40. P. Roth, Idaho National Laboratory, P.O. Box 6188, Idaho Falls, ID 83415 (*Paul.Roth@inl.gov*)
41. P. Staples, NA-212, U.S. Department of Energy, 1000 Independence Avenue SW, Washington, DC 20585 (*Parrish.Staples@nnsa.doe.gov*)
42. J. G. Stevens, Argonne National Laboratory, 9700 S. Cass Avenue, Argonne, IL 60439 (*johnste-vens@anl.gov*)
43. D. M. Wachs, MFC 791 B-147, Idaho National Laboratory, P.O. Box 6188, Idaho Falls, ID 83415 (*Dan-iel.Wachs@inl.gov*)
44. R. E. Williams, NIST Center for Neutron Research, 100 Bureau Drive, Stop 8560, Gaithersburg, MD 20899-8560 (*robert.williams@nist.gov*)
45. S. O'Kelly, NIST Center for Neutron Research, 100 Bureau Drive, Stop 8560, Gaithersburg, MD 20899-8560 (*sean.okelly@nist.gov*)
46. W. C. Richardson, Babcock & Wilcox Nuclear Operations Group, 2016 Mount Athos Rd., Lynchburg, VA 24504 (*WCRichardson@bwxt.com*)

47. E. C. Woolstenhulme, P.O. Box 1625, Idaho Falls, ID 83415-3750 (*Eric.Woolstenhulme@inl.gov*)
48. Peter Lee, Office of Basic Energy Sciences, U.S. Department of Energy, 1000 Independence Avenue SW, Washington, DC 20585 (*peter.lee@science.doe.gov*)
49. C. Sohn, Office of Basic Energy Sciences, U.S. Department of Energy, 1000 Independence Avenue SW, Washington, DC 20585 (*carol.sohn@pnso.science.doe.gov*)
50. J. O. Moore, U.S. Department of Energy (*moorejo@ornl.gov*)
51. L. Foyto, Research Reactor Center, 1513 Research Park Drive, Columbia, MO 65211 (*foytol@missouri.edu*)
52. L. Jollay, Y-12 National Security Complex (*jollayl@y12.doe.gov*)
53. D. Rosine, U.S. Department of Energy (*rosinedb@ornl.gov*)
54. D. Reed, U.S. Department of Energy (*reeddr@ornl.gov*)
55. G. Solbrekken, University of Missouri, Columbia, MO 65211 (*solbrekkeng@missouri.edu*)
56. D. McDaniel, Idaho National Laboratory, P.O. Box 6188, Idaho Falls, ID 83415 (*David.McDaniel@inl.gov*)
57. Hollie Longmire, Y-12 National Security Complex (*longmireha@y12.doe.gov*)
58. Michael J. Nilles, Babcock & Wilcox Nuclear Operations Group, 2016 Mount Athos Rd., Lynchburg, VA 24504 (*mjnilles@babcock.com*)
59. Jared M. Wight, Babcock & Wilcox Nuclear Operations Group, 2016 Mount Athos Rd., Lynchburg, VA 24504 (*jmwight@babcock.com*)
60. Mitch Meyer, P.O. Box 1625, Idaho Falls, ID 83415-3750 (*Mitchell.Meyer@inl.gov*)
61. Anthony Vinnola, P.O. Box 1625, Idaho Falls, ID 83415-3750 (*Anthony.vinnola@inl.gov*)
62. Ann Marie Phillips, P.O. Box 1625, Idaho Falls, ID 83415-3750 (*AnnMarie.Phillips@inl.gov*)
63. Wade Marcum, Oregon State University (*marcumw@engr.orst.edu*)
64. Joe Cleary, Pacific Northwest National Laboratory (*joe.cleary@pnl.gov*)
65. MaryJane Ross-Lee, US Nuclear Regulatory Commission (*maryjane.ross-lee@nrc.gov*)
66. Harriet Kung, Office of Basic Energy Sciences, U.S. Department of Energy, 1000 Independence Avenue SW, Washington, DC 20585 (*harriet.kung@science.doe.gov*)
67. Van T. Nguyen, Office of Basic Energy Sciences, U.S. Department of Energy, 1000 Independence Avenue SW, Washington, DC 20585 (*van.nguyen@science.doe.gov*)
68. Kenneth B. Sheely, NA-21, U.S. Department of Energy, 1000 Independence Avenue SW, Washington, DC 20585 (*ken.sheely@hq.doe.gov*)
69. Michele G. Branton, U.S. Department of Energy (*brantonmg@ornl.gov*)
70. H. Randall Persinger, U.S. Department of Energy (*persingerhr@ornl.gov*)
71. Douglas Burkes, Pacific Northwest National Laboratory (*douglas.burkes@nnsa.doe.gov*)
72. Aurelien Bergeron, Argonne National Laboratory (*abergeron@anl.gov*)
73. Adrien Tentner, Argonne National Laboratory (*tentner@anl.gov*)
74. Kivanc Ekici, 315 Perkins Hall, MABE Dept., The University of Tennessee, Knoxville, TN 37996-2030 (ekici@utk.edu)
75. Rao V. Arimilli, 235 Dougherty Engr. Bldg., MABE Dept., The University of Tennessee, Knoxville, TN 37996-2030 (arimilli@utk.edu)
76. A. J. Baker, 316A Perkins Hall, MABE Dept., The University of Tennessee, Knoxville, TN 37996-2030 (abaker@utk.edu)
77. Arthur E. Ruggles, Pasqua Engr. Bld.g., NE Dept., The University of Tennessee, Knoxville, TN 37996-2300 (aruggles@utk.edu)
78. Ronald E. Pevey, 213 Pasqua Engr. Bldg., NE Dept., The University of Tennessee, Knoxville, TN 37996-2300 (rpevey@utk.edu)
79. Adrian M. Tenter, B208, 9700 S. Cross Avenue, Argonne, IL 60439-2842 (tenter@anl.gov)
80. Trent Primm, Primm Consulting, LLC, 945 Laurel Hill Road, Knoxville, TN 37923(trentprimm@primmconsultingllc.com)
81. Bjorn Sjodin, COMSOL, Inc., 1 New England Executive Park, Suite 359, Burlington, MA 01803 (bjorn@comsol.com)
82. Joe Iannelli, Robert Moon University, 6001 University Blvd., Moon Township, PA, 15108-1189 (iannelli@rmu.edu)

83.	Roy Wilcox, LMU, 6965 Cumberland Gap Parkway, Harrogate, TN 37752 (roy.wilcox@lmunet.edu)
84.	Ed Fontes, COMSOL, AB, Tegnergatan 23, SE-111 40 Stockholm (edu@consol.com)